

2014

# Ionic Liquids and GUMBOS for Biomedical and Sensing Applications

Paul Kipkorir Sang Magut

Louisiana State University and Agricultural and Mechanical College, pmagut1@gmail.com

Follow this and additional works at: [https://digitalcommons.lsu.edu/gradschool\\_dissertations](https://digitalcommons.lsu.edu/gradschool_dissertations)



Part of the [Chemistry Commons](#)

---

## Recommended Citation

Magut, Paul Kipkorir Sang, "Ionic Liquids and GUMBOS for Biomedical and Sensing Applications" (2014). *LSU Doctoral Dissertations*. 718.

[https://digitalcommons.lsu.edu/gradschool\\_dissertations/718](https://digitalcommons.lsu.edu/gradschool_dissertations/718)

This Dissertation is brought to you for free and open access by the Graduate School at LSU Digital Commons. It has been accepted for inclusion in LSU Doctoral Dissertations by an authorized graduate school editor of LSU Digital Commons. For more information, please contact [gradetd@lsu.edu](mailto:gradetd@lsu.edu).

# IONIC LIQUIDS AND GUMBOS FOR BIOMEDICAL AND SENSING APPLICATIONS

A Dissertation

Submitted to the Graduate Faculty of the  
Louisiana State University and  
Agricultural and Mechanical College  
in partial fulfillment of the  
requirements for the degree of  
Doctor of Philosophy

in

The Department of Chemistry

by

Paul Kipkorir Sang Magut  
B.Ed (Science), Egerton University, 2001  
August 2014

*To My Lord and Savior Jesus Christ*

*“You will keep in perfect peace him whose mind is steadfast, because he trusts in you.”*

*Isaiah 26:3*

*To my wife Anne Wanjiku Sang and my daughters Shalom Chepchumba Sang and Shawna Njoki Sang for the sacrifices, support, love and encouragement throughout the years.*

*To My Parents: Joel Kimuigei Magut and Esther Chelagat Magut*

*To My Parents in- law: John Baptist Njagi and Lucy Njoki Njagi*

*To my siblings: Mike, Rose, Richard, Julius, Millicent, Shamila, Bernard, and Hillary*

*To my entire family past, present and future!*

## ACKNOWLEDGEMENTS

First I would like to thank Professor Isiah M. Warner for providing me with the opportunity to join his research group, for his encouragement, guidance and persistent support. Thank you for believing in me and inspiring me toward excellence.

Secondly, I would like to thank my doctoral committee members: Drs. Samuel Gilman, Megan Macnaughtan, Daniel Hayes, and Jack Losso for taking the time out of their schedules to serve on my committee and for always perpetuating my boundless curiosity with their insightful questions.

Thirdly, I would like to thank Dr. Susmita Das for introducing me to fluorescence spectroscopy, ionic liquids, and nanotechnology, and for working closely with me throughout my graduate career.

I am grateful to Dr. David Bwambok and Dr. Min Li for useful discussion at the beginning of my research and for helping me transition to graduate school and to Warner research group.

I thank the following collaborators: Ms. Karen McDonough, Dr. Daniel Hayes, Dr. Vivian Fernand and Ammar Qureshi for introducing me to biological work and especially cell culture. Prof. Jack Losso, Dr. Sita Aggrawal, Dr. Xiaochu Wu and Dr. David Burk for help with fluorescence microscopy, TEM, confocal microscopy, and useful discussions on biological experiments.

I also thank Ms. Danielle Thomas, Dr. Vivian Fernand, Dr. Priya Pathak, Dr. Farhana Hasan, and Dr. Noureen Siraj for reading and editing my dissertation. I am grateful to the following students, Dr. Chengfei Lu, Dr. Ammar Qureshi, Ms. Namrata Karki, Ms. Diana Carvajal and Mr. Kevin Roberson graduate students whom I worked with in various projects.

Ms. Ivana Deyl, Ms. Brittini Naylor and Mr. Joshua Mason undergraduate students, whom I worked with and mentored in the course of my Ph.D.

I am indebted to the family of Erin and Jed Marsolf, my American family for their support and friendship over the years. I am grateful to Mr. Willy Mutai, a phenomenal High School Chemistry Teacher whose teaching ignited a love for Chemistry in me.

I also want to thank the following pastors and their families, James Kisormoi, Peter Muema, Christopher Mujesia, Hans Googer, Kevin Mckee, Jeff Ginn for their spiritual support and friendship.

I would like to thank Drs. Maurice Okoth, Samuel Lutta, Fred Segor, Kituyi Lusweti, Yulita Mitei-Cheruiyot, and Claire Muhanji, the faculty from University of Eldoret (formerly Chepkoilel Campus of Moi University), who encouraged and ignited my desire to pursue Ph.D. in Chemistry!

Last but not least, I am forever grateful to the members of the Warner Research Group, past and present, for their friendship and great moments we shared together in group meetings.

Thank y'all!

## TABLE OF CONTENTS

ACKNOWLEDGEMENTS .....	iii
LIST OF TABLES .....	ix
LIST OF FIGURES .....	x
LIST OF SCHEMES.....	xv
ABSTRACT.....	xvi
CHAPTER 1. INTRODUCTION .....	1
1.1. Characteristics of Cancer .....	1
1.1.1. Causes of Cancer .....	4
1.1.2. Treatment.....	4
1.2. Ionic Liquids .....	7
1.2.2. Synthesis of Ionic Liquids .....	9
1.2.3. Physical and Chemical Properties of ILs.....	11
1.3. From Ionic Liquids to Group of Uniform Materials Based on Organic Salts .....	12
1.3.1. Nanoparticles Derived from ILs and GUMBOS .....	14
1.3.2. Synthesis of NanoGUMBOS by Reprecipitation Method.....	14
1.3.3. Active Pharmaceutical Ingredients Based on Ionic liquids and GUMBOS ...	16
1.3.4. Ionic Liquids and GUMBOS with Anticancer Properties .....	18
1.4. Analytical Methods Used.....	19
1.4.1. Ultraviolet- Visible Spectroscopy .....	19
1.4.2. Mammalian Cell Cytotoxicity .....	20
1.4.3. Fluorescence Spectroscopy.....	22
1.4.4. Fluorescence Microscopy .....	23
1.4.5. Confocal Laser Scanning Microscopy.....	24
1.4.6. Transmission Electron Microscopy .....	25
1.4.7. Zeta Potential Analysis.....	27
1.4.8. Superconducting Quantum Interference Device.....	27
1.5. Scope of the Dissertation .....	28
1.6. References.....	29
CHAPTER 2. TUNABLE CYTOTOXICITY OF RHODAMINE 6G VIA ANION VARIATIONS .....	37

2.1. Introduction.....	37
2.2. Materials and Methods.....	40
2.2.1. Materials .....	40
2.2.2. Synthesis and Characterization of Rhodamine 6G-based GUMBOS .....	40
2.2.3. Synthesis of Rhodamine 6G-based NanoGUMBOS .....	42
2.2.4. Absorption and Fluorescence Spectroscopy.....	43
2.2.5. Quantum Yields and Lifetime Measurements .....	43
2.2.6. Photostability Measurements.....	44
2.2.7. Stability Studies .....	44
2.2.8. Determination of Hydrophobicity .....	44
2.2.9. Cell Studies.....	45
2.3. Results and Discussion .....	49
2.3.1. Synthesis and Characterization of Rhodamine 6G GUMBOS .....	49
2.3.2. Physical and Morphological Properties.....	49
2.3.3. Absorption and Fluorescence Studies.....	52
2.3.4. Stability of Rhodamine 6G-based NanoGUMBOS.....	55
2.3.5. Cell Studies.....	56
2.4. Conclusion .....	64
2.5. References.....	65
<b>CHAPTER 3. PHOSPHONIUM-DYSPROSIUM DERIVED NANOPARTICLES WITH CANCER TARGETING PROPERTIES .....</b>	<b>69</b>
3.1. Introduction.....	69
3.2. Materials and Methods.....	71
3.2.1. Materials .....	71
3.2.2. Synthesis and Characterization of the Phosphonium-dysprosium Salts.....	72
3.2.3. Synthesis and Characterization of Nanoparticles from Phosphonium- dysprosium Salts.....	73
3.2.4. Magnetic Properties .....	73
3.2.5. UV-Vis Absorption and Fluorescence Spectroscopy .....	74
3.2.6. Cell Studies.....	74
3.2.7. Statistics.....	75
3.3. Results and Discussion .....	76
3.3.1. Synthesis and Characterization of the Phosphonium-dysprosium Compounds	76
3.3.2. Physical and Morphological Properties of the Nanoparticles .....	79

3.3.3. Magnetic Properties .....	80
3.3.4. UV-Vis Absorption and Fluorescence Spectroscopy .....	82
3.3.5. Cell Studies.....	83
3.4. Conclusion .....	86
3.5. References.....	86
CHAPTER 4. MULTIMODAL STIMULI RESPONSIVE THERANOSTIC NANOMATERIALS DERIVED FROM IRON (III) PHTHALOCYANINE DEOXYCHOLATE SALT .....	90
4.1. Introduction.....	90
4.2. Materials and Methods.....	92
4.2.1. Materials .....	92
4.2.2. Synthesis of [Ptc][DC].....	93
4.2.3. Synthesis and Characterization of the Nanomaterials .....	93
4.2.4. UV-Vis Absorption and Fluorescence Spectroscopy .....	93
4.2.5. Magnetic Property Measurement.....	94
4.2.6. Drug Encapsulation in Nanoparticles .....	94
4.2.7. Cell Studies.....	94
4.3. Results and Discussions .....	95
4.3.1. Synthesis and Characterization of [Ptc][DC] .....	96
4.3.2. Spectral Characterization of [Ptc][DC] Nanoparticles .....	96
4.3.3. TEM Studies of [Ptc][DC] Nanoparticles .....	97
4.3.4. Magnetic Properties of [Ptc][DC] Nanoparticles .....	98
4.3.5. pH Responsive Properties of [Ptc][DC] Nanoparticles .....	100
4.3.6. Cell Studies.....	100
4.4. Conclusions.....	102
4.5. References.....	102
CHAPTER 5. IONIC LIQUID-BASED NANOMATERIALS FOR PH SENSING AND CHEMOTHERAPY .....	105
5.1. Introduction.....	105
5.2. Materials and Methods.....	107
5.2.1. Materials .....	107
5.2.2. Synthesis and Characterization of Ionic Liquids .....	108
5.2.3. Synthesis and Characterization of Nanomaterials from Ionic Liquids.....	109
5.2.4. Absorption and Fluorescence Studies.....	110



5.2.5. Cytotoxicity Studies .....	111
5.3. Results and Discussions .....	111
5.3.1. Physical Characterization of the ILs.....	112
5.3.2. Optical Properties of pH Dependent TTP Nanomaterials .....	113
5.3.3. Morphological Changes in TTP Nanomaterials with Changes in pH .....	118
5.3.4. Anticancer Activity of TTP-based ILs .....	123
5.4. Conclusions.....	126
5.5. References.....	126
CHAPTER 6. CONCLUSIONS AND FUTURE DIRECTIONS .....	130
APPENDIX: LETTERS OF PERMISSION.....	134
VITA.....	140

## LIST OF TABLES

Table 2.1. Elemental analysis of rhodamine 6G-based GUMBOS .....	50
Table 2.2. Yields, melting points, logarithm of 1-octanol/water partition coefficients of rhodamine 6G-based GUMBOS and size of corresponding particles. ....	50
Table 2.3. Dissociation constants of rhodamine-based GUMBOS in buffer solutions .....	52
Table 2.4 IC <sub>50</sub> (μM) of R6G-based compounds towards breast cell lines .....	58
Table 3.1. Solubility of phosphonium-dysprosium compounds in water .....	79
Table 3.2. Summary of magnetic properties of phosphonium-dysprosium compounds .....	81
Table 3.3. Summary of IC <sub>50</sub> values for phosphonium-dysprosium nanoparticles and the bulk materials.....	85
Table 5.1. Size of [TTP] <sub>2</sub> [FL] and [TTP][FL] nanodroplets at various pH values obtained from dynamic light scattering. ....	120
Table 5.2. Zeta potential of [TTP][FL] and [TTP] <sub>2</sub> [FL] nanodroplets at various pH values.....	122
Table 5.3. IC <sub>50</sub> values of [TTP][FL], [TTP] <sub>2</sub> [FL] and the starting materials [TTP][Cl] and Na <sub>2</sub> FL ILs in breast normal and cancer cell lines. ....	125

## LIST OF FIGURES

Figure 1.1. The hallmarks of cancer. (Adapted from reference 5 and 6).....	2
Figure 1.2. Quantification of tumor deposits <i>ex vivo</i> a) color image b) corresponding tumor-specific fluorescence image of a representative area in the abdominal cavity, and c) scoring based on three different color images (median 7, range 4–22) and their corresponding fluorescence images (FLI) (median 34, range 8–81); $P < 0.001$ by five independent surgeons. (Reproduced from reference 20 with permission from Nature Publishing Group). .....	5
Figure 1.3. Synthesis of 1-alkyl-3-methylimidazolium hexafluorophosphate.....	9
Figure 1.4. Synthesis of ethyl ammonium nitrate. ....	10
Figure 1.5. Synthesis of 1-butyl-3-methylimidazolium tetrachloroferrate. ....	10
Figure 1.6. Illustration of frustrated packing in ILs due to asymmetry of component ions. ....	12
Figure 1.7. Reprecipitation process of nanoGUMBOS fabrication showing (A) 1 mM stock solution of GUMBOS solution in ethanol, (B) injection of 100 $\mu\text{L}$ of the GUMBOS solution into 5 mL of deionized water while sonicating the mixture at room temperature, and (C) reprecipitation of GUMBOS to afford nanoGUMBOS dispersed in water. ....	15
Figure 1.8. Examples of ions employed in synthesis of a) first generation b) second generation and c) third generation ILs and GUMBOS .....	16
Figure 1.9. Schematic diagram of a UV-vis spectrophotometer.....	19
Figure 1.10. Conversion of MTT to insoluble formazan by cellular enzymes in viable cells.....	21
Figure 1.11. Conversion of MTS to soluble formazan by cellular enzymes in viable cells. ....	21
Figure 1.12. Perrin- Jablonski diagram.....	22
Figure 1.13. Schematic representation of a fluorometer.....	23
Figure 1.14. Schematic representation of a conventional fluorescence microscope .....	24
Figure 1.15. Schematic depiction of a confocal laser scanning microscope .....	25
Figure 1.16. Schematic representation of a transmission electron microscope .....	26
Figure 1.17. Schematic representation of a SQUID .....	28
Figure 2.1. NanoGUMBOS TEM micrographs of a) [R6G][TPB] size: $92 \pm 17$ nm and b) [R6G][BETI] size: $101 \pm 21$ nm. Scale bars represent 500 nm. ....	51

Figure 2.2. Absorption spectra of [R6G]-based a) GUMBOS in ethanol b) nanoGUMBOS in PBS. Inset; deconvoluted absorption spectrum of [R6G][TPB] and [R6G][BETI] nanoGUMBOS (black line), representing randomly oriented aggregates absorbing at $\lambda = 525$ nm (red line) and J- aggregates absorbing at $\lambda = 582$ nm (blue line).....	53
Figure 2.3. Fluorescence studies in PBS displaying a) fluorescence excitation and emission spectra of 4 $\mu$ M [R6G][TPB] nanoGUMBOS and b) photostability of 0.1 $\mu$ M [R6G] - based compounds. $F_0$ and $F$ are fluorescence intensities at $t = 0$ and at different times respectively. Maximum slit widths of 14 nm were maintained on both excitation and emission.....	54
Figure 2.4. Stability of nanoGUMBOS in a) PBS b) 10% serum and c) absorbance spectra corresponding to [R6G][TPB] in PBS showing transition from J-aggregates ( $\lambda = 582$ nm) to randomly oriented aggregates ( $\lambda = 525$ nm).....	55
Figure 2.5. TEM images of a suspension of a) [R6G] [BETI] and b) [R6G] [TPB] GUMBOS. This displays micro- and nano-sized particles. Bars represent 2 $\mu$ m. ....	56
Figure 2.6. Cell viability assay of Hs578Bst, Hs578T and MDA-MB-231 cell lines upon treatment with a) [R6G][BETI] and b) [R6G][TPB]. * Statistically different from control, $P < 0.0001$ .....	57
Figure 2.7. Light microscopy images of a) normal breast cell line, Hs578Bst and breast cancer cell lines b) Hs578T and c) MDA-MB-231 after treatment with 50 $\mu$ M [R6G][TPB] for 48h. Cell images were obtained using a light microscope equipped with a camera at a magnification of 20X. ....	58
Figure 2.8. Cell viability assay of Hs578Bst, Hs578T and MDA-MB-231 cell lines upon treatment with 0–100 $\mu$ M of a) [Li][BETI] and b) [Na][TPB] controls. *Statistically different from control, $P < 0.0001$ for [Li][BETI] Hs578T. Statistical analysis shows no difference from control for all the others ( $P > 0.05$ )...	59
Figure 2.9. Effect of a) [R6G][BETI] and b) [R6G][TPB] on cell death of MDA-MB-231 breast cancer cells. MCF7 and Hs578T cancer cell lines displayed similar trends. The enrichment factor is the ratio of the absorbance of the sample (dying/dead cells) and the absorbance of the control (viable cells). *Statistically different from control, $P < 0.0001$ .....	59
Figure 2.10. Clonogenic assay images of MDA-MB-231 breast cancer cells showing a) colonies formed from control wells and b) zero colonies formed in wells treated with 12.5 $\mu$ M [R6G][BETI]. Similar results were obtained for [R6G][TPB]. ....	60
Figure 2.11. Mean Fluorescence intensity (M.F.I) of breast cancer cell line, MDA-MB-231 (blue) and normal breast cell line, Hs578Bst (red) treated with a) [R6G][BETI] and b) [R6G][TPB]. *Statistically different from corresponding concentration in Hs578Bst for the same compound ( $P < 0.0001$ ). ....	61

Figure 2.12. Mean Fluorescence intensity (M.F.I) of normal breast cell line, Hs578Bst treated with a) [R6G][BETI] and b) [R6G][TPB] at a pH of 6.5 (blue) and 7.4 (red).....	62
Figure 2.13. Confocal microscopy analysis of a) [R6G][BETI] and b) [R6G][TPB] in MDA-MB-231. The fluorescent images show the DAPI-labeled nucleus (blue), mitotracker deep red 633-labeled mitochondria (red), [R6G][BETI] or [R6G][TPB] (green) and a merged image that shows the two compounds mainly localize in the mitochondria. ....	63
Figure 2.14. Profiles of mitochondrial toxicity of a) [R6G][BETI] and b) [R6G][TPB] using a Mitochondrial ToxGlo™ Assay. MDA-MB-231 cells were plated at 10,000 cells/ well and treated in serial dilutions of compounds resuspended in glucose free (galactose supplemented) DMEM media for 2 h. A reduction in ATP with discordant changes in membrane integrity (cytotoxicity) indicates that the two compounds are mitochondrial toxins.....	64
Figure 3.1. FT-IR spectra of KSCN, [Ph <sub>4</sub> P][Br], [Ph <sub>4</sub> P][SCN], [Ph <sub>4</sub> P] <sub>5</sub> [Dy(SCN) <sub>8</sub> ].....	76
Figure 3.2. FT-IR spectra of [Ph <sub>3</sub> PBn][Br], [Ph <sub>3</sub> PBn][SCN], [Ph <sub>3</sub> PBn] <sub>5</sub> [Dy(SCN) <sub>8</sub> ].....	77
Figure 3.3. FT-IR spectra of [Ph <sub>3</sub> PBnNO <sub>2</sub> ][Br], [Ph <sub>3</sub> PBn NO <sub>2</sub> ][SCN], Ph <sub>3</sub> PBnNO <sub>2</sub> ] <sub>5</sub> [Dy(SCN) <sub>8</sub> ].....	78
Figure 3.4. FT-IR spectra of [Ph <sub>3</sub> PBnOEt][Br], [Ph <sub>3</sub> PBnOEt] [SCN], [Ph <sub>3</sub> PBnOEt] <sub>5</sub> [Dy(SCN) <sub>8</sub> ] .....	78
Figure 3.5. Transmission electron micrographs of a) [Ph <sub>4</sub> P] <sub>5</sub> [Dy(SCN) <sub>8</sub> ] nanoparticles, size: 54 ± 8nm b) [Ph <sub>3</sub> PBnOEt] <sub>5</sub> [Dy(SCN) <sub>8</sub> ] nanoparticles, size: 65 ± 13 nm. c) [Ph <sub>3</sub> PBnNO <sub>2</sub> ] <sub>5</sub> [Dy(SCN) <sub>8</sub> ] nanoparticles, size: 21 ± 3 nm and d) [Ph <sub>3</sub> PBn] <sub>5</sub> [Dy(SCN) <sub>8</sub> ] nanoparticles, size: 92.3 ± 15.2 nm. Bars represent 500 nm. 79	79
Figure 3.6. Magnetic property of [Ph <sub>3</sub> PBnNO <sub>2</sub> ] <sub>5</sub> [Dy(SCN) <sub>8</sub> ]. a) Field dependence of molar magnetization at 300 K. b) Temperature dependence of static molar magnetic susceptibility $\chi_{mol}$ at a field of 1,000 Oe and c) field dependence of molar magnetization at 200 K.....	81
Figure 3.7. Fluorescence emission spectra of the phosphonium based nanoparticles with transition assignments for [Ph <sub>4</sub> P] <sub>5</sub> [Dy(SCN) <sub>8</sub> ] (red), Ph <sub>3</sub> PBnOEt] <sub>5</sub> [Dy(SCN) <sub>8</sub> ] (green), [Ph <sub>3</sub> PBnNO <sub>2</sub> ] <sub>5</sub> [Dy(SCN) <sub>8</sub> ] (purple), and [Ph <sub>3</sub> PBn] <sub>5</sub> [Dy(SCN) <sub>8</sub> ] (blue) in acetonitrile (1 mM), $\lambda_{ex} = 365$ nm.....	82
Figure 3.8. Cytotoxicity of a) [Ph <sub>4</sub> P] <sub>5</sub> [Dy(SCN) <sub>8</sub> ], b) [Ph <sub>3</sub> PBnOEt] <sub>5</sub> [Dy(SCN) <sub>8</sub> ], c) [Ph <sub>3</sub> PBnNO <sub>2</sub> ] <sub>5</sub> [Dy(SCN) <sub>8</sub> ], and d) [Ph <sub>3</sub> PBn] <sub>5</sub> [Dy(SCN) <sub>8</sub> ] nanoparticles against breast cancer (Hs578T, red) and normal breast (Hs578Bst, blue) cell lines, 48 h incubation. All points are mean ± s.d of triplicate wells of three independent experiments. *Statistically different from the corresponding concentration for the same compound in Hs578T (P < 0.05). ....	84

Figure 3.9. Clonogenic assay images of MDA-MB-231 breast cancer cells showing a) Colonies formed from control wells and b) zero colonies formed in wells treated with 5 $\mu$ M $[\text{Ph}_3\text{PBnNO}_2]_5[\text{Dy}(\text{SCN})_8]$ . Similar results were obtained for all the other phosphonium-dysprosium nanoparticles. ....	85
Figure 4.1. FT-IR spectrum of A) $[\text{Ptc}][\text{Cl}]$ and B) $[\text{Ptc}][\text{DC}]$ . ....	96
Figure 4.2. (A) Absorption spectra and (B) fluorescence emission spectra ( $\lambda_{\text{ex}}=400$ nm) of $[\text{Ptc}][\text{DC}]$ nanoparticles with varying pH. ....	97
Figure 4.3. TEM micrographs of $[\text{Ptc}][\text{DC}]$ nanoparticles respectively at A) pH 7.4 and B) pH 6. ....	98
Figure 4.4. Magnetic properties of $[\text{Ptc}][\text{DC}]$ (A) bulk M vs H at 300 K, (B) nanoparticles M vs H at 300 K, (C) nanoparticles $\chi$ vs T at 0.2 Tesla and (D) nanoparticles M vs H at 200 K. ....	99
Figure 4.5. Cell viability studies of free $[\text{Ptc}][\text{DC}]$ and doxorubicin loaded $[\text{Ptc}][\text{DC}]$ nanoparticles in (A) Hs578Bst (normal breast) and (B) MDA-MB-231 (breast cancer) cell lines. (C) Release profile of doxorubicin from $[\text{Ptc}][\text{DC}]$ nanoparticles with varying pH. (D) Confocal microscopic image of MDA-MB 231 cells after 2 h incubation with Dox free $[\text{Ptc}][\text{DC}]$ nanoparticles. ..	101
Figure 5.1. Pictures of the compounds (A) $[\text{TTP}][\text{FL}]$ and (B) $[\text{TTP}]_2[\text{FL}]$ . ....	113
Figure 5.2. Thermogravimetric analysis of (A) $[\text{TTP}][\text{FL}]$ and (B) $[\text{TTP}]_2[\text{FL}]$ . ....	113
Figure 5.3. pH dependent color change of (a) $[\text{TTP}]_2[\text{FL}]$ nanodroplets, (b) $[\text{TTP}][\text{FL}]$ nanoparticles and (c) $\text{Na}_2\text{FL}$ in water (inherent pH 8.4) and buffers of different pH. ....	114
Figure 5.4. (a, c) absorption and fluorescence spectra of $[\text{TTP}]_2[\text{FL}]$ and (b, d) of $[\text{TTP}][\text{FL}]$ , respectively. ....	115
Figure 5.5. Schematic representation of the type of aggregation in (A) $[\text{TTP}]_2[\text{FL}]$ and (B) $[\text{TTP}][\text{FL}]$ . ....	117
Figure 5.6. a) Photostabilities of $[\text{TTP}]_2[\text{FL}]$ nanoparticles compared to $\text{Na}_2\text{FL}$ solution in water and b) fluorescence emission anisotropy of $[\text{TTP}]_2[\text{FL}]$ nanodroplets in buffer of varying pHs. ....	118
Figure 5.7. TEM micrographs of $[\text{TTP}]_2[\text{FL}]$ nanoparticles in (A) water (pH 8.4) ( $28 \pm 8$ nm) and buffers of (B) pH 5.4 ( $453 \pm 197$ nm), (C) pH 4.0 ( $1.6 \pm 0.2$ $\mu$ m), (D) pH 2.2 ( $797 \pm 171$ nm, $167 \pm 46$ nm). ....	119
Figure 5.8. NMR of $[\text{TTP}]_2[\text{FL}]$ nanodroplets synthesized and incubated at pH 4. ....	123

Figure 5.9. Cytotoxicity studies of (A) [TTP][FL] and (B) [TTP]<sub>2</sub>[FL] in normal breast (Hs578Bst) and breast cancer (MDA-MB-231, MCF-7) cell lines. .... 124

## LIST OF SCHEMES

Scheme 2.1. Synthesis of a) hydrophobic and b) hydrophilic R6G based GUMBOS.....	41
Scheme 3.1. Synthesis of phosphonium-dysprosium compounds .....	73
Scheme 4.1. Synthesis of Iron (III) phthalocyanine based pH sensitive organic salt [Ptc][Dc]...	93
Scheme 5.1. Synthesis of (A) [TTP] <sub>2</sub> [FL] and (B) [TTP][FL] ionic liquids .....	108



## ABSTRACT

This dissertation is a synopsis of advancements in the field of ionic liquids and a group of uniform materials based on organic salts (GUMBOS) in biomedical applications, especially with regard to cancer research. The toxicity of chemotherapeutic agents to normal tissues and drug resistance are a major concern in cancer treatment. In this dissertation, GUMBOS and nanoGUMBOS as well as ionic liquids and nanodroplets are explored as possible chemotherapeutic agents with minimal toxicity to normal cells.

In the first part of my dissertation, exploitation of ionic liquid chemistry to modulate toxicity of rhodamine 6G is reported. Rhodamine 6G-based GUMBOS with varying counter-anions that are stable under physiological conditions, display excellent fluorescence photostability, and more importantly have tunable chemotherapeutic properties were synthesized. *In vitro* studies indicate that the hydrophobic compounds of this series allow production of nanoGUMBOS which are non-toxic to normal cells and toxic to cancer cells. Furthermore, the anions, in combination with cations such as sodium, were observed to be non-toxic to both normal and cancer cells. Thus, we demonstrate that both the cation and anion play an extremely important and cooperative role in the anticancer properties of these compounds.

In the second part, the concept of multifunctional nanoparticles is introduced and exploited for theranostic applications. Nanoparticles possessing multiple properties such as luminescence, magnetism, and cancer targeting, were synthesized and explored for use in cancer therapy. In this regard, it is demonstrated that these nanoparticles can not only be used in diagnostics and as drug delivery agents, but also as active pharmacophores.

Finally, the third part of this dissertation is a report of novel ionic liquid based pH sensitive colorimetric nanosensors based on phosphonium and fluorescein. The pH dependent

size changes in the nanodroplets are demonstrated and potential applications in detecting acidic environment and anticancer activity are investigated.

## CHAPTER 1. INTRODUCTION

### 1.1. Characteristics of Cancer

Cancer is a pervasive disease that remains a primary health concern in the world today since its cure has evaded man's innovativeness and technology for generations. For example, in the United States, one in every four deaths is the result of cancer.<sup>1</sup> Cancer is a group of diseases characterized by unrestrained growth and spread of abnormal cells. Cancer is a consequence of multiple abnormalities in the genetic composition of the normal cell.<sup>2</sup> These abnormalities lead to progressive conversion of normal cells to cancer cells, a process known as carcinogenesis. Cancer cells experience excessive stimulation due to mutations in the deoxyribonucleic acid (DNA) sequence which leads to increased expression of oncogenes and/or loss of tumor suppressor genes. This stimulation triggers a state of chaos in the growth of cancer vasculature (highly disorganized with excessive branching) as cancer cells multiply in the body. In contrast, normal cells live in nearly complete harmony with their environment. Typically, normal genes have programmed growth machinery that ensure controlled growth, cell division and programmed cell death, which maintains a balance in cell numbers as required for a healthy body. When genetic modifications occur, one or all of these patterns are broken and oncogenes transform the normal cells to cancer cells.<sup>3,4</sup> For example, when programmed cell death (apoptosis) is suppressed, progressive cell division leads to an abnormal increase in the number of cells and results in a tumor. Thus, by absence of apoptosis, cancer cells become immortalized and continue to multiply over and over, resulting in suffocation of the neighboring cells due to the demand of cancer cells for nutrients and oxygen.

Various types of cancers are defined based on the location or organ in which they develop in the body. One of the greatest challenges in combating cancer is to mitigate its ability to migrate to other parts of the body through a process known as metastasis. For example,

prostate cancer is known to migrate over time to the brain. If metastasis is not terminated, the entire body or organs may be quickly invaded with cancer, making it difficult to treat and often leading to death.<sup>2</sup>

In general, all types of cancers have certain characteristics or features that are similar as a result of physiological changes they undergo during carcinogenesis. In 2000, Hanahan and Weinberg outlined six such characteristics referred to as the “hallmarks of cancer”, and two more were added in 2011 (Figure 1.1).<sup>5,6</sup> These are; 1) self-reliance in growth signals, 2) insensitivity to anti-growth signals, 3) evasion of apoptosis, 4) infinite replicative ability, 5) initiation of angiogenesis, 6) invasion and metastasis, 7) reprogramming of energy metabolism, and 8) evading immune destruction.<sup>6</sup>

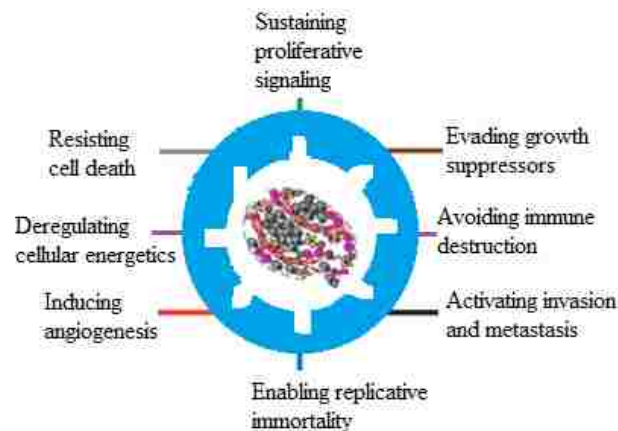


Figure 1.1. The hallmarks of cancer. (Adapted from reference 5 and 6).

The first alteration in cell physiology comprises the production of growth signals by cancer cells to eliminate dependence on stimulus from normal tissue growth microenvironment. To achieve this autonomy, tumor cells apply molecular strategies that alter the extracellular growth signals, cell surface growth receptors, and signal transduction.<sup>5</sup> The second physiological change involves avoidance of anti-proliferative signals by evading cytostatic antigrowth signals. This enables the cancer cells to multiply rapidly without end.<sup>7</sup> Thirdly, cancer cells develop apoptotic resistance via activation of oncogenes and inactivation of the p53 protein. The p53

protein is a product of p53 tumor suppressor gene which regulates apoptosis. As a result of inactivation of p53, cancer cells fail to die and hence become immortal. The fourth physiological change leads to a crisis that makes cancer cells not only immortal, but also allows them to escape the natural deterioration that aging brings. Cancer cells accomplish this by disabling pRb and p53 tumor suppressor proteins, hence avoiding senescence.<sup>8,9</sup> The fifth physiological change encompasses initiation of angiogenesis by cancer cells. This is the stage where cancer cells develop new blood vessels. These new vessels are especially useful in supplying nutrients and oxygen to cancerous tissue. As a result, cancer cells avoid starvation that would otherwise ensue because of the skyrocketing number of cells needing respiration and nutrients.<sup>10</sup> The sixth physiological change of cancer cells consists of their invasion and metastatic ability. This is facilitated by cell adhesion molecules that activate communication between cells and integrins that associate cells to extracellular environment substrates. Metastasis is made possible by transport of tumor cells via the newly formed blood vessels and lymph circulation.<sup>11</sup> The seventh hallmark involves reprogramming of energy metabolism to generate enough energy to fuel the increased cell growth and division. Cancer cells accomplish this by utilizing both aerobic and anaerobic glycolysis as compared to normal cells, which are limited to processing glucose via glycolysis under aerobic conditions.<sup>12</sup> The final hallmark ensures evasion of immune destruction. Proponents of this hallmark propose that human cells and tissue are under a constant surveillance from the immune system which destroys any detected cancer cells promptly. Accordingly, solid tumors that eventually survive are those that have managed to evade recognition by the immune system or limit immunological killing. Collectively, these factors lead to autonomous functioning of cancer cells and hence the loss of contact/communication with normal cells due to created gap junctions.<sup>6</sup>

Research geared toward treatment of cancer seeks to inhibit one or a combination of these hallmarks of cancer. The chemotherapeutic compounds outlined in this dissertation induce apoptosis and stop uncontrolled proliferation of cancer cells *in vitro*.<sup>13-15</sup>

### **1.1.1. Causes of Cancer**

Cancer is caused by internal and external factors. Internal factors are those that are within the individual. External factors are derived from an individual's interaction with the surrounding environment.<sup>2</sup> Internal factors include inherited mutations, immune conditions, hormones, and mutations that occur from metabolism. Internal factors are more difficult to control. However, prior knowledge of family history coupled with early diagnosis may be useful in combating the type of cancer to which these factors may lead.<sup>16,17</sup> External factors include tobacco, infectious organisms, radiation, and chemicals. Cancer caused by external factors may easily be prevented by minimizing exposure to, or avoiding, aforementioned factors.<sup>17</sup> The unfortunate reality is that more than ten years may elapse after exposure to external factors before cancer is detected. It is also important to note that these causal factors may act together or in sequence to initiate cancer.<sup>2</sup>

### **1.1.2. Treatment**

There is currently no cure for cancer. However, four methods are currently being employed to treat cancer: surgery, radiation, immunotherapy, and chemotherapy.<sup>1</sup> All four may be used concurrently or independently depending on the progression of the disease and the benefits to the patient. Surgery involves the removal of cancerous cells. However, re-infection may occur due to the possibility of residual cancer cells after surgery.<sup>18</sup> To increase success rate of surgery, researchers are currently exploring ways of coupling surgery with fluorescence, whereby fluorescent labelled selective compounds are used to light up cancer cells in order to guide the surgeons in removal of affected cells.<sup>19,20</sup> For instance, folate conjugated fluorescent

labels were used recently during surgeries of ten women with ovarian cancer. The surgeons involved reported a significantly increased number of tumor deposits detected by fluorescence as compared to conventionally visualized (Figure 1.2).<sup>21</sup> Fluorescent chemotherapeutic agents, such as the ones reported in this dissertation, may offer the advantage of not only lighting up cancerous cells for effective surgery, but also killing any residual cancer cells after surgery.<sup>13</sup>

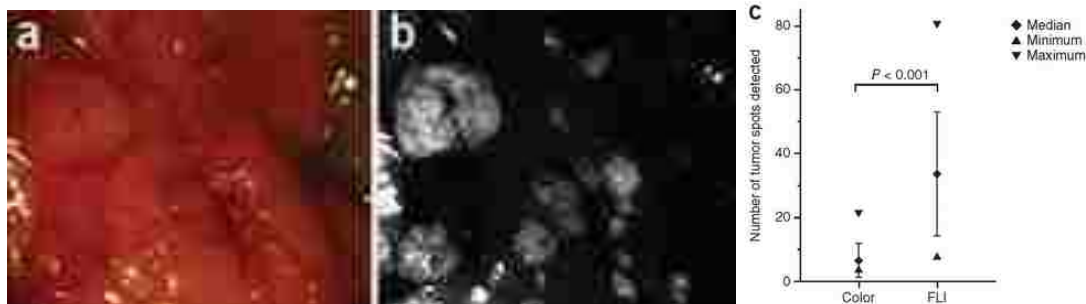


Figure 1.2. Quantification of tumor deposits *ex vivo* a) color image b) corresponding tumor-specific fluorescence image of a representative area in the abdominal cavity, and c) scoring based on three different color images (median 7, range 4–22) and their corresponding fluorescence images (FLI) (median 34, range 8–81);  $P < 0.001$  by five independent surgeons. (Reproduced from reference 20 with permission from Nature Publishing Group).

The second most common method used to treat cancer is known as radiotherapy or radiation oncology. It involves use of high energy x-rays to kill or slow cancer cells from proliferating. Radiotherapy may be used as a palliative or therapeutic treatment.<sup>22</sup> When used for palliative treatment, the goal is for local disease control or symptomatic relief in cases where a cure is not possible. The success of radiotherapy depends on the radiosensitivity of the particular cancer as well as the size of the tumor. Smaller tumors that are more radiosensitive require a lower radiation dose to kill the cells. Unfortunately, most epithelial cells are poorly radiosensitive and therefore the use of radiation therapy must be weighed against the benefits and side effects of using high radiation. In addition, the right dose of radiation is important, since an under dose increases the risk of recurrence while an overdose leads to toxicity. Furthermore, care

must be taken to prevent accidental exposure to normal cells and the personnel operating the equipment to radiation.<sup>22,23</sup>

Thirdly, drugs that stimulate the immune system to reject or kill tumor cells have been exploited. This is referred to as immunotherapy.<sup>16</sup> Although the tumor microenvironment is predominantly immunosuppressive,<sup>24,25</sup> T-cell and antibody responses against antigens associated with tumors can be induced in cancer patients.<sup>26-28</sup> This introduces antitumor immunity that may result in spontaneous tumor regression or control of tumor cell proliferation. Immunotherapy has been demonstrated in patients with melanoma<sup>26</sup> and paraneoplastic neurological disorders.<sup>29</sup>

The fourth most popular method for treatment of cancer is chemotherapy. In this method, chemotherapeutic drugs are used to treat, slow, or halt the proliferation of cancer cells.<sup>30,31</sup> Drug resistance and toxicity of the developed drugs towards normal cells within the proximity of the tumor, are two major challenges of chemotherapy. In addition, systemic toxicity whereby the drug targets other fast multiplying cells such as those lining the bone marrow or those responsible for hair growth is another limitation of chemotherapy. The latter is responsible for hair loss among cancer patients on chemotherapy. In a quest to address off target toxicity, scientists are exploring ways of functionalizing current drugs with targeting agents to ensure they are delivered selectively to cancer cells.<sup>32</sup> Design and development of drugs that are selective to cancer cells rather than rapid cell division is highly sought to minimize systemic toxicity.

Development of nanoparticles for drug delivery and/or as cancer therapeutics is an emerging area to overcome drug resistance, improve selectivity, and reduce toxicity of chemotherapeutics. This is driven by research that indicates that nanoparticles can achieve improved intracellular concentration, while achieving minimal toxicity in normal cells.<sup>32-34</sup> Thus,



exploitation of nanoparticles to deliver anticancer agents is an area that is growing rapidly. Drugs that can be easily modified to evade recognition by proteins responsible for drug resistance in cancer cells would be ideal candidates. A class of compounds known for ease of tunability should therefore be a natural group to turn to. Ionic liquids (ILs) and group of uniform materials based on organic salts (GUMBOS) meet this criteria because they are easy to synthesize and amenable to tunability. Furthermore, since these compounds are composed entirely of ions, they may be synthesized from cationic or anionic compounds with inherent chemotherapeutic properties.<sup>35-37</sup> By varying the counterions, an array of compounds with varying anticancer properties and selectivity towards cancer cells can and has been synthesized.<sup>13</sup>

My dissertation research focusses on synthesis of ILs and GUMBOS, synthesized from cationic compounds known to have anticancer properties for use in cancer therapeutics and other biomedical applications. Nanoparticles (nanoGUMBOS) were derived from the hydrophobic GUMBOS of this series to achieve selectivity towards various cancer cell lines.<sup>13</sup> The cationic compounds selected for this work are highly fluorescent. Consequently, the nanoGUMBOS derived thereof are fluorescent and hence may have potential applications in cancer imaging in addition to their therapeutic value.<sup>13,15</sup>

## **1.2. Ionic Liquids**

Ionic liquids (ILs) are a class of organic salts with melting points below 100 °C.<sup>38</sup> The cation and anion pair may be composed purely of organic ions or a combination of organic and inorganic ions. In most cases, the cation is an organic compound of low symmetry with positively charged nitrogen or phosphorous.<sup>39</sup> Commonly used cations are derived from ammonium, imidazolium, phosphonium, sulfonium, picolinium, thiazolium, pyridinium, and

ammonium, among others. Examples of popular anions are hexafluorophosphate, tetraphenyl borate, and trifluoroborate.

There are two broad categories of ILs: room temperature ILs (RTILs) that melt below 25 °C, and frozen ILs (FILs) which are typically solids at room temperature (25 °C) but melt below 100 °C. It is worth noting that the choice of the upper limit temperature, 100 °C, is arbitrary and serves the purpose of distinguishing IL salts from inorganic salts which have high melting points. Low melting points for ILs are a result of symmetric packing of the cations and anions that constitute ILs. The role played by symmetry in dictating the melting points of ILs is well explained by Seddon *et al.* who demonstrated that replacing inorganic cations such as sodium with unsymmetrical organic cations such as 1-ethyl-3-methylimidazolium significantly lowers the melting point of the resulting ILs.<sup>40</sup>

Ionic liquids were first attributed to a report by Paul Walden in 1914 when he synthesized ethyl ammonium nitrate which has a melting point of 12 °C.<sup>41</sup> However, there are reports indicating that researchers started working with ILs prior to 1914.<sup>38</sup> Two decades later, the first patent on ILs emerged, which was geared towards application of ILs in cellulose dissolution.<sup>42</sup> In 1948, a series of chloroaluminate ILs were used for electroplating.<sup>43</sup> What followed was a series of works in which ILs were investigated for use in the fields of electrochemistry, organic chemistry and catalysis in the mid-1970s and early 1980s.<sup>44-48</sup> Investigations involving the application of ILs in electrochemistry continued into the 1990s with synthesis of more versatile ILs. Perhaps the most significant advancement was the discovery that a variety of different anions or cations could be paired to yield ILs. Consequently, the number of ILs synthesized grew exponentially with significant research being devoted to their physical and chemical properties in the 1980s through 2000s.<sup>49-51</sup> Currently, it is estimated that the theoretical number of possible ILs

that can be achieved via combination of a broad variety of cations and anions is at least a million for binary ILs, and close to  $10^{18}$  for ternary ILs.<sup>52</sup> In the last two decades, ILs chemistry has blossomed, with applications expanding beyond electrochemistry, organic chemistry, and catalysis to other fields such as separation science, engineering, sensing, biological sciences, and drug discovery, among others.<sup>15,53-56</sup> This dissertation will focus on biomedical and sensing applications.

### 1.2.2. Synthesis of Ionic Liquids

One aspect that makes it easy to conduct studies on ILs is the simplicity with which they can be synthesized. There are several approaches employed in synthesis of ILs. A metathesis or ion-exchange reaction is a common method for synthesis of water immiscible ILs.<sup>57</sup> An example is the synthesis of 1-butyl-3-methylimidazolium hexafluorophosphate from 1-butyl-3-methylimidazolium chloride and sodium hexafluorophosphate. The reaction is typically performed in a biphasic medium such as dichloromethane (DCM)/water. The IL is extracted in organic phase while the byproduct is generally soluble in water. Several washes with water affords the IL free from the byproduct.<sup>57</sup> A general scheme of such a reaction is shown in Figure 1.3.

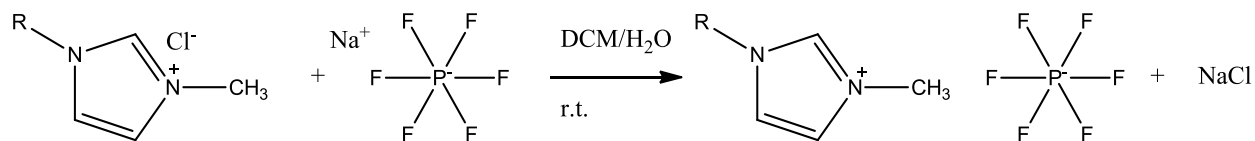


Figure 1.3. Synthesis of 1- alkyl-3-methylimidazolium hexafluorophosphate.

For water miscible ILs, this approach cannot be used since both the product and byproduct are soluble in water. Thus, they may be synthesized by reaction of a silver salt of the desired anion (if available) with the desired cation. In this case, the resulting silver salt byproduct is insoluble in water and can be removed easily. Another route is to conduct the experiment in an organic solvent. The byproduct should be insoluble in the organic solvent e.g. NaCl in DCM. In

such a case, both starting materials are not completely soluble in the organic solvent, and so the reaction is carried out as a suspension for a longer period of time. The suspension is then filtered. A good example is the synthesis of 1-alkyl-3-methylimidazole with metal salt. This reaction can be performed in a DCM and the suspension filtered. However, the resulting halide may be slightly soluble in the IL/ DCM mixture and hence several washes of the organic layer with water would be necessary to completely eliminate the byproduct. Another method that has been employed is the acid-base reaction. Indeed, this was the method used when ethyl ammonium nitrate, the first reported ionic liquid, was synthesized (Figure 1.4).<sup>41</sup> This reaction is performed by reacting ethylamine with nitric acid in an aqueous environment at 4 °C. Upon completion of the reaction, water is removed by lyophilization.

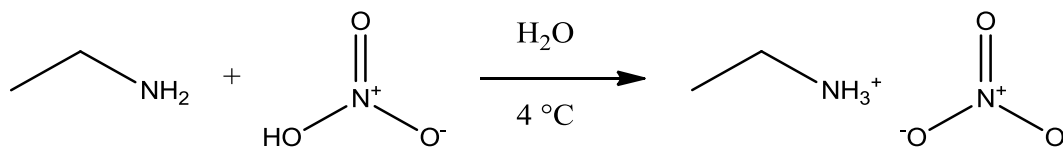


Figure 1.4. Synthesis of ethyl ammonium nitrate.

Direct combination of a halide salt and a metal halide is another method that has been used recently, particularly in the synthesis of magnetic ionic liquids such as [bmim][FeCl<sub>4</sub>]. In such a method, there are no byproducts formed. An equimolar amount of [bmim][Cl] and FeCl<sub>3</sub> are mixed in a dry box with N<sub>2</sub> to yield [bmim][FeCl<sub>4</sub>] (Figure 1.5) which is a brown liquid. Alternatively, FeCl<sub>3</sub>·6H<sub>2</sub>O may be used in place of FeCl<sub>3</sub>. This leads to formation of two layers, water and the IL.<sup>58</sup>

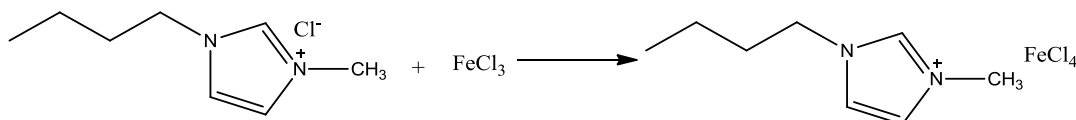


Figure 1.5. Synthesis of 1-butyl-3-methylimidazolium tetrachloroferrate

### 1.2.3. Physical and Chemical Properties of ILs

Physical and chemical properties of ILs can be tuned by changing the structure of the cation or anion. Alternatively, this may be achieved by varying the counterions without any modification of the chemical structure of the IL. Interest in ILs is driven by the uniqueness of this class of compounds, notably low vapor pressure, non-volatility, recyclability, wide liquidus range and ionic conductivity. Wide liquidus range is a result of ILs high thermal stability and non-volatility. Liquidus range is the temperature between the freezing point and boiling point of a liquid. Consequently, by having a wide liquidus range ILs are non-volatile organic solvents and therefore referred to as green solvents.<sup>38</sup> Their non-volatility means that they may not lead to environmental pollution. This was, however, confused to imply that ILs are intrinsically nontoxic, which is far from the truth.<sup>52</sup> Indeed, toxicity data on ILs is now increasingly available.<sup>59</sup> Low vapor pressure of ILs is due to strong interactions between the ions. Good conductivity of ILs arises from the fact that they are composed entirely of ions which have fairly high mobility in liquid state or in aqueous media.<sup>60</sup>

Traditional ILs are polar in nature and therefore are miscible with polar solvents such as ethanol, acetone and methylene chloride but immiscible with non-polar ones. Polarity and water solubility of ILs is largely dictated by the type of cation and anion pair.<sup>61</sup> In general, if cations are paired with anions from halides and metal containing complexes, they tend to be highly soluble in water. On the contrary, bis(trifluoromethanesulfonylimide), tetraphenylborate, and tetrafluorophosphate anions lead to poor water solubility of resulting ILs.<sup>61</sup> Similarly, different substituents attached to the cation or anion impact polarity and water solubility of ILs.<sup>62</sup>

The melting points of ILs are also dependent on the structure as well as substituents on the respective ions. Van der Waals forces are increased with longer alkyl chain substituents. On

the other hand, this leads to reduced lattice energy and hence a decrease in melting points. Likewise, larger anions containing delocalized charges tend to result in lower melting ILs.<sup>63</sup> Another reason that contributes to ILs displaying lower melting points in comparison to inorganic salts is the size and asymmetry of the component ions which result in poor crystal packing (Figure 1.6).<sup>64</sup>

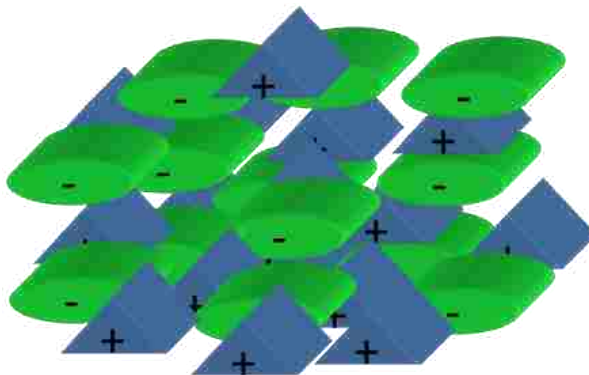


Figure 1.6. Illustration of frustrated packing in ILs due to asymmetry of component ions.

### 1.3. From Ionic Liquids to Group of Uniform Materials Based on Organic Salts

Perhaps the greatest driving force for research involving ILs is the fact that ILs are tunable via simple variations in the anion/cation or by modification of the cationic or anionic moiety of the IL. Almost every chemical and/or physical property of ILs can be modified by simply changing the anion or cation. For instance, variable solubilities, melting points and other physicochemical properties discussed earlier are largely accomplished via introduction of an alkyl chain length on the cation. Subsequent increase in the size of this alkyl chain leads to variations in hydrophobicity.<sup>65</sup>

In 2007, The Warner research group reported a new class of organic salts with similar properties as ILs, and defined them as Group of Uniform Materials Based on Organic Salts (GUMBOS). These materials are solids at room temperature with melting points between 25 °C and 250 °C. Thus, by definition, there is an overlap between ILs and GUMBOS, particularly

FILs. However, while most ILs require modification for task specificity (hence the advent of task specific ILs), most GUMBOS are inherently task specific as they are drawn from non-traditional cations and anions selected based on the desired application or property of the cation/anion. For example, cationic dyes known to have biological applications such as rhodamine, ethidium, and fluorescein have been employed in the synthesis of GUMBOS. It is worth noting that GUMBOS have similar physical and chemical properties as ILs. Like ILs they are amenable to tunability and are synthesized using similar methods. Recently, anion variations on GUMBOS was demonstrated to lead to variations in physicochemical properties as well as anticancer properties.<sup>13</sup> In addition, magnetic<sup>66</sup> GUMBOS have been synthesized via use of magnetic counterion while GUMBOS with antibacterial properties have been made from well-known antibiotics starting materials.<sup>67</sup> In the same breath, multifunctional ILs/GUMBOS can be synthesized by carefully selecting cations and anions with desired properties. For instance, the anion may possess magnetism while the cation possesses anticancer and fluorescent properties.<sup>14</sup>

Probably the greatest contribution of GUMBOS is the meaning it has brought to FILs. In the past, considerable efforts have been made to lower the melting points of FILs because the most important application was use as green solvents. Concerted efforts to replace volatile organic solvents drove the notion that solid ILs were useless and needed modifications to depress the melting points to room temperature range. The development of GUMBOS and applications in many varied fields has revolutionized ionic liquid chemistry. Currently, ILs and GUMBOS are being investigated in the Warner research group for biomedical applications,<sup>13,67</sup> sensing applications,<sup>15,68</sup> and solar cells,<sup>69</sup> among others. This dissertation is devoted to discussing biomedical and sensing applications.

### **1.3.1. Nanoparticles Derived from ILs and GUMBOS**

Nanotechnology is becoming a part of every aspect of life. Nanoparticles are defined as particles with sizes below 100 nm and often display unique intrinsic properties such as changes in morphology, electronic and atomic structure, typically leading to increased surface reactivity compared to bulk samples.<sup>70</sup> NanoGUMBOS are nanomaterials synthesized from GUMBOS. Nanoparticles have found applications in many industries, including the manufacture of electronics, automobiles, paints, coatings, appliances, cosmetics and fabrics. Most recently, nanoparticles are on the cutting edge of biomedical research, and are being explored as therapeutics, drug delivery agents, cellular imaging, and biological sensors among other applications.<sup>71-76</sup> This is driven by the many abilities nanomaterials possess in comparison to the bulk form of the compounds used to synthesize them. Use of ILs as solvents or templates in the synthesis of nanomaterials has gained popularity in the recent past. This is due to ILs ability to solubilize most compounds as well as their low vapor pressure that enables reactions at elevated temperatures in comparison to traditional organic solvents. In addition, ILs are capable of undergoing hydrogen bonding, which allows for ‘self-organization’ and ‘molecular recognition’.<sup>77</sup> More recently, nanoparticles derived from FILs and GUMBOS have been synthesized. This allows the advantages of ILs and GUMBOS to be translated and possibly enhanced at nanoscale.<sup>78-80</sup> The applications outlined herein exploits the advantages associated with tunability of ILs and GUMBOS, as well as valuable properties associated with nanoparticles.<sup>13,15</sup>

### **1.3.2. Synthesis of NanoGUMBOS by Reprecipitation Method**

Generally, there are many methods for synthesis of nanoGUMBOS and other nanoparticles. These include aerosol preparation, sol-gel process, micro emulsion templates and



reprecipitation methods, and many others are being explored and developed. In this dissertation however, nanoGUMBOS were prepared by additive free reprecipitation method by dispersing hydrophobic GUMBOS solution in water under sonication.<sup>76</sup> Reprecipitation method is preferred for biological applications because resulting nanoparticles are free from impurities associated with template assisted methods. Drawbacks of reprecipitation method are the requirement that the starting materials be hydrophobic and the lack of size control of the resulting nanoparticles.

For the reprecipitation method used in this study, the target compound was dissolved in a suitable organic solvent to make 1 mM solution. A small volume of this solution was then injected rapidly into a poor solvent such as water (or cell media) under sonication at room temperature. Finally, the resulting nanoparticles dispersion was left to age in the dark for 1 h before characterization or further use. An example of this method is depicted in Figure 1.7.

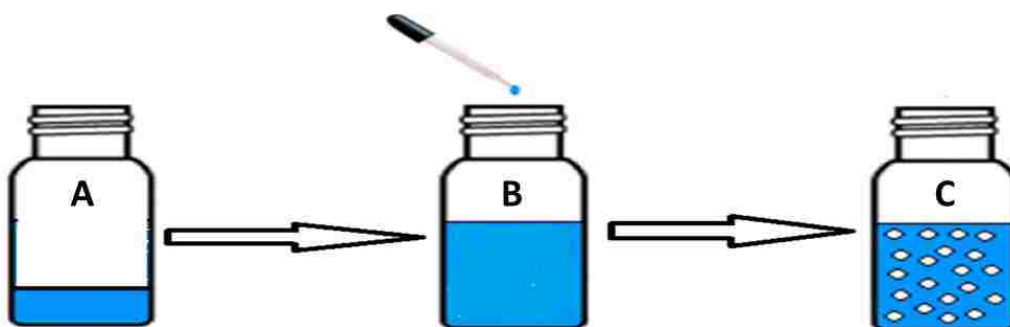


Figure 1.7. Reprecipitation process of nanoGUMBOS fabrication showing (A) 1 mM stock solution of GUMBOS solution in ethanol, (B) injection of 100  $\mu\text{L}$  of the GUMBOS solution into 5 mL of deionized water while sonicating the mixture at room temperature, and (C) reprecipitation of GUMBOS to afford nanoGUMBOS dispersed in water.

Hydrocarbon solvents like hexane, heptane, and iso-octane may be used in place of water for nanoparticle synthesis of hydrophilic compounds. However, the target compound should be soluble in corresponding hydrocarbon miscible solvents such as acetone. Factors such as concentration of the injected solution, temperature of the poor solvent, and aging time may affect the size, shape and spectral properties of nanoparticles fabricated via this method.<sup>81-83</sup>

### 1.3.3. Active Pharmaceutical Ingredients Based on Ionic liquids and GUMBOS

The search for more versatile ILs has led to the development and application of three generations of ILs. The ions that make up each of these generations of ILs have also been employed in the synthesis of GUMBOS. Thus, it is reasonable to refer to the generations as being of ILs and GUMBOS. Figure 1.8 depicts a number of the ions involved in each of the generations.

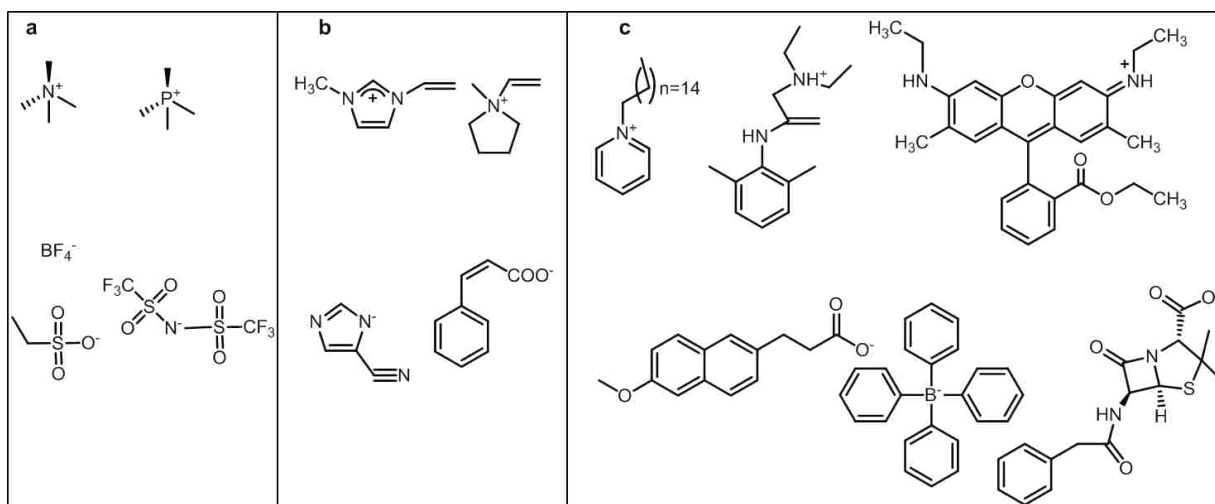


Figure 1.8. Examples of ions employed in synthesis of a) first generation b) second generation and c) third generation ILs and GUMBOS

The first generation was geared towards understanding the intrinsic physical and chemical properties of ILs. Some of the properties that were investigated in detail included viscosity, density, solubility, chemical stability, conductivity, and thermal stability. The second generation of ILs focused on the tuning of the physical and chemical properties to yield ‘task-specific’ ILs as well as environmentally friendly (green) solvents. The third and most current generation of ILs encompasses active pharmaceutical ingredients (API). The goal of the third generation ILs is to generate ILs with biological activity geared towards overcoming present hurdles associated with APIs.<sup>84,85</sup> Therefore, the cations and anions were judiciously chosen to possess properties useful for biological applications. For instance, while the first generations ILs

were mostly non-luminescent, this property was introduced in the third generation ILs by selecting cations from fluorescent compounds. It is estimated that half of all drugs are administered as salts. Thus, salt formation of drug targets is an important pre-design step. This is because salts in APIs are expected to improve solubility in water, safety, industrial processing as well as biological properties. Most importantly, these properties can be enhanced by variation of the counterion of the active component.<sup>13,85</sup>

A more current concept where therapeutic ILs and GUMBOS are being developed, as opposed to being simply ingredients, has the potential to revolutionize the pharmaceutical industry. Indeed, reports have emerged exploring this concept on ILs and GUMBOS.<sup>13,67,86</sup> Theoretically, it is possible to form a combination of two or more drugs with opposite ions as long as the resulting cation and anion pair is stable. Newly formed IL/GUMBOS therapeutic consist of an API, which may be either a cation or an anion, and a counterion selected from a non-toxic, pharmaceutically acceptable compound. The ILs/GUMBOS introduce unique properties not found in ordinary crystalline salt forms. These properties may include improved solubilization as well as uptake in diseased tissue. Most importantly, these properties may be tuned to arrive at an ideal drug whose efficacy and uptake is highly improved. For example, an active compound with tendencies to undergo polymorphism may be paired with a counterion with known tendencies to produce low melting ILs/GUMBOS to overcome polymorphism. Similarly, an active compound with negative side effects may be paired with a counterion that neutralizes the side effects. Another interesting example involves pairing two active ions for dual treatment with synergistic rather than additive results. In this regard, anesthetic lidocaine was converted to lidocainium docusate ionic liquid. The latter was found to have enhanced and prolonged effect on rats as compared to traditionally used solid hydrochloride salt.<sup>87</sup> While most

of these examples are of RTILs,<sup>88</sup> FILs and GUMBOS are increasingly emerging to address problems associated with drugs that may not be converted to liquids. In this regard, GUMBOS have widened the tunable range in comparison to ILs. In one report, the Warner research group has demonstrated the usefulness of GUMBOS in antibacterial therapy,<sup>67</sup> while several reports from the same group document applications of GUMBOS and nanoGUMBOS towards cancer therapy and bioimaging.<sup>13,14,78</sup>

#### **1.3.4. Ionic Liquids and GUMBOS with Anticancer Properties**

Limited reports exist on use of ILs as anticancer agents.<sup>89,90</sup> Recently, three classes of ILs (imidazolium, phosphonium and ammonium) were investigated for anticancer activity and cytotoxicity towards 60 human cell lines by the National Cancer Institute's (NCI). Preliminary structure-activity relationship (SARS) from this data suggested that the length of the alkyl chain on the cation plays a significant role in the antitumor activity and cytotoxicity of ILs. Phosphonium-based ILs were found to be more active and less cytotoxic in comparison to the ammonium and imidazolium-based ILs.<sup>91</sup> Substitutions on the N-3 position in the imidazole ring of the imidazolium ILs played a critical role in antitumor activity and cytotoxicity. It was observed that ILs with C-12 chain length were effective against all 60 tumor cell lines and displayed low cytotoxicities. In general, further increase in alkyl chain length was accompanied with improved antitumor inhibition as well as high cytotoxicity.<sup>92</sup> Frozen ILs and GUMBOS have recently started gaining popularity as anticancer agents, and is the subject of this dissertation.<sup>13,14</sup>

## 1.4. Analytical Methods Used

### 1.4.1. Ultraviolet- Visible Spectroscopy

Ultraviolet-Visible Spectroscopy is a characterization technique for analyses of molecules that absorb light in the ultraviolet and visible region of the electromagnetic spectrum. Absorbance-based techniques are widely used in clinical experiments to evaluate the viability of microorganisms because the devices are simple to use and rapid. A UV-vis spectrophotometer (Figure 1.9) measures the amount of energy that molecules absorb when exposed to light.

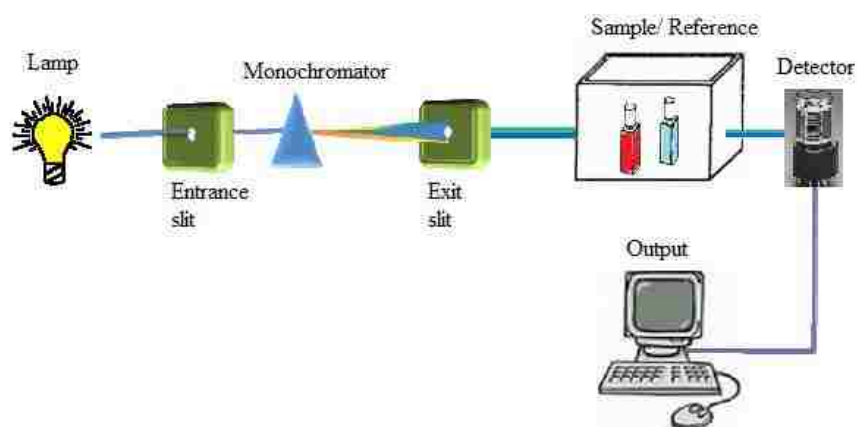


Figure 1.9. Schematic diagram of a UV-vis spectrophotometer

The light source (lamp) generates energy which is passed through a monochromator that selects the desired wavelengths. A beam splitter divides the light into two beams of light through the sample and reference cells respectively. Light absorbed or transmitted by the sample is recorded by a detector (photomultiplier tube or diode array). The absorbance or transmittance may then be plotted against the wavelength to produce a spectrum. The amount of light absorbed, termed as absorbance ( $A$ ) is related to the molar absorptivity ( $\epsilon$ ) and concentration of the analyte as well as the path length ( $b$ ) of the cuvette by the Beer- Lambert's law, symbolized as  $A = \epsilon b C$ . From this equation, a calibration curve with known concentrations of analytes may be used to determine an unknown concentration of a sample.<sup>93</sup>

A 96- well microplate reader was used to perform absorbance measurements for the biological assays in this dissertation. In general, UV-vis spectrophotometers and microplate readers differ mainly in their beam geometry. In conventional spectrophotometers, samples are read through a cuvette with a horizontal (cross-sectional) light path. In microplate readers, the light beam is vertical which results in a pathlength that depends on the volume of fluid in each well.<sup>94</sup> A microplate reader is capable of reading several samples at the same time compared to one sample at a time for conventional spectrophotometer. Sample holders for microplate readers are made of optically transparent multiple well plates, the most common being a 96- well plate.<sup>94</sup>

#### **1.4.2. Mammalian Cell Cytotoxicity**

*In vitro* cytotoxicity assays are important to assess cellular damage that may arise from exposure of cells to different chemical agents. Cell viability assay is an important tool in drug discovery because it offers a rapid method to screen potential drugs. The most common of these assays is based on the absorbance of tetrazolium-converted formazan dyes. This method is dependent on the sensitivity of an absorbance microplate plate reader, cell types, metabolic markers, incubation time, and the number of cells. The principle behind tetrazolium-based assays is founded upon the cellular metabolic activity of live cells. Cellular enzymes in viable cells reduce tetrazolium dye into formazan while dead cells do not lead to this conversion. As a result, the absorbance of the formazan is proportional to the amount of viable cells. Typically, cells are treated with test compounds for 24-72 hours prior to this type of assay. At least 24 h treatment of the cells is required before cell viability assay is performed to eliminate absorbance that may result from dying cells and limit the result to cells that survive the treatment.

The first tetrazolium based assay for measuring cell viability was developed by Mosmann in 1983. In this assay, viable cells reduce the yellow aqueous MTT (3-(4,5-dimethylthiazol-2-yl)-

2,5-diphenyltetrazolium bromide) solution into a purple formazan solid (Figure 1.10).<sup>95</sup> Thus, an organic solvent must be added to dissolve formazan solid to make absorbance measurements possible.

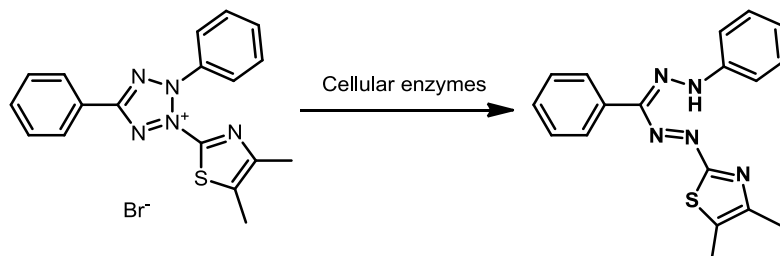


Figure 1.10. Conversion of MTT to insoluble formazan by cellular enzymes in viable cells.

Commonly used organic solvents are isopropanol, dimethylsulfoxide, and sodium dodecyl sulfate/dimethylformamide solutions. This two-step assay produces a homogeneous purple solution with absorbance maxima at 570nm that is directly proportional to the number of viable cells.<sup>96</sup> In a quest to avoid use of toxic organic solvents, a second tetrazolium, MTS (3-(4,5-dimethylthiazol-2-yl)-5-(3-carboxymethoxyphenyl)-2-(4-sulfophenyl)-2H-tetrazolium, inner salt) was developed (Figure 1.11).<sup>97</sup>

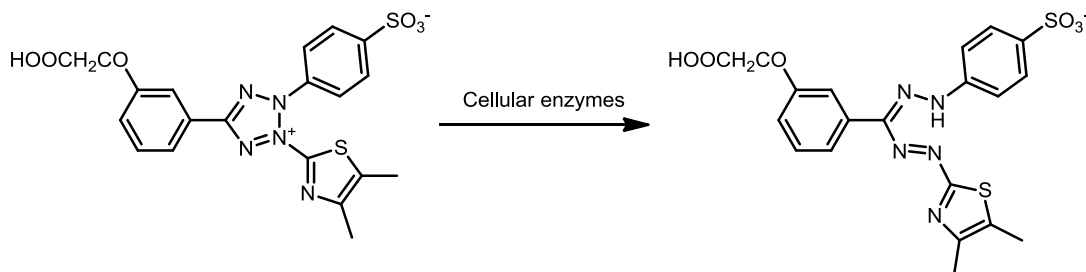


Figure 1.11. Conversion of MTS to soluble formazan by cellular enzymes in viable cells.

This differs from MTT assay in that the product is water-soluble, and hence a co-solvent is not necessary. In addition, it absorbs at 490 nm and has similar benefits as MTT.<sup>98</sup> Thus, in choosing the best tetrazolium based assay method, one must be aware of the region at which test compounds absorb. In addition, other factors such as assay length and amount of MTT/MTS to use per well must be optimized for each cell line to capitalize on the benefits of these assays. In

this dissertation, MTT assay was preferred for rhodamine based GUMBOS while MTS assay was used for phosphonium based GUMBOS.

### 1.4.3. Fluorescence Spectroscopy

Fluorescence is a radiative transition of excited molecules from the first excited singlet state to ground state. The principle of fluorescence is demonstrated by use of the Jablonski diagram (Figure 1.12).

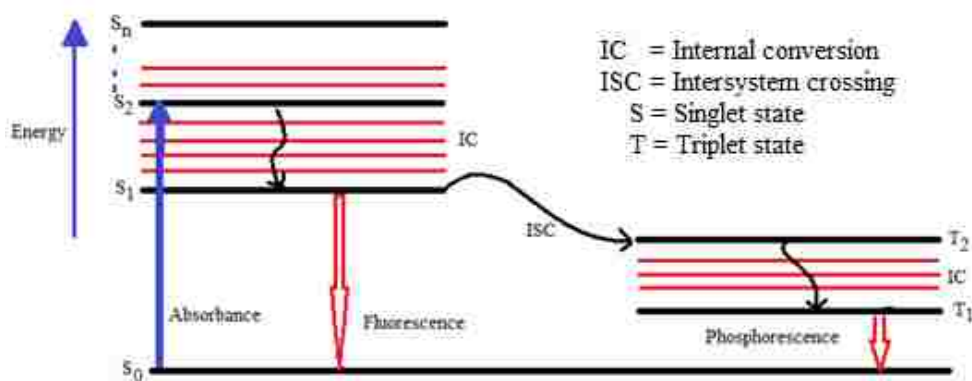


Figure 1.12. Perrin- Jablonski diagram

Briefly, molecules are irradiated and upon absorbing light they are promoted to the first excited singlet electronic state or higher. For fluorophores that are excited to higher electronic states ( $>S_1$ ), they undergo non-radiative decay via internal conversion (IC) to  $S_1$  prior to fluorescence. A photon that undergoes IC emits less energy than it absorbed leading to a shift in the emission spectrum to a longer wavelength (lower energy) relative to excitation wavelength. This change is referred to as Stokes shift. Stokes shift may result from factors such as solvent effects, energy transfer, and the formation of complexes.<sup>94</sup> Excited molecules may also undergo a less probable radiative decay process known as phosphorescence. Phosphorescence occurs when an excited photon undergoes intersystem crossing (ISC) to the excited triplet state followed by radiative transition to the ground state. Phosphorescence is a slower process with an excited state lifetime between  $10^{-6}$  and 1 s, compared to fluorescence which is between  $1 \times 10^{-7}$  to  $1 \times 10^{-9}$



seconds.<sup>94</sup> A fluorometer comprises of a light source, excitation and emission monochromators, and a sample chamber and detector, which may be a photomultiplier tube, photodiode or a CCD (Figure 1.13).

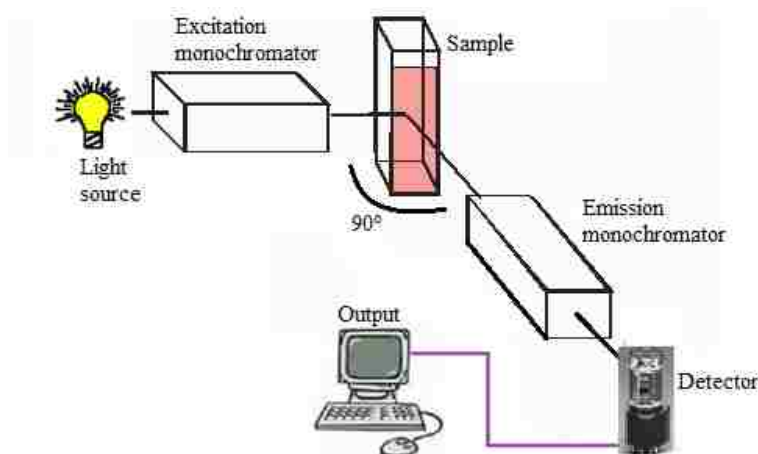


Figure 1.13. Schematic representation of a fluorometer

The excitation monochromator allows light of selected wavelength, usually between 200 to 900 nm, to illuminate the sample. Emitted light is collected at a right angle to the incident light and passes through the emission monochromator which eliminates scattered rays prior to reaching the detector. Common light sources used in fluorescence spectroscopy include lasers, photodiodes, and lamps. Optically-transparent cuvettes (e.g. quartz, glass, polystyrene) are used in a conventional fluorometer to maximize on the transmission and collection of excited and emitted light.

#### 1.4.4. Fluorescence Microscopy

Fluorescence microscopy is a popular technique in biomedical studies.<sup>99</sup> In this dissertation, fluorescence microscopy was utilized in visualizing GUMBOS and nanoGUMBOS in mammalian cells. The principle is the same as for the conventional fluorometer discussed earlier with the only fundamental difference being the ability to visualize samples at the

microscopic level. Hence, cellular compartments can be visualized with the help of fluorescent probes or cellular markers.<sup>100</sup>

A fluorescence microscope consists of a xenon- arc or mercury vapor lamp, dichroic mirror, excitation, and emission filter (Figure 1.14). The dichroic mirror reflects the excitation light and transmits the emitted light. The excitation filter is used to select light of specific wavelengths and to ensure that the light incident on a sample is monochromatic. The emission filter allows light of longer wavelength to pass through to the detector. It is worth noting that all the filters are interference filters with very specific wavelength selectivity.<sup>100</sup>

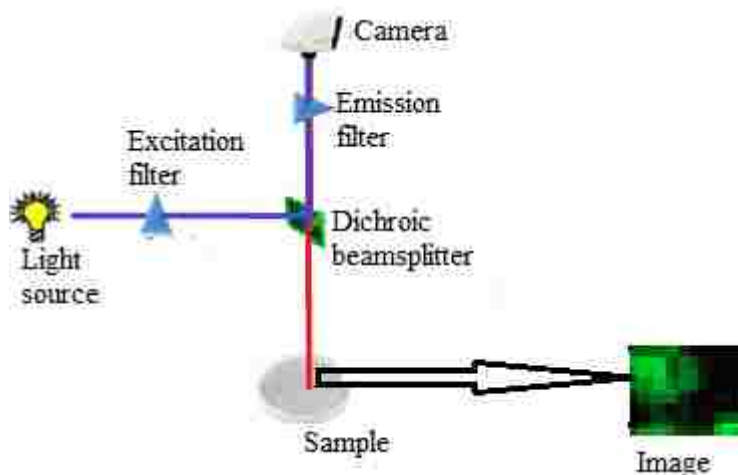


Figure 1.14. Schematic representation of a conventional fluorescence microscope

#### 1.4.5. Confocal Laser Scanning Microscopy

Confocal laser scanning microscopy (CLSM) is a powerful technique for acquiring high resolution fluorescence images, otherwise challenging for the regular fluorescence microscope. It achieves this through optical sectioning of the sample.<sup>101</sup> A CLSM consists of a laser source, dichroic mirror, pin-hole, photomultiplier tube (PMT), and a computer (Figure 1.15). Optical sections of a sample are produced via point by point scanning of the specimen with a laser beam. A pin-hole or a slit eliminates out-of-focus fluorescence from below and above the focal plane under investigation.<sup>102</sup> The dichroic mirror separates the emitted light from the excitation light

and passes the emitted light to a pin-hole. The PMT detects the emitted light emerging from the pin-hole, and the computer processes this signal to produce an image.<sup>102</sup>

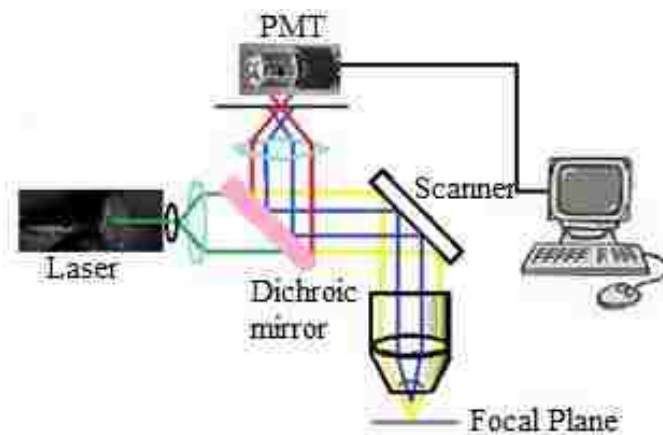


Figure 1.15. Schematic depiction of a confocal laser scanning microscope

Optical paths in a CLSM are designed in such a way that the laser beam focused on a sample is confocal with the point of light focused at the pinhole in front of the photodetector.<sup>101,103</sup> Therefore, unlike a conventional fluorescence microscope, CLSM ensures that the only information that reaches the detector emanates from the focal plane of interest. This technique has made it possible to image thick specimens with high resolution.<sup>104</sup> For example, with a lens of 1.4 numerical aperture, structures with discrete levels in an intact biological sample can be imaged to a theoretical lateral resolution of 0.14  $\mu\text{m}$  and a vertical resolution of 0.23  $\mu\text{m}$ .<sup>101,104</sup> A series of images from several focal planes can be merged together to reconstruct a 3-D image, making CLSM a powerful tool for biologists.<sup>102</sup> In addition to imaging thick specimens, CLSM has been successfully employed in imaging mammalian cells and particularly in visualizing fluorescently labeled subcellular compartments.<sup>103</sup>

#### 1.4.6. Transmission Electron Microscopy

Transmission electron microscopy (TEM) is a powerful tool for analysis of nanoparticle size and morphology. The specimen should however be transparent to electrons. A series of

magnetic lenses are used to focus a beam of electrons which in turn bombard a sample mounted on a carbon coated copper grid.<sup>105</sup> Some of the electrons are transmitted through the sample onto a detector (fluorescent screen) on the opposite side of the electron beam, while most of the electron impinges on the sample. The transmitted electrons generate electronic signals that are utilized to create a TEM image. The transmission electron microscope consists of a vacuum chamber, the electron gun, condensers and electromagnetic lenses (Figure 1.16).

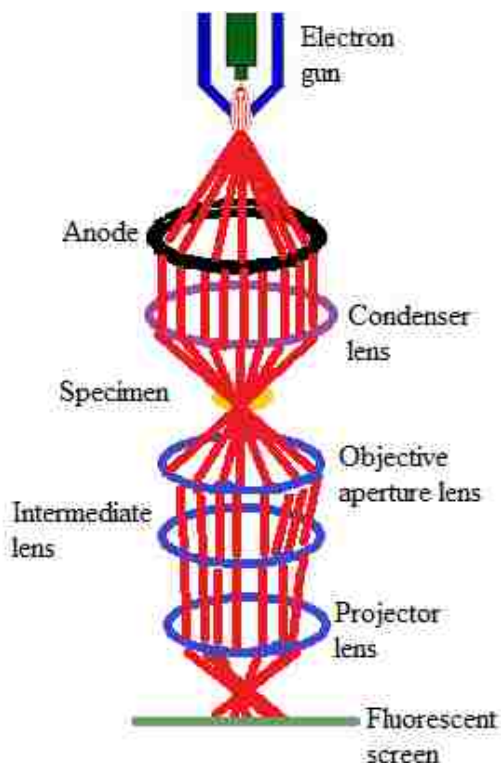


Figure 1.16. Schematic representation of a transmission electron microscope

The vacuum is necessary to protect electrons from being absorbed by air.<sup>105</sup> The electron gun is the source of electrons and consists of a heated tungsten filament (cathode), a cylinder and an anode maintained at a high positive potential relative to the cathode in order to accelerate electrons away from the filament. The condenser focuses the electron beam emerging from the anode into a narrow intense beam of electrons. An objective lens, intermediate lens and a

projector lens successively increases magnification of the image. The image may be formed on a fluorescent screen or on a photographic plate.<sup>105</sup>

#### **1.4.7. Zeta Potential Analysis**

Measurement of zeta potential is used to determine the surface charge of particles in solution.<sup>106</sup> Zeta potential measurements of nanoparticles in this dissertation was performed using a Malvern Zetasizer Nano ZS instrument equipped with a HeNe laser operating at 632.8 nm and a scattering detector at 173 degrees. Nanoparticles have a surface charge that attracts a thin layer of ions of opposite charge on its surface. Therefore, as the nanoparticle travels via diffusion through the solution, the double layer of ions travel with it, creating an electric potential at the surface of the double layer.<sup>107</sup> This potential is referred to as zeta potential and is used to predict the relative stability of nanoparticles in solution. Generally, nanoparticles with a zeta potential greater than +25 mV or smaller than -25 mV are said to have a higher degree of stability.<sup>108</sup> Those with zeta potentials between these two values are expected to aggregate or fall out of solution with time as a result of Van der Waals inter-particle attractions. However, these generalizations are only true for samples that are highly monodispersed, have a high concentration enough to scatter 633 nm light, and are suspended in water of high purity free from any particulates. Unfortunately, this rigorous criterion is rarely met with most samples. For instance, a highly conductive sample may lead to polarization and degradation of the electrode, while very dilute samples will not provide enough light scattering events for accurate zeta potential measurements.<sup>108</sup>

#### **1.4.8. Superconducting Quantum Interference Device**

A superconducting quantum interference device (SQUID) was used to determine the magnetic properties of the multifunctional materials reported in this dissertation. A

superconducting quantum interference device is a magnetometer that consists of a semiconductor loop interrupted with one or more Josephson junctions. It has patterned multilayer structures with superconducting and insulating thin films.<sup>109,110</sup> An interference signal resulting from tunneling of electron pairs is quantified when an electric current is passed across the Josephson junction (Figure 1.17). The variation in electrical current is directly proportional to the magnetic susceptibility of the sample.<sup>110</sup>

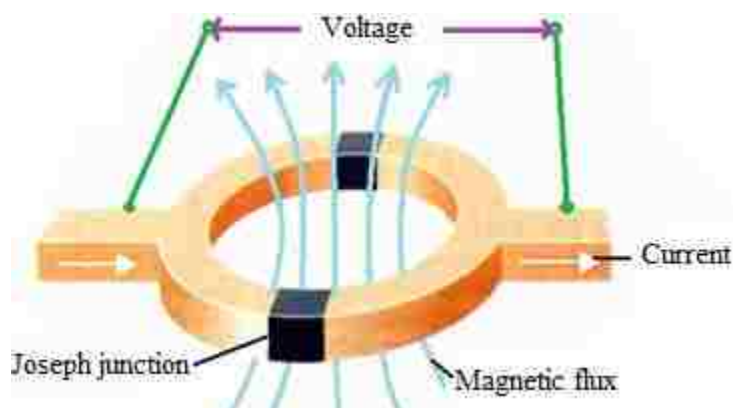


Figure 1.17. Schematic representation of a SQUID

### 1.5. Scope of the Dissertation

This dissertation is composed of two parts. In the first part, ILs, GUMBOS and nanoGUMBOS are explored as possible chemotherapeutic agents. The second part outlines the use of ILs based nanomaterials as a colorimetric pH sensor and use of the pH responsive nanodroplets as anticancer agents.

In the second chapter, the synthesis and characterization of rhodamine 6G based GUMBOS and nanoGUMBOS is discussed. The effect of counterion variations on rhodamine 6G is explored, and interesting findings are reported. A close attention is paid on the influence of variations of hydrophobicity on selectivity of these GUMBOS towards breast cancer cell lines.<sup>13</sup> In the third chapter, the synthesis and characterization of multifunctional organic nanoparticles derived from phosphonium-dysprosium salts is presented. The effect of the synthesized

nanoparticles on five mammalian cancer cell lines and one normal cell line is presented and compared with previously published literature involving the bulk materials. Interesting results in which the nanoparticles formulations were found to be more effective than their bulk counterparts is revealed and discussed.<sup>14</sup> In the fourth chapter, another group of multifunctional nanomaterials based on iron (III) phthalocyanine cation and deoxycholate anion is presented. These materials were designed to possess magnetic properties from iron (III) and near infra-red fluorescence useful for low energy tissue imaging from the phthalocyanine moiety. Responsiveness of the nanomaterials to pH is reported. Chapter five outlines the synthesis, characterization, and application of ionic liquid nanomaterials based on tetraphenyl phosphonium and fluorescein. The application of these nanomaterials as pH nanosensors is discussed.<sup>15</sup> In addition, the wide applicability of these ILs nanomaterials is demonstrated via evaluation of their anticancer properties.

## 1.6. References

1. Siegel, R.; Naishadham, D.; Jemal, A., Cancer statistics, 2013. *CA: A Cancer Journal for Clinicians* **2013**, *63*, 11-30.
2. *Cancer facts and figures 2013*, American Cancer Society 2013.
3. Albin, A.; Benelli, R.; Noonan, D. M.; Brigati, C., The "chemoinvasion assay": A tool to study tumor and endothelial cell invasion of basement membranes. *International Journal of Developmental Biology* **2004**, *48*, 563-571.
4. Coradini, D.; Daidone, M. G., Biomolecular prognostic factors in breast cancer. *Current Opinion in Obstetrics and Gynecology* **2004**, *16*, 49-55.
5. Hanahan, D.; Weinberg, R. A., The hallmarks of cancer. *Cell* **2000**, *100*, 57-70.
6. Hanahan, D.; Weinberg, R. A., Hallmarks of cancer: The next generation. *Cell* **2011**, *144*, 646-674.
7. Weinberg, R. A., The retinoblastoma protein and cell-cycle control. *Cell* **1995**, *81*, 323-330.
8. Wright, W. E.; Pereirasmith, O. M.; Shay, J. W., Reversible cellular senescence - implications for immortalization of normal human-diploid fibroblasts. *Molecular and Cellular Biology* **1989**, *9*, 3088-3092.

9. Bodnar, A. G.; Ouellette, M.; Frolkis, M.; Holt, S. E.; Chiu, C. P.; Morin, G. B.; Harley, C. B.; Shay, J. W.; Lichtsteiner, S.; Wright, W. E., Extension of life-span by introduction of telomerase into normal human cells. *Science* **1998**, *279*, 349-352.
10. Hanahan, D.; Folkman, J., Patterns and emerging mechanisms of the angiogenic switch during tumorigenesis. *Cell* **1996**, *86*, 353-364.
11. Aplin, A. E.; Howe, A.; Alahari, S. K.; Juliani, R. L., Signal transduction and signal modulation by cell adhesion receptors: The role of integrins, cadherins, immunoglobulin-cell adhesion molecules, and selectins. *Pharmacological Reviews* **1998**, *50*, 197-263.
12. Warburg, O., Note on the metabolism of tumours. *Biochemische Zeitschrift* **1930**, *228*, 257-258.
13. Magut, P. K. S.; Das, S.; Fernand, V. E.; Losso, J.; McDonough, K.; Naylor, B. M.; Aggarwal, S.; Warner, I. M., Tunable cytotoxicity of rhodamine 6g via anion variations. *Journal of the American Chemical Society* **2013**, *135*, 15873-15879.
14. Li, M.; Ganea, G. M.; Lu, C.; De Rooy, S. L.; El-Zahab, B.; Fernand, V. E.; Jin, R.; Aggarwal, S.; Warner, I. M., Lipophilic phosphonium-lanthanide compounds with magnetic, luminescent, and tumor targeting properties. *Journal of Inorganic Biochemistry* **2012**, *107*, 40-46.
15. Das, S.; Magut, P. K. S.; de Rooy, S. L.; Hasan, F.; Warner, I. M., Ionic liquid-based fluorescein colorimetric ph nanosensors. *RSC Advances* **2013**, *3*, 21054-21061.
16. Liu, Y.; Zeng, G., Cancer and innate immune system interactions: Translational potentials for cancer immunotherapy. *Journal of Immunotherapy* **2012**, *35*, 299-308.
17. Miller, A. B., Perspectives on cancer prevention. *Risk Analysis* **1995**, *15*, 655-660.
18. Winter, W. E., III; Maxwell, G. L.; Tian, C.; Sundborg, M. J.; Rose, G. S.; Rose, P. G.; Rubin, S. C.; Muggia, F.; McGuire, W. P., Tumor residual after surgical cytoreduction in prediction of clinical outcome in stage IV epithelial ovarian cancer: A gynecologic oncology group study. *Journal of Clinical Oncology* **2008**, *26*, 83-89.
19. Troyan, S. L.; Kianzad, V.; Gibbs-Strauss, S. L.; Gioux, S.; Matsui, A.; Oketokoun, R.; Ngo, L.; Khamene, A.; Azar, F.; Frangioni, J. V., The flare(TM) intraoperative near-infrared fluorescence imaging system: A first-in-human clinical trial in breast cancer sentinel lymph node mapping. *Annals of Surgical Oncology* **2009**, *16*, 2943-2952.
20. Luker, G. D.; Luker, K. E., Optical imaging: Current applications and future directions. *Journal of Nuclear Medicine* **2008**, *49*, 1-4.
21. van Dam, G. M.; Themelis, G.; Crane, L. M. A.; Harlaar, N. J.; Pleijhuis, R. G.; Kelder, W.; Sarantopoulos, A.; de Jong, J. S.; Arts, H. J. G.; van der Zee, A. G. J.; Bart, J.; Low, P. S.; Ntziachristos, V., Intraoperative tumor-specific fluorescence imaging in ovarian cancer by folate receptor-alpha targeting: First in-human results. *Nature Medicine* **2011**, *17*, 1315-U1202.
22. Shafiq, J.; Barton, M.; Noble, D.; Lemer, C.; Donaldson, L. J., An international review of patient safety measures in radiotherapy practice. *Radiotherapy and Oncology* **2009**, *92*, 15-21.



23. Delaney, G.; Jacob, S.; Featherstone, C.; Barton, M., The role of radiotherapy in cancer treatment - estimating optimal utilization from a review of evidence-based clinical guidelines. *Cancer* **2005**, *104*, 1129-1137.
24. Zou, W. P., Immunosuppressive networks in the tumour environment and their therapeutic relevance. *Nature Reviews Cancer* **2005**, *5*, 263-274.
25. Ostrand-Rosenberg, S., Immune surveillance: A balance between protumor and antitumor immunity. *Current Opinion in Genetics & Development* **2008**, *18*, 11-18.
26. Rosenberg, S. A., Progress in human tumour immunology and immunotherapy. *Nature* **2001**, *411*, 380-384.
27. Scanlan, M. J.; Gure, A. O.; Jungbluth, A. A.; Old, L. J.; Chen, Y. T., Cancer/testis antigens: An expanding family of targets for cancer immunotherapy. *Immunological Reviews* **2002**, *188*, 22-32.
28. Dunn, G. P.; Old, L. J.; Schreiber, R. D., The immunobiology of cancer immunosurveillance and immunoediting. *Immunity* **2004**, *21*, 137-148.
29. Darnell, R. B.; Posner, J. B., Paraneoplastic syndromes involving the nervous system. *New England Journal of Medicine* **2003**, *349*, 1543-1554.
30. Mesner, P. W., Jr.; Budihardjo, I. I.; Kaufmann, S. H., Chemotherapy-induced apoptosis. *Advances in pharmacology (San Diego, Calif.)* **1997**, *41*, 461-499.
31. Kaufmann, S. H.; Earnshaw, W. C., Induction of apoptosis by cancer chemotherapy. *Experimental Cell Research* **2000**, *256*, 42-49.
32. Allen, T. M., Ligand-targeted therapeutics in anticancer therapy. *Nature Reviews Cancer* **2002**, *2*, 750-763.
33. Maeda, H. The enhanced permeability and retention (EPR) effect in tumor vasculature: The key role of tumor-selective macromolecular drug targeting. In *Advances in enzyme regulation, vol 41*; Weber, G., Ed. 2001; Vol. 41, p 189-207.
34. Cho, K.; Wang, X.; Nie, S.; Chen, Z.; Shin, D. M., Therapeutic nanoparticles for drug delivery in cancer. *Clinical Cancer Research* **2008**, *14*, 1310-1316.
35. Kawakami, M.; Koya, K.; Ukai, T.; Tatsuta, N.; Ikegawa, A.; Ogawa, K.; Shishido, T.; Chen, L. B., Structure-activity of novel rhodacyanine dyes as antitumor agents. *Journal of Medicinal Chemistry* **1998**, *41*, 130-142.
36. Lampidis, T. J.; Hasin, Y.; Weiss, M. J.; Chen, L. B., Selective killing of carcinoma-cells invitro by lipophilic-cationic compounds - a cellular basis. *Biomedicine and Pharmacotherapy* **1985**, *39*, 220-226.
37. Kelland, L., The resurgence of platinum-based cancer chemotherapy. *Nature Reviews Cancer* **2007**, *7*, 573-584.
38. Wilkes, J. S., A short history of ionic liquids - from molten salts to neoteric solvents. *Green Chemistry* **2002**, *4*, 73-80.
39. Clare, B.; Sirwardana, A.; Macfarlane, D. R., Synthesis, purification and characterization of ionic liquids. *Topics in Current Chemistry* **2010**, *290*, 1-40.

40. Seddon, K. R., Ionic liquids for clean technology. *Journal of Chemical Technology and Biotechnology* **1997**, *68*, 351-356.
41. Walden, P., *Bull. Acad. Imper. Sci. (St. Petersburg)* **1914**, *1800*, 405-422.
42. Graenacher, C. Cellulose solution. In; US Patents: 1934.
43. Hurley, F. H.; Wier, T. P., The electrodeposition of aluminum from nonaqueous solutions at room temperature. *Journal of the Electrochemical Society* **1951**, *98*, 207-212.
44. Chum, H. L.; Koch, V. R.; Miller, L. L.; Osteryoung, R. A., Electrochemical scrutiny of organometallic iron complexes and hexamethylbenzene in a room-temperature molten-salt. *Journal of the American Chemical Society* **1975**, *97*, 3264-3265.
45. Wilkes, J. S.; Levisky, J. A.; Wilson, R. A.; Hussey, C. L., Dialkylimidazolium chloroaluminate melts - a new class of room-temperature ionic liquids for electrochemistry, spectroscopy, and synthesis. *Inorganic Chemistry* **1982**, *21*, 1263-1264.
46. Sun, I. W.; Ward, E. H.; Hussey, C. L.; Seddon, K. R.; Turp, J. E., Electrochemistry and spectroelectrochemistry of the hexachloroiridate (III) and hexachloroiridate (IV) complexes in the basic aluminum-chloride 1-methyl-3-ethylimidazolium chloride room-temperature ionic liquid. *Inorganic Chemistry* **1987**, *26*, 2140-2143.
47. Ward, E. H.; Barnard, P. A.; Sun, I. W.; Hussey, C. L., Spectroelectrochemistry in room-temperature haloaluminate ionic liquids. *Journal of the Electrochemical Society* **1987**, *134*, C510-C510.
48. Scheffler, T. B.; Hussey, C. L.; Seddon, K. R.; Kear, C. M.; Armitage, P. D., Molybdenum chloro complexes in room-temperature chloroaluminate ionic liquids: stabilization of hexachloromolybdate(2-) and hexachloromolybdate(3-). *Inorganic Chemistry* **1983**, *22*, 2099-2100.
49. Fannin, A. A.; King, L. A.; Stech, D. J.; Vaughn, R. L.; Wilkes, J. S.; Williams, J. L., Transport processes in imidazolium chloroaluminate molten-salts. *Journal of the Electrochemical Society* **1982**, *129*, C122-C122.
50. Wilkes, J. S.; Levisky, J. A.; Pflug, J. L.; Hussey, C. L.; Scheffler, T. B., Composition determinations of liquid chloroaluminate molten-salts by nuclear magnetic-resonance spectrometry. *Analytical Chemistry* **1982**, *54*, 2378-2379.
51. Plechkova, N. V.; Seddon, K. R., Applications of ionic liquids in the chemical industry. *Chemical Society Reviews* **2008**, *37*, 123-150.
52. Rogers, R. D.; Seddon, K. R., Ionic liquids - solvents of the future? *Science* **2003**, *302*, 792-793.
53. Visser, A. E.; Swatloski, R. P.; Huddleston, J. G.; Rogers, R. D., Room temperature ionic liquids as alternatives to organic solvents in liquid/liquid extraction of metal ions. *Abstracts of Papers of the American Chemical Society* **1999**, *217*, U881-U881.
54. Chen, P. Y.; Sun, I. W., Electrochemical study of copper in a basic 1-ethyl-3-methylimidazolium tetrafluoroborate room temperature molten salt. *Electrochimica Acta* **1999**, *45*, 441-450.

55. Ke, M.; Zhou, A.; Song, Z.; Jiang, Q., Toxicity of ionic liquids. *Progress in Chemistry* **2007**, *19*, 671-679.
56. Akdogan, Y.; Junk, M. J. N.; Hinderberger, D., Effect of ionic liquids on the solution structure of human serum albumin. *Biomacromolecules* **2011**, *12*, 1072-1079.
57. Kasai, H.; Nalwa, H. S.; Oikawa, H.; Okada, S.; Matsuda, H.; Minami, N.; Kakuta, A.; Ono, K.; Mukoh, A.; Nakanishi, H., A novel preparation method of organic microcrystals. *Japanese Journal of Applied Physics Part 2* **1992**, *31*, L1132-L1134.
58. Hayashi, S.; Hamaguchi, H. O., Discovery of a magnetic ionic liquid [bmim]FeCl<sub>4</sub>. *Chemistry Letters* **2004**, *33*, 1590-1591.
59. Kaushik, N. K.; Attri, P.; Kaushik, N.; Choi, E. H., Synthesis and antiproliferative activity of ammonium and imidazolium ionic liquids against T98G brain cancer cells. *Molecules* **2012**, *17*, 13727-13739.
60. Vranes, M.; Zec, N.; Tot, A.; Papovic, S.; Dozic, S.; Gadzuric, S., Density, electrical conductivity, viscosity and excess properties of 1-butyl-3-methylimidazolium bis(trifluoromethylsulfonyl) imide plus propylene carbonate binary mixtures. *Journal of Chemical Thermodynamics* **2014**, *68*, 98-108.
61. Ranke, J.; Othman, A.; Fan, P.; Mueller, A., Explaining ionic liquid water solubility in terms of cation and anion hydrophobicity. *International Journal of Molecular Sciences* **2009**, *10*, 1271-1289.
62. Patinha, D. J. S.; Alves, F.; Rebelo, L. P. N.; Marrucho, I. M., Ionic liquids based aqueous biphasic systems: Effect of the alkyl chains in the cation versus in the anion. *Journal of Chemical Thermodynamics* **2013**, *65*, 106-112.
63. Fredlake, C. P.; Crosthwaite, J. M.; Hert, D. G.; Aki, S.; Brennecke, J. F., Thermophysical properties of imidazolium-based ionic liquids. *Journal of Chemical and Engineering Data* **2004**, *49*, 954-964.
64. Del Popolo, M. G.; Voth, G. A., On the structure and dynamics of ionic liquids. *Journal of Physical Chemistry B* **2004**, *108*, 1744-1752.
65. Kagimoto, J.; Taguchi, S.; Fukumoto, K.; Ohno, H., Hydrophobic and low-density amino acid ionic liquids. *Journal of Molecular Liquids* **2010**, *153*, 133-138.
66. Tesfai, A.; El-Zahab, B.; Kelley, A. T.; Li, M.; Garno, J. C.; Baker, G. A.; Warner, I. M., Magnetic and nonmagnetic nanoparticles from a group of uniform materials based on organic salts. *ACS Nano* **2009**, *3*, 3244-3250.
67. Cole, M. R.; Li, M.; Jadeja, R.; El-Zahab, B.; Hayes, D.; Hobden, J. A.; Janes, M. E.; Warner, I. M., Minimizing human infection from escherichia coli o157:H7 using GUMBOS. *Journal of Antimicrobial Chemotherapy* **2013**, *68*, 1312-1318.
68. Regmi, B. P.; Monk, J.; El-Zahab, B.; Das, S.; Hung, F. R.; Hayes, D. J.; Warner, I. M., A novel composite film for detection and molecular weight determination of organic vapors. *Journal of Materials Chemistry* **2012**, *22*, 13732-13741.
69. Jordan, A. N.; Das, S.; Siraj, N.; de Rooy, S. L.; Li, M.; El-Zahab, B.; Chandler, L.; Baker, G. A.; Warner, I. M., Anion-controlled morphologies and spectral features of

- cyanine-based nanoGUMBOS - an improved photosensitizer. *Nanoscale* **2012**, *4*, 5031-5038.
70. Rao, C. N. R.; Cheetham, A. K., Science and technology of nanomaterials: Current status and future prospects. *Journal of Materials Chemistry* **2001**, *11*, 2887-2894.
  71. Sahay, G.; Alakhova, D. Y.; Kabanov, A. V., Endocytosis of nanomedicines. *Journal of Controlled Release* **2010**, *145*, 182-195.
  72. Sahay, G.; Kim, J. O.; Kabanov, A. V.; Bronich, T. K., The exploitation of differential endocytic pathways in normal and tumor cells in the selective targeting of nanoparticulate chemotherapeutic agents. *Biomaterials* **2010**, *31*, 923-933.
  73. Du, J.-Z.; Du, X.-J.; Mao, C.-Q.; Wang, J., Tailor-made dual pH-sensitive polymer-doxorubicin nanoparticles for efficient anticancer drug delivery. *Journal of the American Chemical Society* **2011**, *133*, 17560-17563.
  74. Gratton, S. E. A.; Ropp, P. A.; Pohlhaus, P. D.; Luft, J. C.; Madden, V. J.; Napier, M. E.; DeSimone, J. M., The effect of particle design on cellular internalization pathways. *Proceedings of the National Academy of Sciences of the United States of America* **2008**, *105*, 11613-11618.
  75. Haley, B.; Frenkel, E., Nanoparticles for drug delivery in cancer treatment. *Urologic Oncology: Seminars and Original Investigations* **2008**, *26*, 57-64.
  76. Kasai, H.; Murakami, T.; Ikuta, Y.; Koseki, Y.; Baba, K.; Oikawa, H.; Nakanishi, H.; Okada, M.; Shoji, M.; Ueda, M.; Imahori, H.; Hashida, M., Creation of pure nanodrugs and their anticancer properties. *Angewandte Chemie International Edition* **2012**, *51*, 10315-10318.
  77. Antonietti, M.; Kuang, D. B.; Smarsly, B.; Yong, Z., Ionic liquids for the convenient synthesis of functional nanoparticles and other inorganic nanostructures. *Angewandte Chemie-International Edition* **2004**, *43*, 4988-4992.
  78. Bwambok, D. K.; El-Zahab, B.; Challa, S. K.; Li, M.; Chandler, L.; Baker, G. A.; Warner, I. M., Near-infrared fluorescent nanoGUMBOS for biomedical imaging. *ACS Nano* **2009**, *3*, 3854-3860.
  79. Tesfai, A.; El-Zahab, B.; Bwambok, D. K.; Baker, G. A.; Fakayode, S. O.; Lowry, M.; Warner, I. M., Controllable formation of ionic liquid micro- and nanoparticles via a melt-emulsion-quench approach. *Nano Letters* **2008**, *8*, 897-901.
  80. Das, S.; Bwambok, D.; El-Zahab, B.; Monk, J.; de Rooy, S. L.; Challa, S.; Li, M.; Hung, F. R.; Baker, G. A.; Warner, I. M., Nontemplated approach to tuning the spectral properties of cyanine-based fluorescent nanoGUMBOS. *Langmuir* **2010**, *26*, 12867-12876.
  81. An, B. K.; Kwon, S. K.; Jung, S. D.; Park, S. Y., Enhanced emission and its switching in fluorescent organic nanoparticles. *Journal of the American Chemical Society* **2002**, *124*, 14410-14415.
  82. Peng, A. D.; Xiao, D. B.; Ma, Y.; Yang, W. S.; Yao, J. N., Tunable emission from doped 1,3,5-triphenyl-2-pyrazoline organic nanoparticles. *Advanced Materials* **2005**, *17*, 2070-2073.

83. Gesquiere, A. J.; Uwada, T.; Asahi, T.; Masuhara, H.; Barbara, P. F., Single molecule spectroscopy of organic dye nanoparticles. *Nano Letters* **2005**, *5*, 1321-1325.
84. Ferraz, R.; Branco, L. C.; Prudencio, C.; Noronha, J. P.; Petrovski, Z., Ionic liquids as active pharmaceutical ingredients. *Chemmedchem* **2011**, *6*, 975-985.
85. Sekhon, B. S., Ionic liquids: Pharmaceutical and biotechnological applications. *Asian Journal of Pharmaceutical and Biological Research* **2011**, *1*, 395-411.
86. Vineet, K.; Sanjay, V. M. Ionic liquids as pharmaceutical salts: A historical perspective. In *Ionic liquid applications: Pharmaceuticals, therapeutics, and biotechnology*; American Chemical Society: 2010; Vol. 1038, p 1-12.
87. Rodriguez, H.; Bica, K.; Rogers, R. D., Ionic liquid technology: A potential new platform for the pharmaceutical industry. *Tropical Journal of Pharmaceutical Research* **2008**, *7*, 1011-1012.
88. Moniruzzaman, M.; Goto, M., Ionic liquids: Future solvents and reagents for pharmaceuticals. *Journal of Chemical Engineering of Japan* **2011**, *44*, 370-381.
89. Stepnowski, P.; Skladanowski, A. C.; Ludwiczak, A.; Laczynska, E., Evaluating the cytotoxicity of ionic liquids using human cell line HeLa. *Human & Experimental Toxicology* **2004**, *23*, 513-517.
90. Ranke, J.; Stolte, S.; Stoermann, R.; Arning, J.; Jastorff, B., Design of sustainable chemical products - the example of ionic liquids. *Chemical Reviews* **2007**, *107*, 2183-2206.
91. Kumar, V.; Malhotra, S. V., Study on the potential anti-cancer activity of phosphonium and ammonium-based ionic liquids. *Bioorganic & Medicinal Chemistry Letters* **2009**, *19*, 4643-4646.
92. Malhotra, S. V.; Kumar, V., A profile of the in vitro anti-tumor activity of imidazolium-based ionic liquids. *Bioorganic & Medicinal Chemistry Letters* **2010**, *20*, 581-585.
93. Skoog, D. A. W., Donald M., Holler, F. J., *Fundamentals of analytical chemistry*; 7th ed.; Saunders College Publishing: New York, 1996.
94. Lakowicz, J. *Principles of fluorescence spectroscopy*; 3rd ed.; Springer Science: New York, 2006.
95. Mosmann, T., Rapid colorimetric assay for cellular growth and survival: Application to proliferation and cytotoxicity assays. *Journal of Immunological Methods* **1983**, *65*, 55-63.
96. Sylvester, P. Optimization of the tetrazolium dye (mtt) colorimetric assay for cellular growth and viability. In *Drug design and discovery*; Satyanarayanajois, S. D., Ed.; Humana Press: 2011; Vol. 716, p 157-168.
97. Cory, A. H.; Owen, T. C.; Barltrop, J. A.; Cory, J. G., Use of an aqueous soluble tetrazolium formazan assay for cell-growth assays in culture. *Cancer Communications* **1991**, *3*, 207-212.
98. Riss, T. L.; Moravec, R. A., Comparison of mtt, xtt, and a novel tetrazolium compound mts for invitro proliferation and chemosensitivity assays. *Molecular Biology of the Cell* **1992**, *3*, A184-A184.

99. Periasamy, A.; Wodnicki, P.; Wang, X. F.; Kwon, S.; Gordon, G. W.; Herman, B., Time-resolved fluorescence lifetime imaging microscopy using a picosecond pulsed tunable dye laser system. *Review of Scientific Instruments* **1996**, *67*, 3722-3731.
100. Lichtman, J. W.; Conchello, J. A., Fluorescence microscopy. *Nature Methods* **2005**, *2*, 910-919.
101. Paddock, S. W., Confocal laser scanning microscopy. *BioTechniques* **1999**, *27*, 992-+.
102. Fritzky, L.; Lagunoff, D., Advanced methods in fluorescence microscopy. *Analytical Cellular Pathology* **2013**, *36*, 5-17.
103. Shotton, D. M., Confocal scanning optical microscopy and its applications for biological specimens. *Journal of Cell Science* **1989**, *94*, 175-206.
104. White, J. G.; Amos, W. B.; Fordham, M., An evaluation of confocal versus conventional imaging of biological structures by fluorescence light-microscopy. *Journal of Cell Biology* **1987**, *105*, 41-48.
105. Hornyak, G. L.; Peschel, S.; Sawitowski, T.; Schmid, G., TEM, STM and AFM as tools to study clusters and colloids. *Micron* **1998**, *29*, 183-190.
106. Schmut, R., Zeta potential measurement. *Industrial and Engineering Chemistry* **1964**, *56*, 28-33.
107. Binner, J.; Zhang, Y., Characterization of silicon carbide and silicon powders by XPS and zeta potential measurement. *Journal of Materials Science Letters* **2001**, *20*, 123-126.
108. Dukhin, A. S.; Goetz, P. J., Characterization of aggregation phenomena by means of acoustic and electroacoustic spectroscopy. *Colloids and Surfaces A-Physicochemical and Engineering Aspects* **1998**, *144*, 49-58.
109. Koelle, D., High transition temperature superconducting quantum interference devices: Basic concepts, fabrication and applications. *Journal of Electroceramics* **1999**, *3*, 195-212.
110. Kleiner, R.; Koelle, D.; Ludwig, F.; Clarke, J., Superconducting quantum interference devices: State of the art and application's. *Proceedings of the Institute of Electrical and Electronics Engineers* **2004**, *92*, 1534-1548.

## CHAPTER 2. TUNABLE CYTOTOXICITY OF RHODAMINE 6G VIA ANION VARIATIONS\*

### 2.1. Introduction

There has recently been a tremendous growth in the number of compounds developed as chemotherapeutic agents for treatment of cancer. However, two major obstacles are relevant for chemotherapeutic agents: toxicity towards normal cells and drug resistance. Cationic compounds and multilamellar vesicles with positive charges have been vigorously investigated for this purpose.<sup>1-4</sup> For example, cationic rhodamine dyes have been demonstrated to be good candidates for this line of research and a number of reports exist dating back to as early as the 1970's.<sup>5-8</sup> Most of these studies suggest that cationic compounds accumulate in the mitochondria of tumor cells due to the unusually high negative mitochondrial membrane potential of tumor cells as compared to normal cells. Upon accumulation and subsequent retention, cationic compounds lead to disruption of adenosine triphosphate (ATP) synthesis in the mitochondria which eliminates the power source of these cells.<sup>6,7</sup> Other investigations suggest that only the cationic dyes with delocalized positive charge show mitochondrial selectivity<sup>7-9</sup> with little or no focus on the role played by the counter anion. For example, Lampidis and co-workers have performed some very thorough and impressive research on the toxicity of cationic compounds.<sup>10-13</sup> In one of these studies, they report the selective toxicity of cationic rhodamine analogues (rhodamine 123 and 6G), tetraphenyl phosphonium (TTP<sup>+</sup>), and safranin O towards breast cancer cell line (MCF7) in comparison to the normal monkey kidney cell line (CV-1).<sup>6</sup>

\*Reproduced in part with permission from Magut, P. K. S.; Das, S.; Fernand, V. E.; Losso, J.; McDonough, K.; Naylor, B. M.; Aggarwal, S.; Warner, I. M., Tunable cytotoxicity of rhodamine 6g via anion variations. *Journal of the American Chemical Society* **2013**, *135*, 15873-15879. Copyright © 2013, American Chemical Society.

However, later studies with matched pairs of normal and breast cancer cell lines revealed that rhodamine 123 has no preferential retention or toxicity towards either of these cell lines. Thus, the selectivity reported earlier was attributed to drug resistance caused by a multi-drug resistance (mdr-1) gene apparently found in the CV-1 cell line, but absent in normal and breast cancer cell lines.<sup>10</sup> It is with these findings in mind that we chose to investigate the effect of counter anions on the antitumor activity of rhodamine 6G to examine if such a change may impart selectivity, particularly towards matched normal and breast cancer cell lines. These anion variations also led to synthesis of organic nanoparticles from the more hydrophobic compounds as discussed later.

Our interest in organic nanoparticles is driven by the significant attention this area has drawn among researchers in the recent past.<sup>14-18</sup> In addition, many types of organic nanoparticles have the advantage of ease of tunability which allows potential applications in varied fields such as optoelectronics, bioimaging, and optical data storage.<sup>17,19-23</sup> The high load of fluorophores in molecular assemblies within nanoparticles is one property that makes them particularly attractive for biomedical applications.<sup>24</sup> With regard to cancer cells, it has been proposed that nanoparticles can achieve increased intracellular concentration, while achieving minimal toxicity in normal cells.<sup>25</sup> Consequently, many recent advances in cancer research to address toxicity of chemotherapeutic agents towards normal cells have led to exploitation of nanoparticles.<sup>26</sup>

Relative hydrophobicity has been shown to influence drug uptake and subcellular distribution of chemotherapeutic agents.<sup>27</sup> To this end, many approaches to varying the hydrophobicity of potential anticancer drugs, especially cationic compounds, involve addition of new groups via covalent bonding or increasing alkyl chain lengths that leads to tedious synthesis of new organic compounds with a primary focus on the contributions of the cation to their



anticancer properties.<sup>27</sup> In the study outlined in this manuscript, we sought to minimize structural differences from the cationic precursors by investigating the effect of the anion on the hydrophobicity and antitumor properties of these compounds *in vitro*. To achieve this goal, we have employed a much simpler strategy to developing compounds with varying hydrophobicities using the concept of variations in hydrophobicity employed for ionic liquids (ILs).<sup>28</sup> In this approach, the cationic dye of choice is held constant while organic counter-anions of varying sizes and lipophilic properties are coupled via simple ion exchange procedures.<sup>20</sup> These compounds are derived from a new class of compounds referred to as a group of uniform materials based on organic salts (GUMBOS). GUMBOS are typically solids which possess many of the attractive properties of ILs.<sup>29</sup> Although GUMBOS share similar properties to ILs, these solids are defined as having melting points ranging from 25 °C to 250 °C, thus broadening the tunable hydrophobic and melting point ranges for select designer materials applications. Additionally, as hydrophobicity increases, water insoluble nanoparticles known as nanoGUMBOS can be fabricated from GUMBOS.<sup>16,20,30</sup> Recently, using a similar concept for solubility of organic compounds in water, Kasai and co-workers have fabricated nanodrugs with anticancer properties from camptothecin derivatives that are insoluble in water.<sup>14</sup>

In this study, we have used the traditionally measured 1-octanol/water partition coefficients to gauge the relative hydrophobicity of these compounds.<sup>31</sup> On the basis of this measure of hydrophobicity, cell viability results revealed that nanoGUMBOS synthesized from hydrophobic GUMBOS are non-toxic to normal cells and toxic to cancer cells while rhodamine 6G chloride and the hydrophilic GUMBOS inhibited cell proliferation for both normal and cancer cells *in vitro*. The anions in combination with sodium or lithium ions were non-toxic to both normal and cancer cells. In the studies introduced in this manuscript, we demonstrate that

both the cation and anion play an active and cooperative role in the observed cytotoxic properties. To the best of our knowledge, this study is the first of its kind. Furthermore, we believe that this approach may be a general one and that this discovery may be of great significance in medicinal chemistry, cancer therapy, and fluorescence bioimaging.

## **2.2. Materials and Methods**

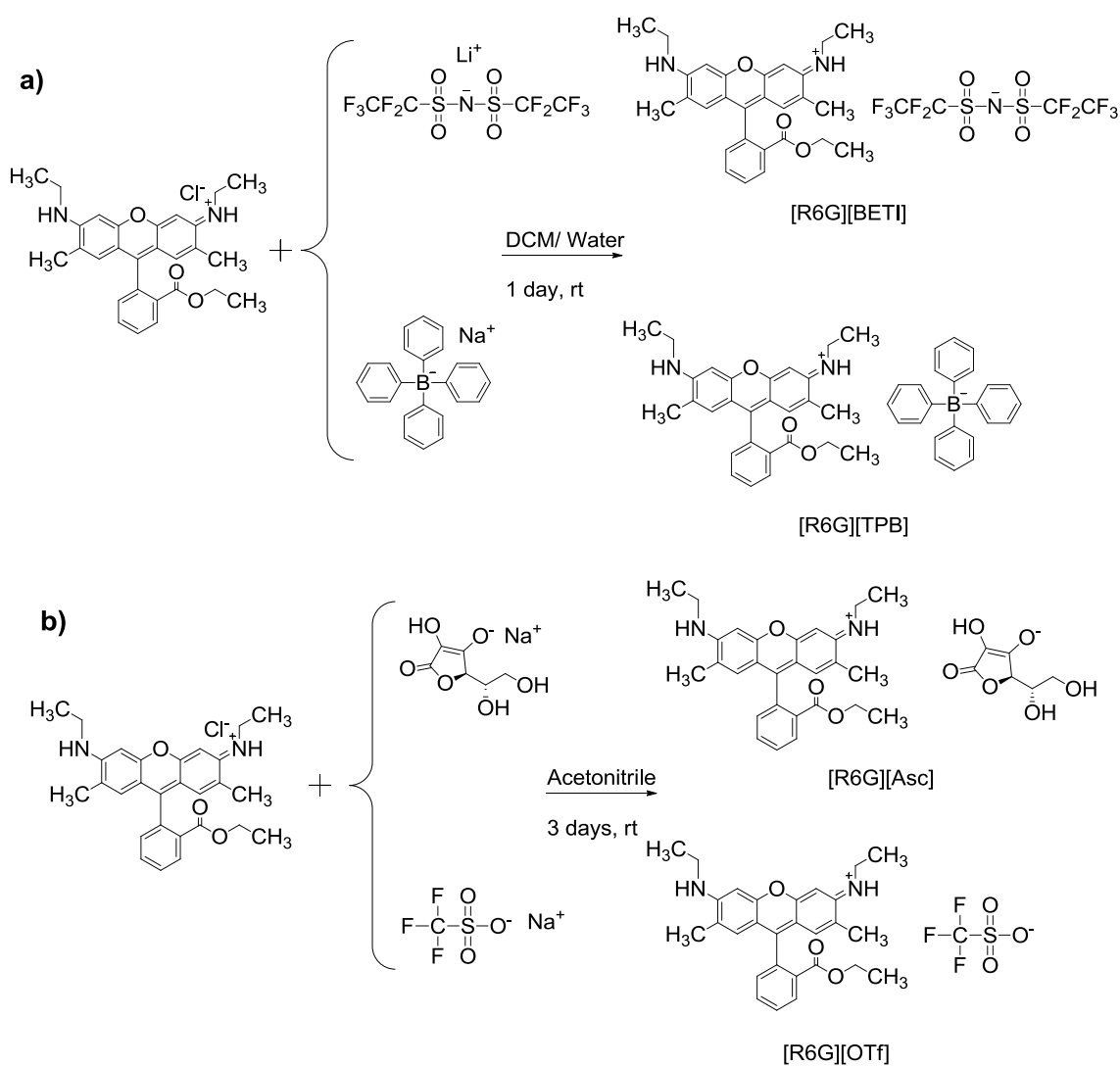
### **2.2.1. Materials**

Human serum and glutaraldehyde were purchased from Sigma Aldrich (St. Louis, MO) and used as received. Sodium tetraphenyl borate (99.5%), sodium trifluoromethanesulfonate (98%), sodium L-ascorbate (98%), rhodamine 6G (95%), phosphate buffered saline, methylene chloride, anhydrous acetonitrile, ethanol (spectroscopic grade), crystal violet, digitonin, carbonyl cyanide 3-chlorophenylhydrazone (CCCP) and 0.2  $\mu\text{m}$  nylon membrane filters were purchased from Sigma Aldrich (Milwaukee, WI). Lithium bis (perfluoroethylsulfonyl) imide was donated by Dr. Gary Baker (Oak Ridge National Laboratory, Oak Ridge, TN). Cell viability MTT (3-[4, 5-Dimethylthiazol-2-yl]-2, 5-diphenyltetrazolium bromide) and Mitochondrial ToxGlo™ Assay kits were purchased from Promega Corporation (Madison, WI). Cell death ELISA assay kit was purchased from Roche Applied Sciences (Indianapolis, IN). Triply deionized water (18.2  $\text{M}\Omega\cdot\text{cm}$ ) from an Elga model PURELAB ultra water filtration system (Lowell, MA) was used for all preparations of GUMBOS. A BRANSON 3510RDTH model bath ultrasonicator (335 W, 40 kHz frequency) (Branson Ultrasonics Corporation, Danbury, CT) was used at room temperature for preparation of nanoGUMBOS.

### **2.2.2. Synthesis and Characterization of Rhodamine 6G-based GUMBOS**

The rhodamine 6G-based organic salts (GUMBOS) were prepared using ion exchange procedures similar to those previously reported in the literature with slight modification.<sup>20,28</sup> The

synthesis of rhodamine tetraphenyl borate ([R6G][TPB]) is herein described as a representative procedure for the hydrophobic GUMBOS. Thirty (30) mg (0.063 mmol) of [R6G][Cl] and 23.6 mg (0.068 mmol) of sodium tetraphenyl borate ([Na][TPB]) salt were dissolved in a mixture of methylene chloride (DCM) and water (2:1, v/v) and allowed to stir for 24 h at room temperature (Scheme 2.1a). Afterwards, the DCM bottom layer was washed several times with water to remove the sodium chloride by-product, and the product was dried by removal of solvent *in vacuo*.



Scheme 2.1. Synthesis of a) hydrophobic and b) hydrophilic R6G-based GUMBOS.

Further freeze-drying to remove traces of water afforded 46.1 mg (Table 2.2) of [R6G][TPB]. A different procedure was employed for synthesis of the hydrophilic GUMBOS, [R6G][Asc] and [R6G][OTf] since these products are relatively more soluble in water <sup>28</sup> (Scheme 2.1b). The starting materials, [R6G][Cl] and sodium ascorbate ([Na][Asc]) were stirred in anhydrous acetonitrile for 72 h. The NaCl byproduct was removed by filtration and [R6G][Asc] or [R6G][OTf] GUMBOS were obtained by removal of acetonitrile under vacuum. The GUMBOS obtained were characterized by use of <sup>1</sup>H NMR (Bruker Avance 400, CDCl<sub>3</sub>) and elemental analysis. For [R6G][BETI] and [R6G][OTf], <sup>19</sup>F NMR (Bruker DPX 250, CDCl<sub>3</sub>) was used to confirm anion exchange. Melting points of the GUMBOS were determined using a MEL-TEMP capillary melting point apparatus (Stanford Research Systems, Sunnyvale, CA).

### **2.2.3. Synthesis of Rhodamine 6G-based NanoGUMBOS**

NanoGUMBOS were synthesized by use of a slightly modified, additive free reprecipitation method.<sup>32</sup> Briefly, 1 mL of 1 mM GUMBOS were prepared by dissolving in DMSO such that the final volume of DMSO was no more than 10% and topped off at the 1 mL mark using cell media (DMEM containing 10% Fetal bovine serum), followed by sonication for 5 min. A 100  $\mu$ L aliquot of this solution was re-suspended in 1 mL cell media under sonication to prepare 100  $\mu$ M of nanoGUMBOS. These nanoGUMBOS were then left to age in the dark for 1 h. For nanoGUMBOS characterization, a few microliters were dropcast onto a carbon coated copper grid and left to dry at room temperature. Upon drying, the grids were washed several times with water to remove the cell media. A similar protocol was used to synthesize nanoGUMBOS for stability studies with water as the solvent instead of cell media. The average particle size and size distribution of nanoGUMBOS were determined by use of transmission electron microscopy (TEM) using an LVEM5 transmission electron microscope (DeLong

America, Montreal, Canada) and dynamic light scattering (DLS). The zeta potentials of nanoGUMBOS at various pH values were measured by using a Zetasizer Nano ZS (Malvern Instruments, UK).

#### **2.2.4. Absorption and Fluorescence Spectroscopy**

UV-vis spectra were collected using a Shimadzu UV-3101 PC UV-Vis-near-IR scanning spectrometer (Shimadzu, Columbia, MD). Steady-state fluorescence measurements were recorded at room temperature by use of a Spex Fluorolog-3 spectrofluorimeter (model FL3-22TAU3; Jobin Yvon, Edison, NJ) equipped with a 450-W xenon lamp and R928P photomultiplier tube (PMT) emission detector. A 0.4 cm<sup>2</sup> quartz cuvette (Starna Cells) was used to collect the fluorescence and absorbance relative to an identical cell filled with relevant solvent as the blank. Both normalized and non-normalized absorption spectra were deconvoluted using principal component analysis, and fits with lowest  $\chi^2$  values were accepted.<sup>16</sup> A two component Gaussian fit was used to deconvolute both the normalized and non-normalized absorption spectra.

#### **2.2.5. Quantum Yields and Lifetime Measurements**

Quantum yields (QY) of the GUMBOS were measured relative to [R6G][Cl], QY= 0.90  $\pm$  0.02.<sup>33</sup> The GUMBOS and solution of [R6G][Cl] in deionized water were optically matched at the excitation wavelength (530 nm) and the QY calculated with corrections for the absorbance of all dispersions and solutions. The optical density was set at around 0.1 at 530 nm, and the integrated intensities of the emission spectra, corrected for differences in index of refraction and concentration.<sup>34</sup> Fluorescence Lifetime measurements were performed at Horiba Scientific (Edison, NJ) using a time domain mode. A picoseconds pulsed laser source of 495 nm was used

and emission was collected at 550 nm with a TBX detector. The Time Correlated Single Photon Counting (TCSPC) mode was used for data acquisition with a resolution of 50 ps per channel.

#### **2.2.6. Photostability Measurements**

Photostability fluorescence measurements were collected as follows: the excitation/emission slit widths were maintained at maximum value (14 nm/ 14 nm) for maximum light exposure of the samples. Appropriate neutral density filters were used in order to avoid saturation of the detector. Data were collected over a period of 5000 seconds. All measurements were performed at room temperature by use of a Spex Fluorolog-3 spectrofluorimeter (model FL3-22TAU3; Jobin Yvon, Edison, NJ) equipped with a 450-W xenon lamp and R928P PMT emission detector.

#### **2.2.7. Stability Studies**

The stability of the nanoGUMBOS in phosphate buffered saline (PBS) at a pH 7.4 and ionic strength,  $I = 0.15$  M, and in blood serum (10 % Serum in PBS), was monitored by use of absorption and fluorescence measurements. In a typical experiment, nanoGUMBOS were freeze-dried and lyophilized to remove water and then re-suspended in 5 mL PBS. Absorbance and fluorescence emission measurements of the re-suspended nanoGUMBOS were acquired at various time intervals. A similar procedure was used for a solution containing 10% blood serum in PBS.

#### **2.2.8. Determination of Hydrophobicity**

1-Octanol/ water partition coefficient was used to gauge relative hydrophobicities of [R6G] - based GUMBOS. High performance liquid chromatography (HPLC) coupled with a UV-vis detector was used.<sup>35</sup> Separation and quantification of the GUMBOS in 1-octanol was performed on a Shimadzu HPLC system (Shimadzu, Kyoto, Japan) consisting of an SCL-10A

system controller, two LC-10AD pumps, a DGU-14A degasser, a SIL-10AD autosampler and an SPD-10AV UV-vis detector ( $\lambda = 530$  nm). Separation of the analytes was performed at room temperature using a Phenomenex Luna C18 column, 100 Å pore size, 4 µm particle sizes, 250 × 4.6 mm i.d. column containing a guard column (Phenomenex, Torrance, CA, USA). The [R6G]-based GUMBOS were eluted isocratically at a flow rate of 0.6 mL/ min using an acetonitrile/ water mobile phase (45/55, v/ v) containing phosphoric acid buffer (pH= 3.0). An injection volume of 20 µL was employed for this study. The concentration of GUMBOS in water phase was determined using mass balance. In a typical study, a known amount of [R6G][TPB] was dissolved in a 1-octanol and water mixture (equal volumes) and shaken for 24 h. The upper 1-octanol phase was then analyzed by use of HPLC with UV detection and quantified using an external calibration method. The equation  $K_{(o/w)} = [\text{GUMBOS}]_{o,e} / [\text{GUMBOS}]_{w,e}$  was used to calculate the partition coefficient, where ‘K’, ‘o’, ‘w,’ and ‘e’ represents partition coefficient, octanol, water, and equilibrium state, respectively. It is worth noting that the 1-octanol used in the partition experiments was pre-saturated with water overnight before use in order to correct for mutual solubility of the two solvents.<sup>35</sup>

## **2.2.9. Cell Studies**

### **2.2.9.1. Cell Culture**

*In vitro* experiments were performed using normal human breast fibroblast (Hs578Bst, ATCC no. HTB-125), human breast carcinoma (Hs578T, ATCC HTB-126), hormone-independent human breast adenocarcinoma (MDA-MB-231, ATCC no. HTB-26), and hormone-dependent human breast adenocarcinoma (MCF7, ATCC no. HTB-22) cell lines were obtained from the American Tissue Culture Collection (ATCC, Manassas, VA). All cell lines were grown to 90% confluence according to ATCC’s instructions before use in further experiments.

### **2.2.9.2. Cell Viability Assay**

Cytotoxicities of [R6G]-based GUMBOS and nanoGUMBOS for each cell line was determined by use of MTT Assay kit (Promega Corporation, Madison, WI, USA) according to the manufacturer's instructions. Briefly, in a 96-well plate, 5,000 cells in 0.1 mL culture medium were seeded to each well. After 24 h, the culture medium was removed and discarded followed by addition of 0.1 mL culture medium containing 0-100  $\mu$ M test compounds. Each concentration was performed in triplicates. Use of cell media and maintaining a sterile environment during the synthesis of nanoGUMBOS allowed their introduction directly into mammalian cells *in vitro* without the need to wash or re-suspend. The cells were then incubated for 48 h at 37 °C, in 5% CO<sub>2</sub> atmosphere. At the end of the incubation period, the cells were treated with 15  $\mu$ L MTT and incubated for 4 h. After four hours, 100  $\mu$ L stop solution was added per well and incubated overnight. Afterwards, the plate was shaken for 20 seconds to homogenize and cell viability determined using a micro plate spectrophotometer (Benchmark plus Bio-Rad Laboratories, Hercules, CA, USA). Absorbance was read at 570 nm with a reference wavelength of 650 nm. Cell viability as a percentage was determined by computing the ratio between absorbance of the treated cells and the absorbance of untreated (control) cells taken as 100%. Data was expressed as mean  $\pm$  SD

### **2.2.9.3. Apoptosis**

Apoptotic cell death was determined using a cell death ELISA assay kit (Roche Applied Sciences, Indianapolis, IN) as per the manufacturer's instruction. In a typical experiment, 10<sup>6</sup> cells/ well were incubated with 0-70  $\mu$ M of the test compound for 48 h to induce apoptosis. The cells were then lysed to produce nucleosomes and apoptotic cell death detected using a



microplate spectrophotometer (Benchmark Plus, Bio-Rad Laboratories, Hercules, CA, USA). Absorbance was read at 405 nm with a reference wavelength of 490 nm.

#### **2.2.9.4. Clonogenic Assay**

Clonogenic assay was performed according to a procedure described in literature with slight modifications.<sup>36</sup> Briefly, breast cancer cell line MDA-MB-231 was cultured in triplicate in 6-well plates at a density of 50 cells/ well and allowed to attach for two hours. Cells were observed under a microscope to confirm attachment and then incubated with the test compound for 48 h. Control wells contained cells with only cell culture medium. After 48 h, the medium was changed and the cells were allowed to form colonies over a period of one week. The colonies were then fixed with glutaraldehyde (6 % v/ v), stained with crystal violet (0.5 % w/ v) and counted using a stereomicroscope.

#### **2.2.9.5. Microscopy**

Approximately 5000 Hs578Bst cells, Hs578T cells and MDA-MB-231 cells were plated on glass bottom culture dishes (35 mm petri dish, 10mm Micro well; Ashland, MA, USA) for cell adherence a day before use. After 24 h, cells were incubated with the test compound at a final concentration of 50  $\mu$ M at 37 °C and 5% CO<sub>2</sub> in a humidified cell culture incubator for 48 h. Cell images were obtained under a light microscope (Nikon Diaphot 300; Hoffman Modulation Contrast) equipped with camera Nikon D70s at a magnification of 20X. Similarly, for confocal microscopy, cells were incubated with test compounds at a final concentration of 50 nM for 30 min. Cell images were acquired under an oil immersion objective (x40) with a confocal laser microscope (Leica TCS SP5 AOBS confocal microscope) equipped with an argon-krypton laser.

### **2.2.9.6. Cellular Uptake**

Cellular uptake was evaluated using flow cytometry following a protocol reported in literature,<sup>37</sup> with slight modifications. Briefly,  $3 \times 10^4$  cells per well were seeded in a 24- well plate and incubated for 24 h. The medium was replaced with medium containing [R6G][BETI] or [R6G][TPB] at 0-50  $\mu$ M. In another set of experiments to investigate the effect of extracellular pH on uptake of nanoGUMBOS by normal breast cell line, Hs578Bst, media was adjusted to pH 6.5 and 7.4. After 4 h, cells were washed three times with PBS and harvested by trypsinization. They were then washed again with centrifugation and resuspended in FACS buffer (0.3% BSA in PBS). Mean Fluorescence intensities were determined by flow cytometry (Becton & Dickinson, Mountain View, CA, USA).

### **2.2.9.7. Determination of Mitochondrial Responses to [R6G][BETI] and [R6G][TPB]**

To determine whether these compounds inhibited oxidative phosphorylation, a Mitochondrial ToxGlo<sup>TM</sup> Assay kit developed by Promega Corporation (Madison, WI) was used. This experiment was performed following the manufacturer's protocol with slight modification. The experiment comprised two parts. In the first part, membrane integrity (MI) was assessed, while in the second part ATP was measured. Briefly, 10,000 cells/ well were grown using standard media in a white 96- well plate (costar®) and allowed to adhere. These cells were then washed in serum-free, galactose-containing medium in order to restrict ATP production to oxidative phosphorylation. Carbonyl cyanide 3-chlorophenylhydrazone (CCCP) was used as a positive control mitochondrial toxin and digitonin was used as a positive control toxicity compound. All test compounds and controls were prepared in serum-free galactose-containing medium. After washing, cells were incubated with the test compounds and controls for 2 h. At the end of 2h, 20  $\mu$ L of a 5x diluted fluorogenic peptide substrate (bis- AAF-R110) was

introduced to each well and mixed by use of orbital shaking for 1 min at 600 rpm. The sample was then incubated for 30 min at 37 °C followed by measurement of fluorescence using excitation at 485 nm and measuring emission at 530 nm. This test was considered valid when the signal from the cytotoxicity control was at least twofold higher than that of the untreated media control. To determine the amount of ATP, the sample plate was equilibrated to room temperature for 5-10 min and 100 µL of prepared ATP detection reagent were added to each well followed by 5 min mixing on an orbital shaker at 600 rpm. Data was expressed as percentage of vehicle control.

#### **2.2.9.8. Statistics**

Statistical analyses were performed using one-way analysis of variance (ANOVA). Tukey's studentized range test was performed to ascertain significant differences between treatments within the 95% confidence interval using SAS 9.2 software (SAS, Cary, NC, USA).  $P < 0.05$  was considered to indicate statistical significance. Results shown are representative of at least three experiments and are expressed as mean  $\pm$  SD.

### **2.3. Results and Discussion**

#### **2.3.1. Synthesis and Characterization of Rhodamine 6G GUMBOS**

The elemental analysis (Table 2.1) and  $^1\text{H}$ NMR of all GUMBOS as well as  $^{19}\text{F}$  NMR of [R6G][BETI] and [R6G][OTf] gave results consistent with expectations.

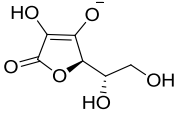
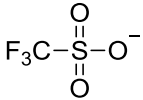
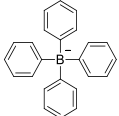
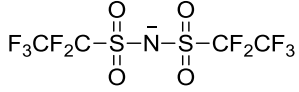
#### **2.3.2. Physical and Morphological Properties**

Rhodamine 6G-based GUMBOS displayed variable physical properties based upon changes in the anion type and size. It was observed that changing the anion affected the melting points of the GUMBOS (Table 2.2), as is commonly observed in other low-melting organic salts, such as ionic liquids, due to attenuation of crystal packing by larger anions in such salts.<sup>38,39</sup>

Table 2.1. Elemental analysis of rhodamine 6G-based GUMBOS

GUMBOS	C				N		S	
	Theory (%)	Found (%)	Theory (%)	Found (%)	Theory (%)	Found (%)	Theory (%)	Found (%)
[R6GAsc]	66.04	65.96	6.19	5.98	4.73	4.69	5.41	5.30
[R6G][OTf]	58.78	58.60	5.27	5.20	4.68	4.63	-	-
R6G][BETI]	46.67	47.02	3.91	3.79	5.10	5.14	7.78	7.57
[R6G][TPB]	81.88	81.71	6.74	6.75	3.67	3.69	-	-

Table 2.2. Yields, melting points, logarithm of 1-octanol/water partition coefficients of rhodamine 6G-based GUMBOS and size of corresponding particles.

GUMBOS	Yields (%)	Anion Structure	MW of Anion (g/mol)	m.p (°C)	Partition Coefficients (Log $K_{o/w}$ )	Particle Size (nm)
[R6G][Asc]	89		176	138	-0.5	N/A
[R6G][OTf]	94		149	239	0.1	N/A
[R6G][TPB]	96		319	83	0.3	92 ± 17
[R6G][BETI]	96		381	64	1.0	101 ± 21

NanoGUMBOS from rhodamine 6G tetraphenyl borate ([R6G][TPB]) and rhodamine 6G bis(perfluoroethylsulfonyl) imide ([R6G][BETI]) were primarily spherical or slightly ovate as characterized by use of transmission electron microscopy (TEM) (Figure 2.1) with an average size of approximately 100 nm. We note that the polydispersity index obtained for these nanoGUMBOS by use of dynamic light scattering (DLS) was generally good, usually under 0.2.

The agglomeration observed in Figure 2.1, a, may have resulted from evaporation of the dispersant.

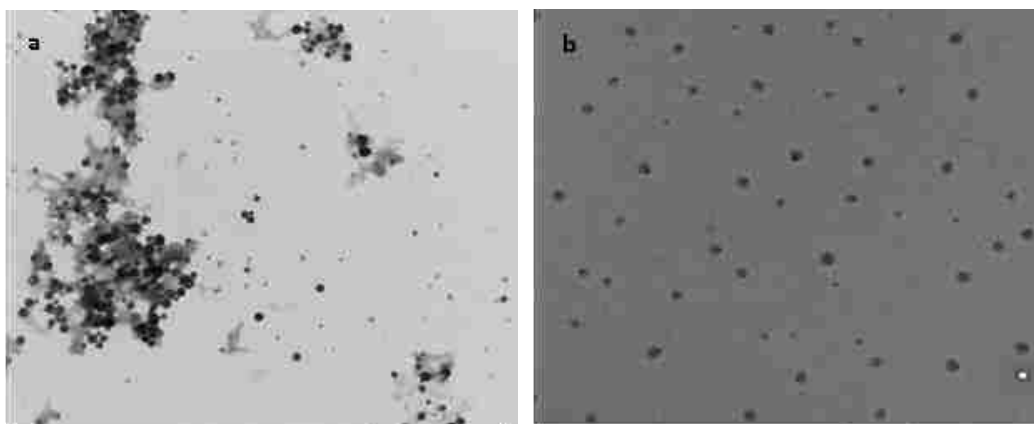


Figure 2.1. NanoGUMBOS TEM micrographs of a) [R6G][TPB] size:  $92 \pm 17$  nm and b) [R6G][BETI] size:  $101 \pm 21$  nm. Scale bars represent 500 nm.

One (1)-octanol/water partition coefficients was determined in order to gauge the relative hydrophobicities of the synthesized compounds<sup>35,40</sup> Trends beginning with least hydrophobic were rhodamine 6G ascorbate ([R6G][Asc]) < rhodamine 6G trifluoromethanesulfonate ([R6G][OTf]) < [R6G][TPB] < [R6G][BETI] (Table 2.2). These observed variations in partition coefficients clearly demonstrate that anions play an important role in determining hydrophobicities of [R6G]-based organic salts. Dissociation constants of rhodamine 6G-based GUMBOS were also determined (Table 2.3) and observed trends were very consistent with our measured octanol/water partition coefficients. Compared to [R6G][Cl], [R6G][BETI] and [R6G][TPB] show very low dissociation constants, while [R6G][OTf], [R6G][Asc] show moderate dissociation constants, which underscores the role played by anions in tuning this physical property of GUMBOS. [R6G][BETI] has dissociation constants of  $1.4 \times 10^{-12}$  and  $7.4 \times 10^{-12}$  and [R6G][TPB] has values of  $1.37 \times 10^{-11}$  and  $1.52 \times 10^{-11}$  in pH 6.5 and pH 7.4 buffer solutions, respectively. The low values of dissociation constants of [R6G][BETI] and [R6G][TPB] in PBS solutions suggest that these two GUMBOS are very insoluble in PBS

solution, where they form nanoGUMBOS. This study also demonstrates that pH is an important factor for evaluating solubility of rhodamine 6G-based GUMBOS. Generally, lower pH values favor less dissociated GUMBOS.

Table 2.3. Dissociation constants of rhodamine-based GUMBOS in buffer solutions

Compound	pH	Solubility (g/L)	Solubility (molL <sup>-1</sup> )	Dissociation constants Ks (mol <sup>2</sup> L <sup>-2</sup> )
[R6G][BETI]	6.5	$9.56 \times 10^{-4}$	$1.16 \times 10^{-6}$	$(1.35 \pm 0.70) \times 10^{-12}$
	7.4	$2.23 \times 10^{-3}$	$2.71 \times 10^{-6}$	$(7.36 \pm 0.06) \times 10^{-12}$
[R6G][TPB]	6.5	$2.82 \times 10^{-3}$	$3.71 \times 10^{-6}$	$(1.37 \pm 0.05) \times 10^{-11}$
	7.4	$2.97 \times 10^{-3}$	$3.89 \times 10^{-6}$	$(1.52 \pm 0.040) \times 10^{-11}$
[R6G][OTf]	6.5	$3.28 \times 10^{-2}$	$5.54 \times 10^{-5}$	$(3.07 \pm 0.20) \times 10^{-9}$
	7.4	$3.61 \times 10^{-2}$	$6.10 \times 10^{-5}$	$(3.73 \pm 0.40) \times 10^{-9}$
[R6G][Asc]	6.5	0.50	$8.05 \times 10^{-4}$	$(6.49 \pm 0.08) \times 10^{-7}$
	7.4	0.43	$6.95 \times 10^{-4}$	$(4.83 \pm 0.20) \times 10^{-7}$
[R6G][Cl]	6.5	1.37	$2.85 \times 10^{-3}$	$(8.11 \pm 0.60) \times 10^{-6}$
	7.4	1.68	$3.50 \times 10^{-3}$	$(1.23 \pm 0.07) \times 10^{-5}$

### 2.3.3. Absorption and Fluorescence Studies

Ethanol solutions of [R6G]-based GUMBOS displayed essentially identical absorption spectra with values of  $\lambda_{\max}$  near 525 nm, which were similar to the precursor, [R6G][Cl] (Figure 2.2, a). Use of these compounds in biological systems requires investigations of their spectral behavior at physiological pH. In phosphate buffered saline (PBS, pH= 7.4, ionic strength, I= 0.15 M), [R6G][TPB] and [R6G][BETI] nanoGUMBOS exhibited broad absorption spectra with a shoulder in the red region relative to the peak maxima (Figure 2.2, b).

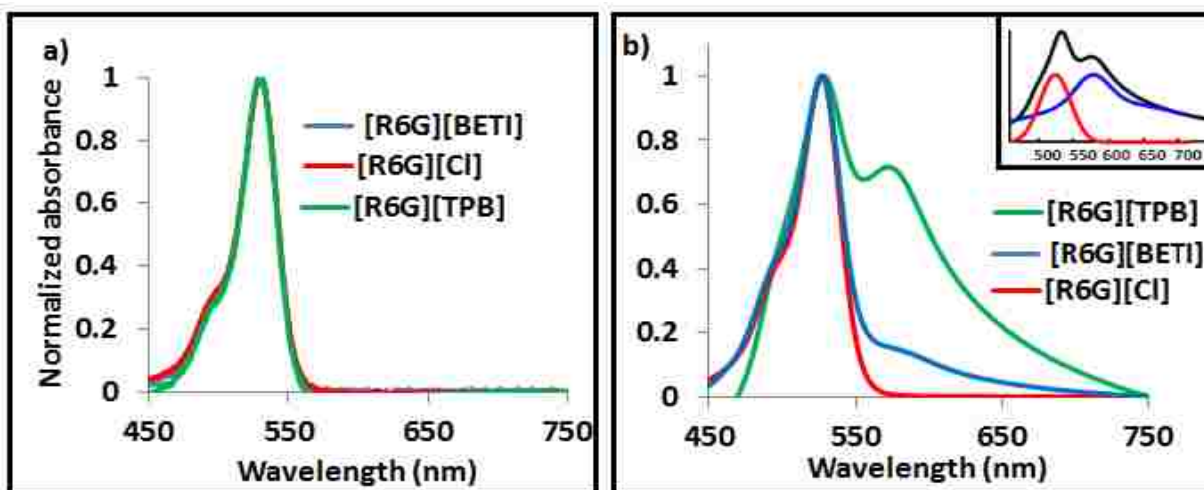


Figure 2.2. Absorption spectra of [R6G]-based a) GUMBOS in ethanol b) nanoGUMBOS in PBS. Inset; deconvoluted absorption spectrum of [R6G][TPB] and [R6G][BETI] nanoGUMBOS (black line), representing randomly oriented aggregates absorbing at  $\lambda=525$  nm (red line) and J-aggregates absorbing at  $\lambda=582$  nm (blue line).

The deconvoluted absorption spectra (inset of Figure 2.2, b) of [R6G][TPB] and [R6G][BETI] nanoGUMBOS reveal that each absorption spectrum can be decomposed into two major bands attributed to two different types of absorbing species.<sup>16</sup> The spectral component absorbing at  $\sim 525$  nm is assigned to aggregates within the dye nanoGUMBOS with transition dipoles that are often randomly oriented in dilute solutions.<sup>41</sup> The red-shifted spectral component is attributed to J-type aggregation in which the transition dipoles are arranged in a staircase manner.<sup>42</sup> Although J-aggregation is expected to lead to narrowing of the spectral line, the absorption profile for our nanoGUMBOS is relatively broader. This broadening may be attributed to imperfect J-aggregation, lack of motional narrowing, or the presence of lattice disorder within nanoGUMBOS.<sup>43,44</sup> The more hydrophilic GUMBOS, [R6G][Asc] and [R6G][OTf], displayed absorbance profiles similar to [R6G][Cl], possibly due to similar solubility in water. An intense fluorescence emission signal from nanoGUMBOS appears near 550 nm with the fluorescence excitation and emission spectra following the expected mirror-image rule as a result of Franck Condon factors (Figure 2.3, a).

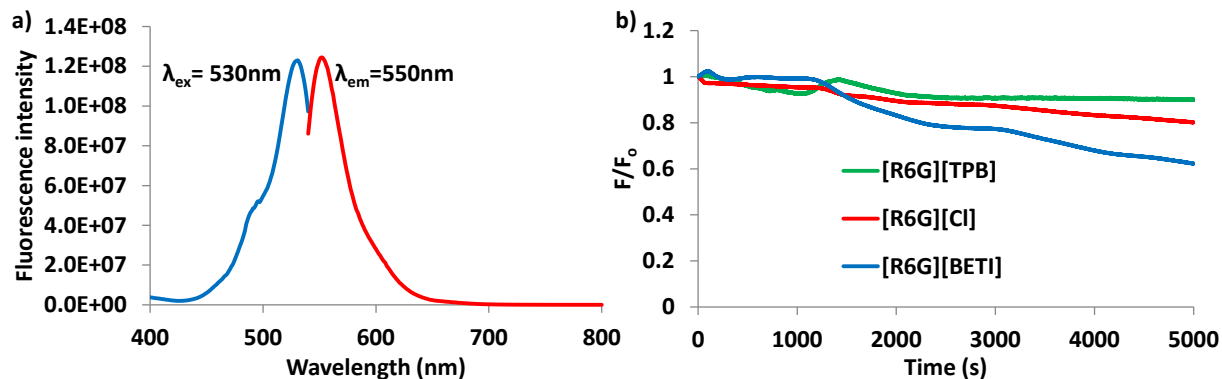


Figure 2.3. Fluorescence studies in PBS displaying a) fluorescence excitation and emission spectra of 4  $\mu\text{M}$  [R6G][TPB] nanoGUMBOS and b) photostability of 0.1  $\mu\text{M}$  [R6G] - based compounds.  $F_0$  and  $F$  are fluorescence intensities at  $t=0$  and at different times respectively. Maximum slit widths of 14 nm were maintained on both excitation and emission.

We determined the quantum yields of the [R6G]-based GUMBOS via a previously reported comparative method,<sup>45</sup> using [R6G][Cl] as the standard.<sup>33</sup> The quantum yields were determined to be 0.87, 1.01, 0.97 and 1.01 for [R6G][Asc], [R6G][OTf], [R6G][TPB], and [R6G][BETI] respectively while the [R6G][Cl] standard used was 0.90. In addition, we have determined the lifetimes of these compounds which were 3.92, 3.92, 3.91 and 3.91 for [R6G][Asc], [R6G][OTf], [R6G][TPB] and [R6G][BETI] respectively. The lifetime of [R6G][Cl] is 3.94. Evaluation of these results reveals minimal differences in quantum yields and lifetimes with changes in the anion. This implies that fluorescence properties of these compounds are strongly influenced by properties of the cationic fluorophore and are minimally affected by the anions.

This feature allowed the fluorescence properties of the R6G moiety to be essentially maintained, while tuning other physical properties of GUMBOS. Intrinsic photostability was also monitored to evaluate the molecular response of the GUMBOS and nanoGUMBOS upon exposure to light. Evaluation of data from these studies revealed excellent photostability with [R6G][TPB] being the most photostable. It was observed that signal retention ranged from 62%



to 90% after 5000 seconds of irradiation (Figure 2.3, b) which suggests relatively long shelf life if these materials were to be developed as drug or imaging contrast agents.

### 2.3.4. Stability of Rhodamine 6G-based NanoGUMBOS

Colloidal stabilities of nanoGUMBOS in phosphate buffered saline (PBS, pH= 7.4, ionic strength, I= 0.15 M), and serum-PBS (10% serum in PBS) were investigated by monitoring absorbance at  $\lambda= 530$  nm and emission at  $\lambda= 550$  nm over a 48 h period. We observed a gradual decrease in the relative absorbance and emission when nanoGUMBOS were dispersed in PBS (Figure 2.4).

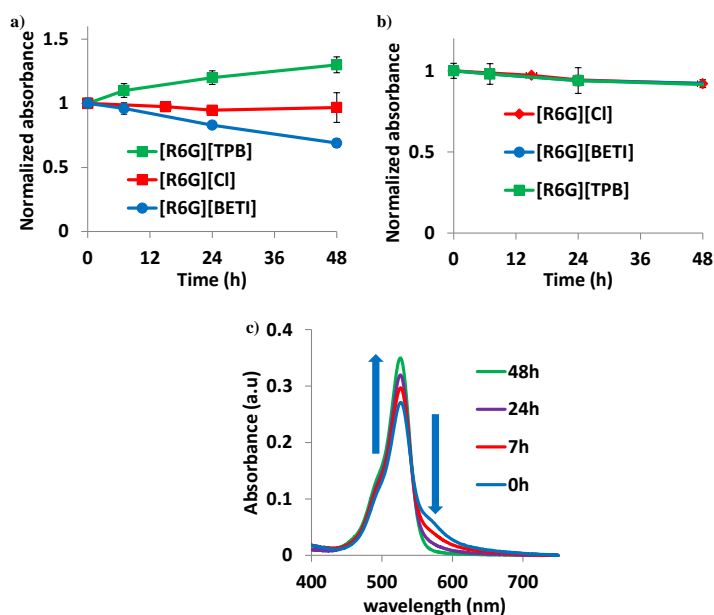


Figure 2.4. Stability of nanoGUMBOS in a) PBS b) 10% serum and c) absorbance spectra corresponding to [R6G][TPB] in PBS showing transition from J-aggregates ( $\lambda = 582$  nm) to randomly oriented aggregates ( $\lambda = 525$  nm).

This decrease in signal is partly attributed to adsorption of nanoGUMBOS on the walls of the glass vial in which they were prepared.<sup>46</sup> Attenuation of intensities may also be a result of nanoparticle aggregation or reorientation with time. It is interesting to note that we observed an increase in absorbance (Figure 2.4, a) and fluorescence emission for [R6G][TPB] nanoGUMBOS in PBS, which is attributed to dye de-aggregation over time. This was confirmed

by monitoring the absorption spectra as depicted in Figure 2.4, c, where the peak earlier attributed to J-aggregates ( $\lambda = 582$  nm) for [R6G][TPB] nanoGUMBOS decreased in absorbance with time as the one attributed to randomly oriented aggregates ( $\lambda = 525$  nm) increased. This suggests a gradual shift from the more ordered J-aggregates to randomly oriented aggregates in PBS. In contrast, when nanoGUMBOS were dispersed in serum-PBS, little or no changes in absorption intensity (Figure 2.4, b) and fluorescence emission were observed. This is likely due to prevention of non-specific adsorption to the walls of the glass vials by serum proteins. This observation is consistent with previous literature where bovine serum albumin was used to prevent non-specific adsorption of PEGylated gold nanoparticles.<sup>46</sup> This study of nanoGUMBOS in serum-PBS suggests a possible fate of these materials if used *in vivo*. Thus, their extraordinary stability enhances their potential for such applications.

### 2.3.5. Cell Studies

MTT assay was used as the primary method for evaluating cytotoxicities, while microscopy was used to corroborate these findings. Initial studies were performed using a suspension of hydrophobic GUMBOS in PBS. After examining these suspensions, we observed the presence of micro- and nano-particles (Figure 2.5).

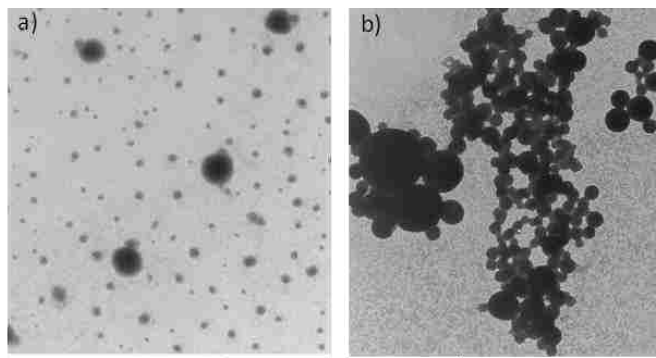


Figure 2.5. TEM images of a suspension of a) [R6G] [BETI] and b) [R6G] [TPB] GUMBOS. This displays micro- and nano-sized particles. Bars represent 2  $\mu$ m.

Therefore, further studies were performed by synthesis of nanoGUMBOS with an average size of approximately 100 nm from hydrophobic [R6G][BETI] and [R6G][TPB]. This ensured uniformity in the size of the nanoGUMBOS. Various cell lines were treated with varying concentrations of nanoGUMBOS and it was observed that viability of the normal breast cell line remained largely unaffected, while breast cancer cell proliferation was inhibited in a concentration dependent manner (Figure 2.6).

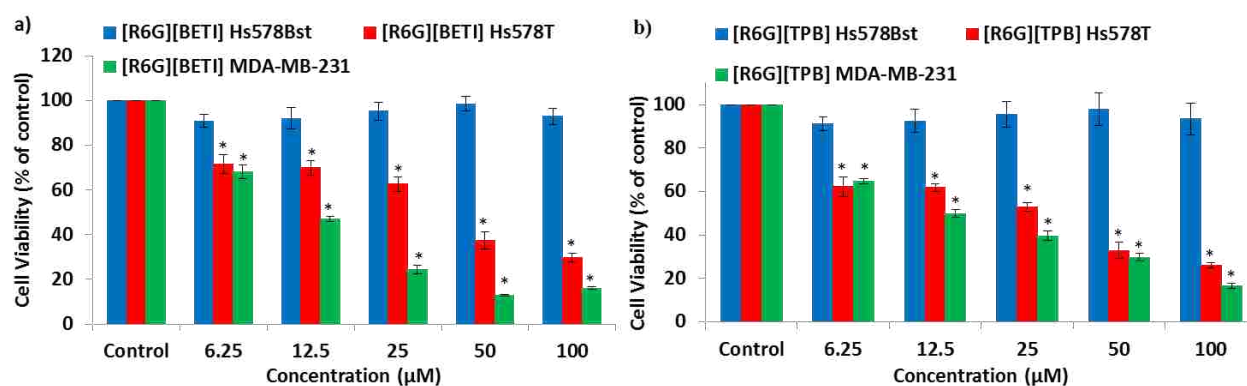


Figure 2.6. Cell viability assay of Hs578Bst, Hs578T and MDA-MB-231 cell lines upon treatment with a) [R6G][BETI] and b) [R6G][TPB]. \* Statistically different from control,  $P < 0.0001$ .

The MTT assay results were consistent with light microscopy images acquired after 48h treatment of the cells with [R6G][BETI] and [R6G][TPB] (Figure 2.7). At the end of 48 h, it was observed that the normal breast cell line (HS578Bst) appeared attached firmly and healthy. In contrast, the breast cancer cell lines (Hs578T and MDA-MB-231) appeared smaller, round up and detached consistent with the morphology observed when adherent cells die. It is also interesting to note that these compounds were found to be more toxic toward more aggressive and invasive cancer cell lines than toward less invasive cell lines. For example, the  $IC_{50}$  values for the more invasive and aggressive MDA-MB-231 were 11.4 μM and 12.2 μM for [R6G][BETI] and [R6G][TPB] respectively, while it was >100 μM for the non-invasive MCF7 (Table 2.4). In contrast, the hydrophilic [R6G][OTf] and [R6G][Asc] inhibited cell proliferation

of both normal and breast cancer cell lines. A summary of the IC<sub>50</sub> values is displayed in Table 2.4.

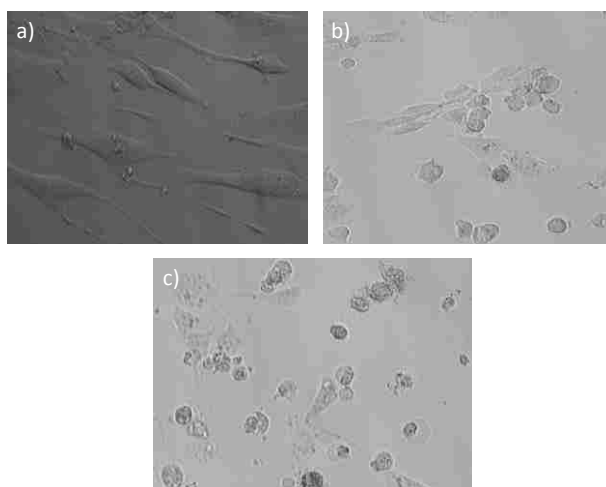


Figure 2.7. Light microscopy images of a) normal breast cell line, Hs578Bst and breast cancer cell lines b) Hs578T and c) MDA-MB-231 after treatment with 50  $\mu\text{M}$  [R6G][TPB] for 48h. Cell images were obtained using a light microscope equipped with a camera at a magnification of 20X.

Table 2.4 IC<sub>50</sub> ( $\mu\text{M}$ ) of R6G-based compounds towards breast cell lines

Compounds	Hs578Bst IC <sub>50</sub> ( $\mu\text{M}$ )	Hs578T IC <sub>50</sub> ( $\mu\text{M}$ )	MDA-MB-231 IC <sub>50</sub> ( $\mu\text{M}$ )	MCF7 IC <sub>50</sub> ( $\mu\text{M}$ )
[R6G][Asc]	10.2	21.0	5.0	13.3
[R6G][Cl]	34.6	19.2	5.1	30.7
[R6G][OTf]	40.6	18.6	10.2	14.2
[R6G][TPB]	-	25.6	12.2	>100
R6G][BETI]	-	23.8	11.4	>100

Using control experiments, it was observed that the cation, rhodamine 6G, inhibited cell proliferation of both normal and breast cancer cell lines in agreement with previous literature,<sup>6</sup> while the anions [Li][BETI] and [Na][TPB] were not observed to have a significant effect on any of the investigated cell lines (Figure 2.8). This definitively demonstrates that the cation and anion combination plays an active and cooperative role in the observed selective properties, particularly for hydrophobic compounds.

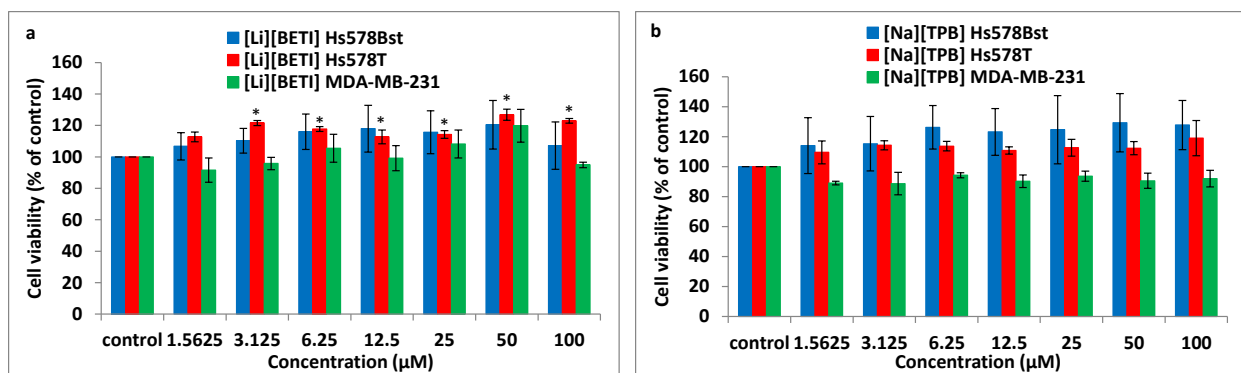


Figure 2.8. Cell viability assay of Hs578Bst, Hs578T and MDA-MB-231 cell lines upon treatment with 0–100 μM of a) [Li][BETI] and b) [Na][TPB] controls. \*Statistically different from control,  $P < 0.0001$  for [Li][BETI] Hs578T. Statistical analysis shows no difference from control for all the others ( $P > 0.05$ ).

Apoptosis is characterized by membrane blebbing, condensation of cytoplasm, and the initiation of an endogenous endonuclease. This nuclease cleaves double-stranded DNA generating mono- and oligonucleosomes. The result is an enrichment of mono- and oligonucleosomes in the cytoplasm of the apoptotic cell because DNA degradation occurs several hours before plasma membrane breakdown. Thus, the enrichment factor for apoptotic cells would be proportional to the concentration of an apoptosis inducing agent. Apoptosis is determined using a cell death ELISA kit. Results from our experiments indicate that [R6G][BETI] and [R6G][TPB] induce apoptosis as the enrichment factor increased with an increase in concentration of the nanoGUMBOS (Figure 2.9).

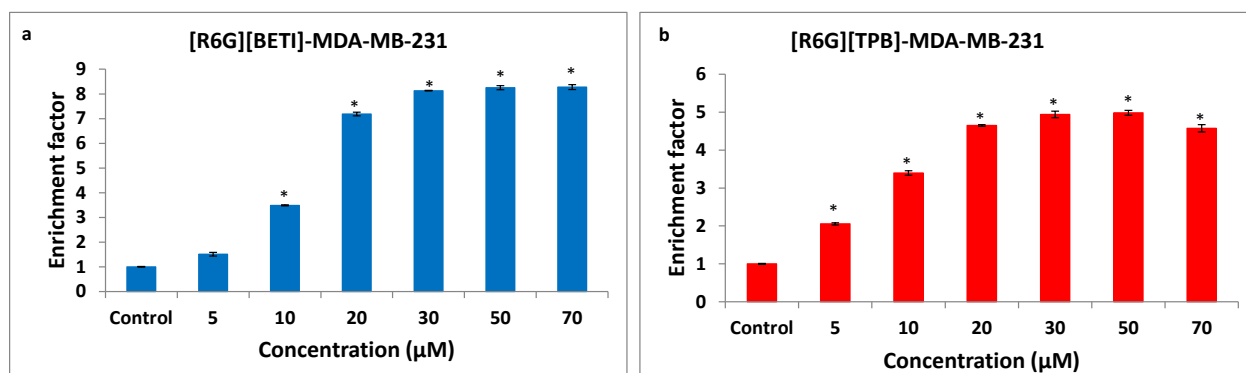


Figure 2.9. Effect of a) [R6G][BETI] and b) [R6G][TPB] on cell death of MDA-MB-231 breast cancer cells. MCF7 and Hs578T cancer cell lines displayed similar trends. The enrichment factor is the ratio of the absorbance of the sample (dying/dead cells) and the absorbance of the control (viable cells). \*Statistically different from control,  $P < 0.0001$ .

In addition, clonogenic assay revealed that [R6G][BETI] and [R6G][TPB] prevented colony formation of cancer cell lines when surviving cells were cultured after treatment with a low dosage of these two compounds (Figure 2.10). Thus, these compounds may be good candidates for further investigations as possible chemotherapeutic agents. Uptake of nanoparticles by individual cells is usually mediated by either non-specific or specific receptor interactions, commonly via endocytosis. The charge, hydrophobicity, and size of nanoparticles greatly influence this cellular uptake.<sup>47,48</sup> The [R6G][BETI] and [R6G][TPB] nanoparticles displayed a net negative surface charge as gauged by measurement of their zeta potentials.

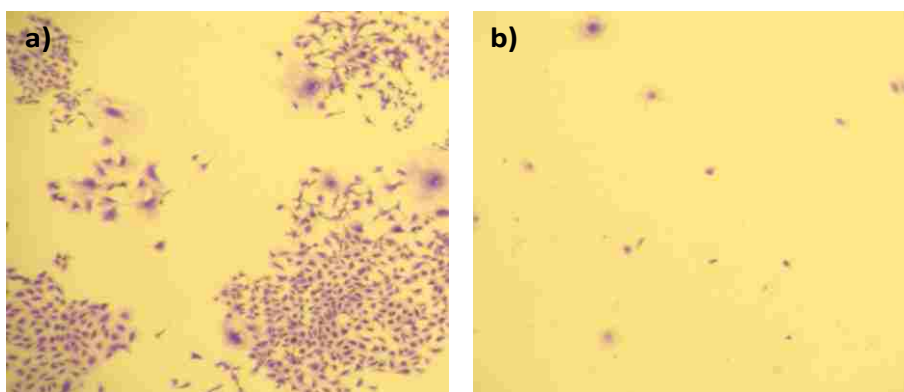


Figure 2.10. Clonogenic assay images of MDA-MB-231 breast cancer cells showing a) colonies formed from control wells and b) zero colonies formed in wells treated with 12.5  $\mu\text{M}$  [R6G][BETI]. Similar results were obtained for [R6G][TPB].

This charge was pH dependent, becoming more negative at physiological pH and less negative at acidic pH. Breast cancer cell lines have been found to have acidic extracellular pH ( $\sim 6.5$ )<sup>49</sup> in comparison to normal cells ( $\sim 7.4$ ).<sup>50</sup> From our results, at pH 6.5 the zeta potential of [R6G][BETI] and [R6G][TPB] were  $-9.9 \pm 0.9$  and  $-8.0 \pm 0.9$  mV respectively while at pH 7.4 they were  $-16.2 \pm 1.2$  and  $-17.8 \pm 1.5$  mV respectively. Since the cell membrane is negatively charged,<sup>27</sup> it is reasonable to expect that at pH 7.4, electrostatic repulsion between the nanoparticles (with high negative charge at this pH) and the cell membrane may lead to reduced uptake in normal breast cells. At lower values of pH, however, repulsive forces are reduced since

nanoGUMBOS possess less net negative surface charge and thus may have greater uptake in cancer cell lines. This uptake may be further enhanced via hydrophobic interactions with cancer cell membrane. This conclusion is supported by cellular uptake data in which MDA-MB-231 displayed a higher mean fluorescence intensities, in comparison to Hs578Bst, when the two cell lines were treated with the same concentrations of [R6G][BETI] and [R6G][TPB] nanoGUMBOS (Figure 2.11).

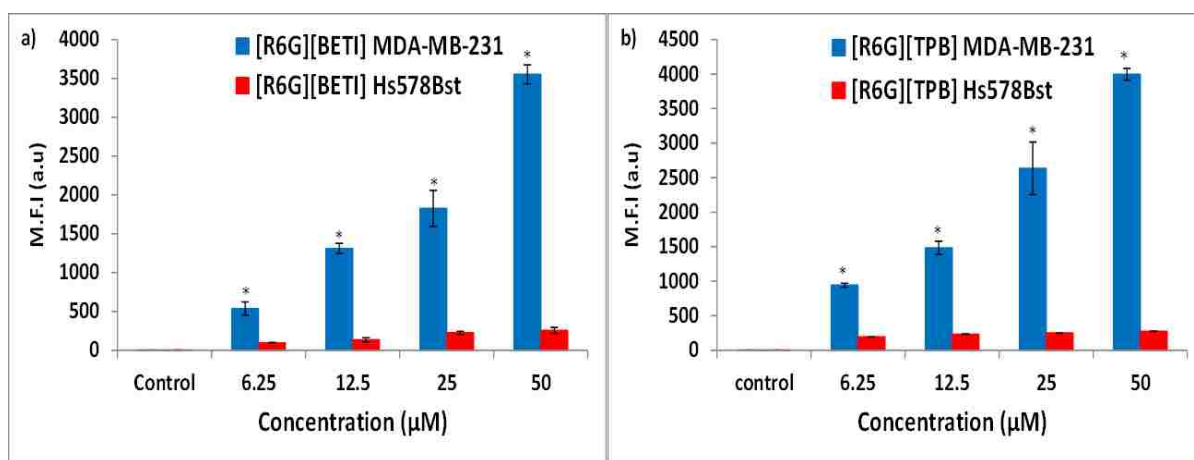


Figure 2.11. Mean Fluorescence intensity (M.F.I) of breast cancer cell line, MDA-MB-231 (blue) and normal breast cell line, Hs578Bst (red) treated with a) [R6G][BETI] and b) [R6G][TPB]. \*Statistically different from corresponding concentration in Hs578Bst for the same compound ( $P < 0.0001$ ).

Furthermore, the acidity of the extracellular pH value in cancer cells is primarily due to production of lactic acid, a consequence of increased glycolytic activity. This acidity is proportional to the number of cells as well as aggressiveness of the cell line.<sup>51</sup> For example, MCF7 which is non-invasive and less aggressive has been shown to acidify its extracellular environment to a lower extent in comparison to the more invasive and aggressive MDA-MB-231.<sup>51</sup> This is consistent with our results in which  $IC_{50}$  values for MCF7 were above 100 μM for the two compounds, while for MDA-MB-231 they were slightly above 10 μM as previously noted. We investigated this line of thought by conducting uptake experiments in the normal breast cell line at pH 6.5 for various concentrations of nanoGUMBOS. We observed a significant

improvement in uptake of at least two-fold (Figure 2.12). However, this improved uptake was still significantly lower in comparison to uptake in the breast cancer cell lines. This implies that there are other factors contributing to improved uptake in breast cancer cell lines. Studies to elucidate these other factors including possible differences in cell membranes of the various cell lines are ongoing in our laboratory.

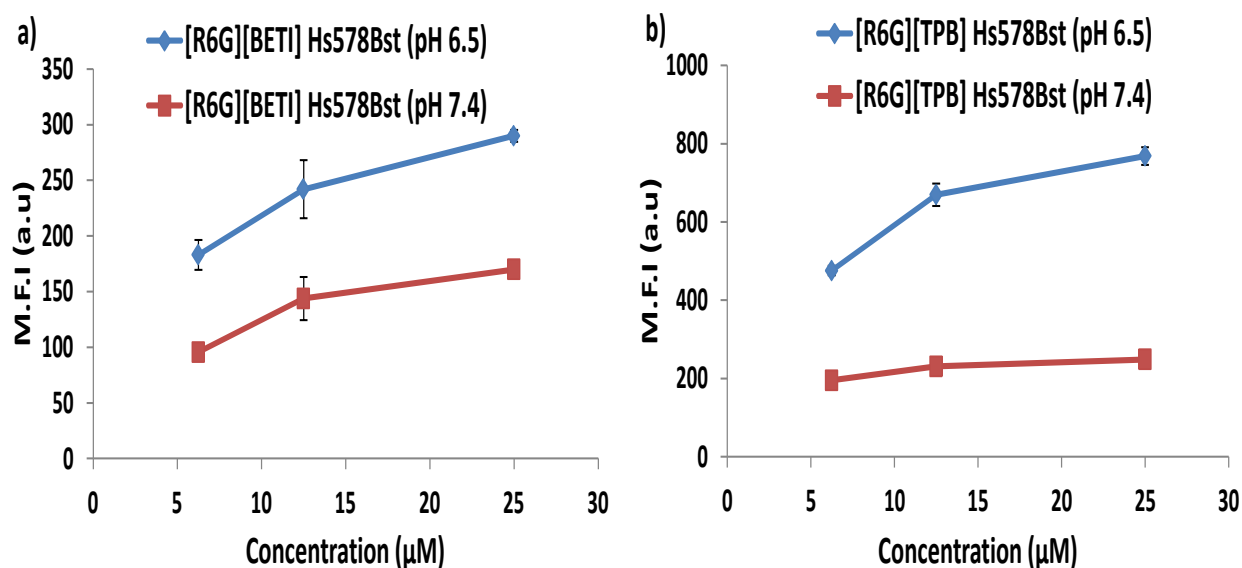


Figure 2.12. Mean Fluorescence intensity (M.F.I.) of normal breast cell line, Hs578Bst treated with a) [R6G][BETI] and b) [R6G][TPB] at a pH of 6.5 (blue) and 7.4 (red).

By use of confocal microscopy, the NanoGUMBOS were determined to primarily localize in the mitochondria (Figure 2.13). Thus, it is reasonable to expect that cell death could be a result of inhibition of mitochondrial function since this is the mechanism previously observed for rhodamine 6G.<sup>5,52</sup> This conclusion was examined by use of a Mitochondrial ToxGlo™ Assay (Promega Corporation) kit which predicts potential mitochondrial dysfunction upon exposure to various drugs. The kit consists of two major components. The first is a fluorogenic peptide substrate (bis- AAF-R110) which cannot cross membranes of live cells; hence its fluorescence is proportional to dead cells (cytotoxicity).<sup>53</sup>



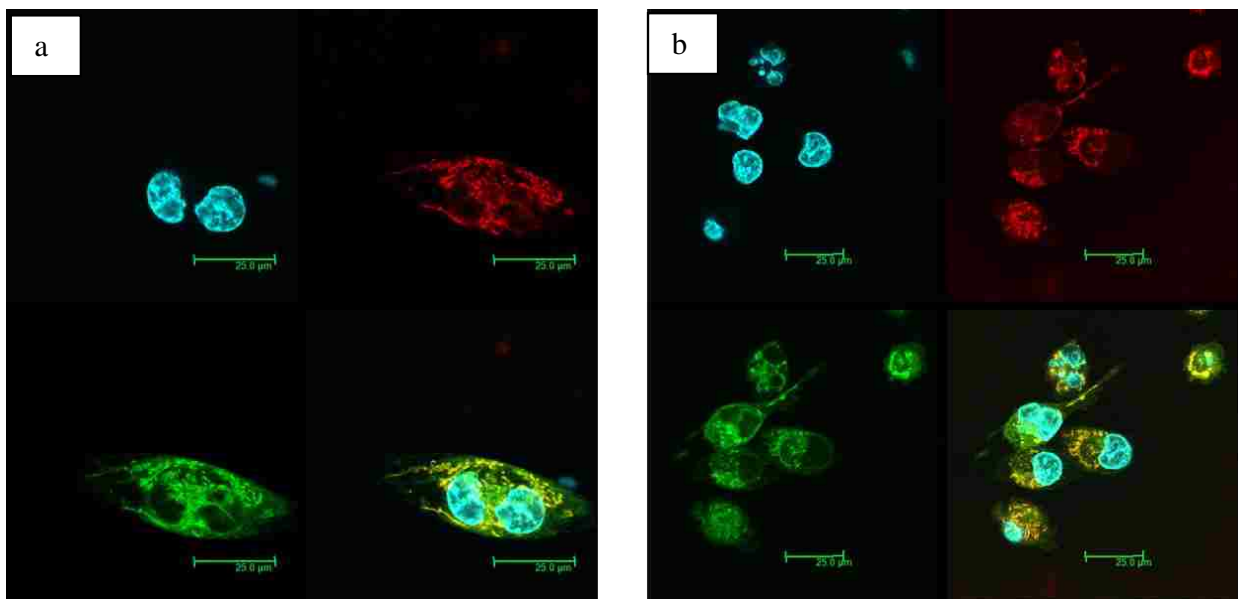


Figure 2.13. Confocal microscopy analysis of a) [R6G][BETI] and b) [R6G][TPB] in MDA-MB-231. The fluorescent images show the DAPI-labeled nucleus (blue), mitotracker deep red 633-labeled mitochondria (red), [R6G][BETI] or [R6G][TPB] (green) and a merged image that shows the two compounds mainly localize in the mitochondria.

The second component is an ATP detection reagent. This reagent lyses viable cells to release ATP, and in the process produces a luminescent signal that is proportional to the quantity of ATP present. Test compounds that inhibit oxidative phosphorylation lead to a decrease in ATP measured with either no change or discordant changes in cytotoxicity. In contrast, concordant decreases in ATP and increases in cytotoxicity are indicative of primary necrosis and hence are non-mitochondrial. Based on our observed results, ATP production was reduced with discordant changes in cytotoxicity of MDA-MB-231 cells exposed to [R6G][BETI] and [R6G][TPB] (Figure 2.14), indicating that these two compounds are mitochondrial toxins. Thus, we conclude that toxicity of these two compounds towards breast cancer cell lines result from inhibition of oxidative phosphorylation in the mitochondria of cancer cells as previously reported for rhodamine 6G.<sup>5,52</sup> This conclusion is consistent with the counter anion of rhodamine 6G playing a significant and cooperative role in the selectivity observed in the studies reported in this manuscript.

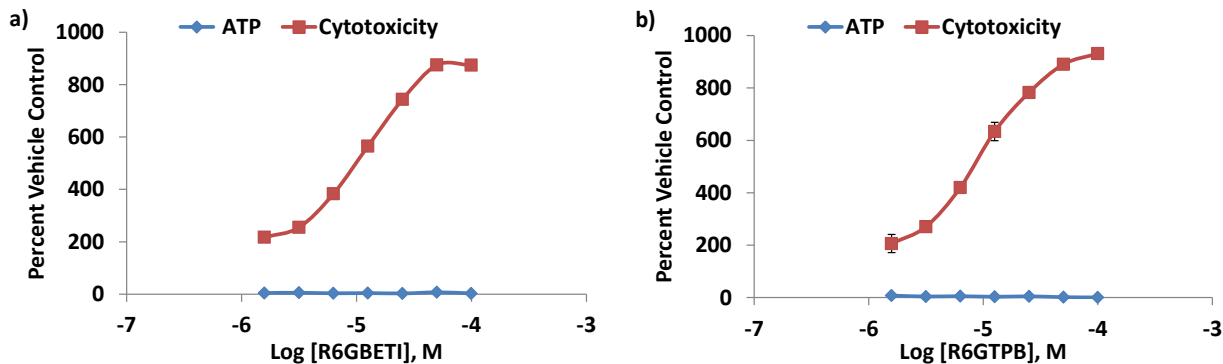


Figure 2.14. Profiles of mitochondrial toxicity of a) [R6G][BETI] and b) [R6G][TPB] using a Mitochondrial ToxGlo™ Assay. MDA-MB-231 cells were plated at 10,000 cells/ well and treated in serial dilutions of compounds resuspended in glucose free (galactose supplemented) DMEM media for 2 h. A reduction in ATP with discordant changes in membrane integrity (cytotoxicity) indicates that the two compounds are mitochondrial toxins.

## 2.4. Conclusion

In summary, we have synthesized and investigated the hydrophobic, luminescence, stability, and cellular uptake properties of novel fluorescent GUMBOS. In addition, nanoGUMBOS with an average size of approximately 100 nm in diameter were fabricated by use of a simple, rapid, reproducible, and additive-free reprecipitation method. We have demonstrated tunability of the physicochemical properties of these compounds. Most notably, this study has demonstrated that both the cation and anion in this class of compounds play an active and cooperative role in the observed selective anti-tumor cell proliferation potential. This is a remarkable finding since the effect of cationic compounds on normal and cancer cell lines has been studied for decades with no similar observations. Achieving selective anti-cancer activity simply by altering the anion of a known anti-cancer agent such as rhodamine 6G opens new avenues for research and discovery of inexpensive anti-cancer drugs since the synthetic routes outlined here for production of GUMBOS and nanoGUMBOS are rather simple. A particularly interesting aspect of this study is that this may be an approach which is generally applicable to other cationic compounds whose toxicities have been previously studied in detail. Finally, the luminescence properties of these compounds may allow the design of probes that

will help to visualize tumor cells for surgical removal, while at the same time inducing cell death in residual cancerous tissue.

## 2.5. References

1. Kelland, L., The resurgence of platinum-based cancer chemotherapy. *Nature Reviews Cancer* **2007**, *7*, 573-584.
2. Kawakami, M.; Koya, K.; Ukai, T.; Tatsuta, N.; Ikegawa, A.; Ogawa, K.; Shishido, T.; Chen, L. B., Structure-activity of novel rhodacyanine dyes as antitumor agents. *Journal of Medicinal Chemistry* **1998**, *41*, 130-142.
3. Abrams, M. J.; Picker, D. H.; Fackler, P. H.; Lock, C. J. L.; Howardlock, H. E.; Faggiani, R.; Teicher, B. A.; Richmond, R. C., Synthesis and structure of bis[rhodamine 123] tetrachloroplatinate dihydrate: the first tetrachloroplatinate(II) salt with anticancer activity. *Inorganic Chemistry* **1986**, *25*, 3980-3983.
4. Takaha, N.; Nakanishi, H.; Kimura, Y.; Hongo, F.; Kamoi, K.; Kawauchi, A.; Mizuno, M.; Yoshida, J.; Wakabayashi, T.; Miki, T., Significant induction of apoptosis in renal cell carcinoma cells transfected with cationic multilamellar liposomes containing the human interferon-beta gene through activation of the intracellular type 1 interferon signal pathway. *International Journal of Oncology* **2012**, *40*, 1441-1446.
5. Gear, A. R. L., Rhodamine 6g - potent inhibitor of mitochondrial oxidative-phosphorylation. *Journal of Biological Chemistry* **1974**, *249*, 3628-3637.
6. Lampidis, T. J.; Hasin, Y.; Weiss, M. J.; Chen, L. B., Selective killing of carcinoma-cells invitro by lipophilic-cationic compounds - a cellular basis. *Biomedicine and Pharmacotherapy* **1985**, *39*, 220-226.
7. Kurtoglu, M.; Lampidis, T. J., From delocalized lipophilic cations to hypoxia: Blocking tumor cell mitochondrial function leads to therapeutic gain with glycolytic inhibitors. *Molecular Nutrition & Food Research* **2009**, *53*, 68-75.
8. Chen, L. B.; Summerhayes, I. C.; Johnson, L. V.; Walsh, M. L.; Bernal, S. D.; Lampidis, T. J., Probing mitochondria in living cells with rhodamine 123. *Cold Spring Harbor Symposia on Quantitative Biology* **1982**, *46 Pt 1*, 141-155.
9. Johnson, L. V.; Walsh, M. L.; Chen, L. B., Localization of mitochondria in living cells with rhodamine-123. *Proceedings of the National Academy of Sciences of the United States of America-Biological Sciences* **1980**, *77*, 990-994.
10. Broutyboye, D.; Kolonias, D.; Wu, C. J.; Savaraj, N.; Lampidis, T. J., Relationship of multidrug-resistance to rhodamine-123 selectivity between carcinoma and normal epithelial-cells - taxol and vinblastine modulate drug efflux. *Cancer Research* **1995**, *55*, 1633-1638.
11. Hu, Y. P.; Moraes, C. T.; Savaraj, N.; Priebe, W.; Lampidis, T. J., Rho(0) tumor cells: A model for studying whether mitochondria are targets for rhodamine 123, doxorubicin, and other drugs. *Biochemical Pharmacology* **2000**, *60*, 1897-1905.

12. Lampidis, T. J.; Castello, C.; Delgiglio, A.; Pressman, B. C.; Viallet, P.; Trevorow, K. W.; Valet, G. K.; Tapiero, H.; Savaraj, N., Relevance of the chemical charge of rhodamine dyes to multiple-drug resistance. *Biochemical Pharmacology* **1989**, *38*, 4267-4271.
13. Lampidis, T. J.; Planas, L.; Tapiero, H., Selectivity of agents which modulate anthracycline and rhodamine resistance. *Proceedings of the American Association for Cancer Research* **1986**, *27*, 397-397.
14. Kasai, H.; Murakami, T.; Ikuta, Y.; Koseki, Y.; Baba, K.; Oikawa, H.; Nakanishi, H.; Okada, M.; Shoji, M.; Ueda, M.; Imahori, H.; Hashida, M., Creation of pure nanodrugs and their anticancer properties. *Angewandte Chemie International Edition* **2012**, *51*, 10315-10318.
15. de Rooy, S. L.; El-Zahab, B.; Li, M.; Das, S.; Broering, E.; Chandler, L.; Warner, I. M., Fluorescent one-dimensional nanostructures from a group of uniform materials based on organic salts. *Chemical Communications* **2011**, *47*, 8916-8918.
16. Das, S.; Bwambok, D.; Ei-Zahab, B.; Monk, J.; de Rooy, S. L.; Challa, S.; Li, M.; Hung, F. R.; Baker, G. A.; Warner, I. M., Nontemplated approach to tuning the spectral properties of cyanine-based fluorescent nanoGUMBOS. *Langmuir* **2010**, *26*, 12867-12876.
17. Tian, Z.; Wu, W.; Li, A. D. Q., Photoswitchable fluorescent nanoparticles: Preparation, properties and applications. *Chemphyschem* **2009**, *10*, 2577-2591.
18. Peng, A. D.; Xiao, D. B.; Ma, Y.; Yang, W. S.; Yao, J. N., Tunable emission from doped 1,3,5-triphenyl-2-pyrazoline organic nanoparticles. *Advanced Materials* **2005**, *17*, 2070-2073.
19. Anthony, J. E., Functionalized acenes and heteroacenes for organic electronics. *Chemical Reviews* **2006**, *106*, 5028-5048.
20. Bwambok, D. K.; El-Zahab, B.; Challa, S. K.; Li, M.; Chandler, L.; Baker, G. A.; Warner, I. M., Near-infrared fluorescent nanoGUMBOS for biomedical imaging. *ACS Nano* **2009**, *3*, 3854-3860.
21. Park, S.; Kwon, J. E.; Kim, S. H.; Seo, J.; Chung, K.; Park, S.-Y.; Jang, D.-J.; Medina, B. M.; Gierschner, J.; Park, S. Y., A white-light-emitting molecule: Frustrated energy transfer between constituent emitting centers. *Journal of the American Chemical Society* **2009**, *131*, 14043-14049.
22. Yoon, S.-J.; Chung, J. W.; Gierschner, J.; Kim, K. S.; Choi, M.-G.; Kim, D.; Park, S. Y., Multistimuli two-color luminescence switching via different slip-stacking of highly fluorescent molecular sheets. *Journal of the American Chemical Society* **2010**, *132*, 13675-13683.
23. An, B.-K.; Kwon, S.-K.; Park, S. Y., Photopatterned arrays of fluorescent organic nanoparticles. *Angewandte Chemie International Edition* **2007**, *46*, 1978-1982.
24. Breton, M.; Prevel, G.; Audibert, J.-F.; Pansu, R.; Tauc, P.; Le Pioufle, B.; Francais, O.; Fresnais, J.; Berret, J.-F.; Ishow, E., Solvatochromic dissociation of non-covalent

- fluorescent organic nanoparticles upon cell internalization. *Physical Chemistry Chemical Physics* **2011**, *13*, 13268-13276.
25. Haley, B.; Frenkel, E., Nanoparticles for drug delivery in cancer treatment. *Urologic Oncology: Seminars and Original Investigations* **2008**, *26*, 57-64.
  26. Cho, K.; Wang, X.; Nie, S.; Chen, Z.; Shin, D. M., Therapeutic nanoparticles for drug delivery in cancer. *Clinical Cancer Research* **2008**, *14*, 1310-1316.
  27. Kandela, I. K.; Lee, W.; Indig, G. L., Effect of the lipophilic/hydrophilic character of cationic triarylmethane dyes on their selective phototoxicity toward tumor cells. *Biotechnic and Histochemistry* **2003**, *78*, 157-169.
  28. Fraga-Dubreuil, J.; Famelart, M. H.; Bazureau, J. P., Ecofriendly fast synthesis of hydrophilic poly(ethyleneglycol)-ionic liquid matrices for liquid-phase organic synthesis. *Org. Process Res. Dev.* **2002**, *6*, 374-378.
  29. Akdogan, Y.; Junk, M. J. N.; Hinderberger, D., Effect of ionic liquids on the solution structure of human serum albumin. *Biomacromolecules* **2011**, *12*, 1072-1079.
  30. Tesfai, A.; El-Zahab, B.; Kelley, A. T.; Li, M.; Garno, J. C.; Baker, G. A.; Warner, I. M., Magnetic and nonmagnetic nanoparticles from a group of uniform materials based on organic salts. *ACS Nano* **2009**, *3*, 3244-3250.
  31. Biagi, G. L.; Recanatini, M.; Barbaro, A. M.; Borea, P. A., Lipophilicity estimation of drugs. *Process Control and Quality* **1997**, *10*, 129-149.
  32. Kasai, H.; Nalwa, H. S.; Oikawa, H.; Okada, S.; Matsuda, H.; Minami, N.; Kakuta, A.; Ono, K.; Mukoh, A.; Nakanishi, H., A novel preparation method of organic microcrystals. *Japanese Journal of Applied Physics Part 2* **1992**, *31*, L1132-L1134.
  33. Magde, D.; Wong, R.; Seybold, P. G., Fluorescence quantum yields and their relation to lifetimes of rhodamine 6g and fluorescein in nine solvents: Improved absolute standards for quantum yields. *Photochemistry and Photobiology* **2002**, *75*, 327-334.
  34. Williams, A. T. R.; Winfield, S. A.; Miller, J. N., Relative fluorescence quantum yields using a computer- controlled luminiscence spectrometer. *Analyst* **1983**, *108*, 1067-1071.
  35. Lee, S. H.; Lee, S. B., Octanol/water partition coefficients of ionic liquids. *Journal of Chemical Technology and Biotechnology* **2009**, *84*, 202-207.
  36. Franken, N. A. P.; Rodermond, H. M.; Stap, J.; Haveman, J.; van Bree, C., Clonogenic assay of cells in vitro. *Nature Protocols* **2006**, *1*, 2315-2319.
  37. Vader, P.; van der Aa, L. J.; Engbersen, J. F. J.; Storm, G.; Schiffelers, R. M., A method for quantifying cellular uptake of fluorescently labeled siRNA. *Journal of Controlled Release* **2010**, *148*, 106-109.
  38. Lopez-Martin, I.; Burello, E.; Davey, P. N.; Seddon, K. R.; Rothenberg, G., Anion and cation effects on imidazolium salt melting points: A descriptor modelling study. *Chemphyschem* **2007**, *8*, 690-695.
  39. Larsen, A. S.; Holbrey, J. D.; Tham, F. S.; Reed, C. A., Designing ionic liquids: Imidazolium melts with inert carborane anions. *Journal of the American Chemical Society* **2000**, *122*, 7264-7272.

40. Kamlet, M. J.; Abraham, M. H.; Doherty, R. M.; Taft, R. W., Solubility properties in polymers and biological media.4. Correlation of octanol water partition- coefficients with solvatochromic parameters. *Journal of the American Chemical Society* **1984**, *106*, 464-466.
41. Kasha, M.; Rawls, H. R.; Ashraf El-Bayoum, M., The exciton model in molecular spectroscopy. *Pure and Applied Chemistry* **1965**, *11*, 371-392.
42. Kumar, V.; Baker, G. A.; Pandey, S., Ionic liquid-controlled J- versus H-aggregation of cyanine dyes. *Chemical Communications* **2011**, *47*, 4730-4732.
43. An, B. K.; Kwon, S. K.; Jung, S. D.; Park, S. Y., Enhanced emission and its switching in fluorescent organic nanoparticles. *Journal of the American Chemical Society* **2002**, *124*, 14410-14415.
44. Jelley, E. E., Spectral absorption and fluorescence of dyes in the molecular state. *Nature* **1936**, *138*, 1009-1010.
45. Williams, A. T. R.; Winfield, S. A.; Miller, J. N., Relative fluorescence quantum yields using a computer-controlled luminescence spectrometer. *Analyst* **1983**, *108*, 1067-1071.
46. Takae, S.; Akiyama, Y.; Otsuka, H.; Nakamura, T.; Nagasaki, Y.; Kataoka, K., Ligand density effect on biorecognition by pegylated gold nanoparticles: Regulated interaction of RCA (120) lectin with lactose installed to the distal end of tethered peg strands on gold surface. *Biomacromolecules* **2005**, *6*, 818-824.
47. Gratton, S. E. A.; Ropp, P. A.; Pohlhaus, P. D.; Luft, J. C.; Madden, V. J.; Napier, M. E.; DeSimone, J. M., The effect of particle design on cellular internalization pathways. *Proceedings of the National Academy of Sciences of the United States of America* **2008**, *105*, 11613-11618.
48. Sahay, G.; Kim, J. O.; Kabanov, A. V.; Bronich, T. K., The exploitation of differential endocytic pathways in normal and tumor cells in the selective targeting of nanoparticulate chemotherapeutic agents. *Biomaterials* **2010**, *31*, 923-933.
49. Du, J.-Z.; Du, X.-J.; Mao, C.-Q.; Wang, J., Tailor-made dual ph-sensitive polymer-doxorubicin nanoparticles for efficient anticancer drug delivery. *Journal of the American Chemical Society* **2011**, *133*, 17560-17563.
50. Zhang, X.; Lin, Y.; Gillies, R. J., Tumor ph and its measurement. *Journal of Nuclear Medicine* **2010**, *51*, 1167-1170.
51. Montcourrier, P.; Silver, I.; Farnoud, R.; Bird, I.; Rochefort, H., Breast cancer cells have a high capacity to acidify extracellular milieu by a dual mechanism. *Clinical & Experimental Metastasis* **1997**, *15*, 382-392.
52. Darzynkiewicz, Z.; Traganos, F.; Staianocoico, L.; Kapuscinski, J.; Melamed, M. R., Interactions of rhodamine-123 with living cells studied by flow-cytometry. *Cancer Research* **1982**, *42*, 799-806.
53. Niles, A. L.; Moravec, R. A.; Hesselberth, P. E.; Scurria, M. A.; Daily, W. J.; Riss, T. L., A homogeneous assay to measure live and dead cells in the same sample by detecting different protease markers. *Analytical Biochemistry* **2007**, *366*, 197-206.

## CHAPTER 3. PHOSPHONIUM-DYSPROSIUM DERIVED NANOPARTICLES WITH CANCER TARGETING PROPERTIES

### 3.1. Introduction

Nanoparticles for biomedical applications have recently gained increased attention among researchers.<sup>1-5</sup> This is driven by the various inherent advantages of nanoparticles including increased length of circulation in blood, improved intracellular penetration, and better retention and accumulation in tumors due to enhanced permeability and retention effect.<sup>6-8</sup> Much effort has been directed towards attaching ligands for guiding these nanoparticles toward diseased organelles. Therefore, functionalized nanoparticles are desirable for targeted drug delivery. Some functions of nanoparticles currently being explored, whether individually or in combination, include nanoparticles attached to surface enhanced cell penetrating molecules, specific organelle targeting molecules, increased stability, response to local stimuli such as pH, and fluorescence capability to allow intracellular visualization among others.<sup>9</sup> Many of these functions are incorporated into nanocarriers such as liposomes, micelles, nanoemulsions, and polymeric nanoparticles.<sup>10,11</sup> However, development of multifunctional nanocarriers requires much effort, engineering, and cost in order to incorporate all desired properties. It is worth noting that each functionality introduced increases complexity, size of the nanoparticle, and cost of production.<sup>9</sup> To overcome these challenges, it is best to incorporate anticipated properties into small molecules prior to nanoparticle synthesis.<sup>8</sup> Hence, it is imperative that compounds synthesized for such nanoparticles possess the preferred properties. This goal requires a class of compounds amenable to tunability.

Ionic liquids (ILs), defined as organic salts with melting points below 100 °C, fit this criteria because they possess tunable properties such as melting points, hydrophobicity, solubility, and thermal stability among others.<sup>12</sup> As a result of tunability, ionic liquids have found

applications in varied fields such as electrochemistry<sup>13</sup>, solar cells,<sup>14</sup> and solvents in industry,<sup>15</sup> and they have very recently been investigated for therapeutic purposes, especially cancer. Several reports have emerged on toxicity of ILs as well as anticancer properties.<sup>16-18</sup> Recently, it was demonstrated that the toxicity of ILs is controlled by several inherent properties of the IL. These include the alkyl chain length in the cation, extent and type of functionalization on the side chain of the cation, chemical nature of the ions, and combined influence of anion and cation.<sup>17</sup> The ionic nature of ionic liquids allows the incorporation of complementary properties in the cation and anion. Using this concept, we recently synthesized and reported a series of organic salts that are solids at room temperature with multifunctional properties for biomedical applications.<sup>18,19</sup> These salts are referred to as a group of uniform materials based on organic salts (GUMBOS). They are similar to ionic liquids in terms of properties and tunability, but unlike ionic liquids, they are solid phase materials with wider melting point ranges between 25 °C and 250 °C.<sup>18</sup> From this definition, it should be obvious that there is an overlap with frozen ionic liquids, which are defined as having melting points between 25 °C and 100 °C.

In this study, multifunctional compounds were designed for therapeutic purposes from aryltriphenylphosphonium-dysprosium thiocyanate salts. The properties incorporated include tumor targeting, magnetism, and luminescence. These compounds were designed to derive fluorescence and paramagnetism from the dysprosium thiocyanate moiety, and mitochondrial cancer targeting property from the phosphonium group.<sup>19</sup> It is important to note that delocalized phosphonium cations have been investigated and reported to have anticancer properties by preferentially accumulating in the mitochondria due to the unusually high mitochondrial membrane potential.<sup>20,21</sup> Upon accumulation, they inhibit oxidative phosphorylation, necessary for energy production in tumor cells, and thus prevent production of adenosine triphosphate



required for normal cellular function.<sup>22-24</sup> Here, we extend this study to nanoparticles derived from these compounds and evaluate their efficacy in cancer cell lines *in vitro*. To achieve this, we had to ensure that the multifunctional properties are retained in the nanoscale through various characterization techniques. In this study, we report drastically improved half maximal inhibitory concentration (IC<sub>50</sub>) values in comparison to those earlier reported for the bulk material,<sup>19</sup> indicating that these phosphonium-dysprosium nanoparticles may be potentially better chemotherapeutic agents than their respective bulk material.

## **3.2. Materials and Methods**

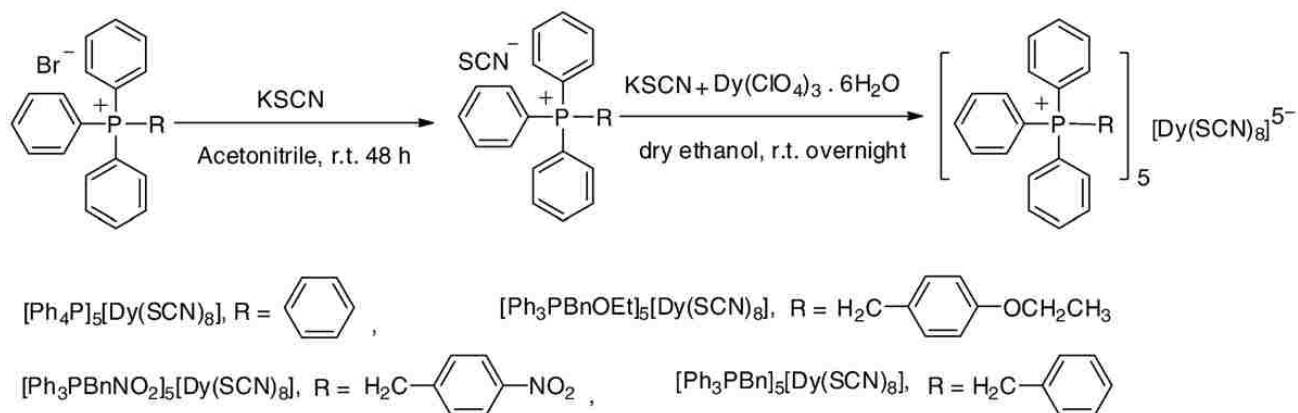
### **3.2.1. Materials**

Tetraphenylphosphonium bromide (98.0%), benzyltriphenylphosphonium bromide (97.0%), (4-ethoxybenzyl)triphenyl phosphonium bromide (98.0%), and (4-nitrobenzyl)triphenyl phosphonium bromide (98.0%) were obtained from TCI America (Portland, Oregon, USA). Potassium thiocyanate, dysprosium (III) oxide, and perchloric acid (70%) were obtained from Sigma-Aldrich (Sigma-Aldrich, Milwaukee, Wisconsin, USA) and used as purchased. Anhydrous grade ethanol, methanol, acetonitrile, chloroform, and carbon tetrachloride were obtained from Sigma Aldrich (Sigma-Aldrich, Milwaukee, WI), and all other high performance liquid chromatography (HPLC) grade organic solvents such as acetone, hexane, and water were obtained from J.T. Baker (J. T. Baker, Phillipsburg, NJ). Normal human breast fibroblast cells (Hs578Bst, ATCC no. HTB-125), human breast carcinoma cells (Hs578T, ATCC no. HTB-126), hormone-independent human breast carcinoma cells (MDA-MB-231, ATCC no. HTB-26), human pancreatic carcinoma cells (PANC-1, ATCC no. CRL-1469), and human colorectal adenocarcinoma cells (HT-29, ATCC no. HTB-38) were obtained from the American Tissue

Culture Collection (ATCC, Manassas, VA) and grown to 90% confluence according to ATCC protocol.

### 3.2.2. Synthesis and Characterization of the Phosphonium-dysprosium Salts

Phosphonium-dysprosium salts ( $[\text{Ph}_4\text{P}]_5[\text{Dy}(\text{SCN})_8]$ ,  $[\text{Ph}_3\text{PBnOEt}]_5[\text{Dy}(\text{SCN})_8]$ ,  $[\text{Ph}_3\text{PBnNO}_2]_5[\text{Dy}(\text{SCN})_8]$ , and  $[\text{Ph}_3\text{PBn}]_5[\text{Dy}(\text{SCN})_8]$ ) were synthesized and characterized as previously described.<sup>19</sup> Briefly, the following steps were adopted for synthesis of all the phosphonium-dysprosium salts: In the first step, the four intermediate compounds ( $[\text{Ph}_4\text{P}][\text{SCN}]$ ,  $[\text{Ph}_3\text{PBnOEt}][\text{SCN}]$ ,  $[\text{Ph}_3\text{PBnNO}_2][\text{SCN}]$ , and  $[\text{Ph}_3\text{PBn}][\text{SCN}]$ ) were synthesized via a facile metathesis reaction between the respective phosphonium bromide (1 equiv.) and KSCN (2 equiv.) in acetonitrile at room temperature for 2 days.<sup>25,26</sup> Dissolving  $\text{Dy}_2\text{O}_3$  in 70%  $\text{HClO}_4$  aqueous solution afforded  $\text{Dy}(\text{ClO}_4)_3 \cdot 6\text{H}_2\text{O}$ , which was lyophilized to remove residual water.<sup>25</sup> In the second step, ( $[\text{Ph}_4\text{P}]_5[\text{Dy}(\text{SCN})_8]$ ,  $[\text{Ph}_3\text{PBnOEt}]_5[\text{Dy}(\text{SCN})_8]$ ,  $[\text{Ph}_3\text{PBnNO}_2]_5[\text{Dy}(\text{SCN})_8]$ , and  $[\text{Ph}_3\text{PBn}]_5[\text{Dy}(\text{SCN})_8]$ ) products were synthesized according to a previously reported protocol with slight modifications.<sup>25,26</sup> As an example, in a typical reaction, a mixture of  $[\text{Ph}_4\text{P}][\text{SCN}]$  (5 equiv.), KSCN (3 equiv.), and  $\text{Dy}(\text{ClO}_4)_3 \cdot 6\text{H}_2\text{O}$  (1 equiv.) was stirred at room temperature overnight in absolute ethanol. The  $\text{KClO}_4$  byproduct (white suspension) was removed by filtration, and ethanol evaporated. The residue was re-dissolved in dry dichloromethane (DCM) and the solution allowed to stand overnight in a refrigerator. Filtration and evaporation of DCM under vacuum afforded the products which were further dried by lyophilization. Scheme 3.1 displays the structures and the synthesis procedure outlined here. The four products were characterized by use of  $^1\text{H}$ ,  $^{13}\text{C}$ , and  $^{31}\text{P}$  NMR, FT-IR, and C, H, N, S elemental analysis.



Scheme 3.1. Synthesis of phosphonium-dysprosium compounds.

### 3.2.3. Synthesis and Characterization of Nanoparticles from Phosphonium-dysprosium Salts

Nanoparticles derived from  $[\text{Ph}_4\text{P}]_5[\text{Dy}(\text{SCN})_8]$ ,  $[\text{Ph}_3\text{PBnOEt}]_5[\text{Dy}(\text{SCN})_8]$ ,  $[\text{Ph}_3\text{PBnNO}_2]_5[\text{Dy}(\text{SCN})_8]$ , and  $[\text{Ph}_3\text{PBn}]_5[\text{Dy}(\text{SCN})_8]$  were synthesized via previously reported template free reprecipitation method with slight modifications.<sup>18,27,28</sup> The synthesis of  $[\text{Ph}_4\text{P}]_5[\text{Dy}(\text{SCN})_8]$  nanoparticles is described as an example. Briefly, 1 mM  $[\text{Ph}_4\text{P}]_5[\text{Dy}(\text{SCN})_8]$  was prepared by dissolving in acetonitrile. A 100  $\mu\text{L}$  aliquot of this solution was rapidly injected into 5 mL deionized water under sonication for 5 min. The resulting nanoparticles were left to age in the dark for 1 h followed by freeze drying to remove water. This process was repeated several times to accumulate enough nanoparticles. Particle sizes and images was determined by use of transmission electron microscopy (TEM) using an LVEM5 transmission electron microscope (DeLong America, Montreal, Canada). The TEM sample was prepared on a carbon-coated copper grid (CF400-Cu, Electron Microscopy Sciences, Hatfield, PA). Zeta potentials were determined using Zetasizer Nano ZS (Malvern Instruments, UK).

### 3.2.4. Magnetic Properties

Magnetic properties were determined using a Quantum Design Superconducting Quantum Interference Device (SQUID) magnetometer (San Diego, CA, USA) at temperatures between 5 and 300 K at a magnetic field of 10,000 Oe.

### 3.2.5. UV-Vis Absorption and Fluorescence Spectroscopy

UV-Vis spectra were collected using a Shimadzu UV-3101 PC UV-Vis-near-IR scanning spectrophotometer (Shimadzu, Columbia, MD). A 0.4 cm<sup>2</sup> quartz cuvette (Starna Cells, Atascadero, CA) was used to collect absorbance relative to an identical cell filled with the relevant solvent as the blank. Steady-state fluorescence measurements were recorded at room temperature by use of a Spex Fluorolog-3 spectrofluorometer (model FL3-22TAU3; Jobin Yvon, Edison, NJ) equipped with a 450-W xenon lamp and R928P photomultiplier tube (PMT) emission detector. Fluorescence emission spectra were collected in a 0.4 cm<sup>2</sup> quartz cuvette with slit widths set for entrance exit bandwidths of 4 nm on both excitation and emission monochromators.

### 3.2.6. Cell Studies

*In vitro* experiments employed normal human breast fibroblast cells (Hs578Bct, ATCC no. HTB-125), human breast carcinoma cells (Hs578T, ATCC no. HTB-126), hormone-independent human breast carcinoma cells (MDA-MB-231, ATCC no. HTB-26), human pancreatic carcinoma cells (PANC-1, ATCC no. CRL-1469), and human colorectal adenocarcinoma cells (HT-29, ATCC no. HTB-38) obtained from the American Tissue Culture Collection (ATCC, Manassas, VA). The cells were grown to 90% confluence prior to any experiments according to ATCC's protocol. Cytotoxicities of the nanoparticles towards each cell line were determined by MTS Assay kit (Promega Corporation, Madison, WI, USA) according to the manufacturer's protocol. Approximately 5,000 cells in 0.1 mL culture medium were seeded to each well in a 96-well plate. After 24 h, the culture medium was removed and discarded, followed by addition of 0.1 mL culture medium containing 0-400 μM of the nanoparticles. The cells were then incubated for 48 h at 37 °C in a humidified atmosphere

containing 5% CO<sub>2</sub>. At the end of the incubation period, the cells were treated with 20 µL MTS and incubated for 1 h. Absorbance measurements were recorded at 490 nm using a microplate spectrophotometer (Benchmark plus Bio-Rad Laboratories, Hercules, CA, USA). Cell viability as a percentage was determined by computing the ratio between absorbance of the treated cells and the absorbance of untreated (control) cells taken as 100%. The concentration at which 50% cell proliferation was inhibited (IC<sub>50</sub>) was computed using a linear fit equation of the linear part of the cell viability graphs. If the linear portion of the graph did not include 50% cell viability, IC<sub>50</sub> was assumed to be higher than the minimum concentration for which constant cytotoxicity was attained irrespective of the increase in concentration. The IC<sub>50</sub> values were used to compare cytotoxicities of the various compounds and their corresponding nanoparticles. All experiments were performed at least three times and the data was expressed as mean ± SD.

Clonogenic assay was performed according to a procedure described by Franken et al., with slight modifications.<sup>29</sup> Briefly, MDA-MB-231 was cultured in triplicate in 6-well plates at a density of 50 cells/ well and allowed to attach for two hours. Cells were then incubated with the test compound for 48h. Control wells contained cells without treatment. The medium was replaced with fresh culture medium. Cells incubated and allowed to form colonies over a period of one week. Finally, cells were fixed with glutaraldehyde (6% v/v), stained with crystal violet (0.5 % w/v), and counted using a stereomicroscope.

### **3.2.7. Statistics**

Statistical analysis was performed using one-way analysis of variance (ANOVA). Tukey's studentized range test was performed to ascertain the significant difference between treatments within the 95% confidence interval using SAS 9.2 software (SAS, Cary, NC, USA). P < 0.05 was considered to indicate statistical significance. All data are expressed as mean ± SD.

### 3.3. Results and Discussion

#### 3.3.1. Synthesis and Characterization of the Phosphonium-dysprosium Compounds

Characterization of the phosphonium-dysprosium compounds by of  $^1\text{H}$ ,  $^{13}\text{C}$ , and  $^{31}\text{P}$  NMR, FT-IR (Figure 3.1-3.4), and C, H, N, S elemental analysis gave results consistent with expectations as follows:

$[\text{Ph}_4\text{P}]_5[\text{Dy}(\text{SCN})_8]$ , pale brown solid. Yield, 76%. Mp: 172-175  $^\circ\text{C}$ .  $^1\text{H}$  NMR (400 MHz,  $\text{DMSO-d}_6$ ),  $\delta$  (ppm): 7.98 (t, 4H), 7.80 (m, 8H), 7.73 (m, 8H).  $^{13}\text{C}$  NMR (100 MHz,  $\text{DMSO-d}_6$ ),  $\delta$  (ppm): 115.8, 135.1, 135.0, 129.3, 118.6, 117.7.  $^{31}\text{P}$  NMR (101 MHz,  $\text{DMSO-d}_6$ ),  $\delta$  (ppm): 23.0. IR (neat),  $\nu$  ( $\text{cm}^{-1}$ ): 2910, 2855, 2039, 1435, 1107, 839, 672. Anal. Calcd for  $\text{C}_{128}\text{H}_{100}\text{DyN}_8\text{P}_5\text{S}_8$ : C, 66.15; H, 4.34; N, 4.82; S, 11.04. Found: C, 66.22; H, 4.35; N, 4.78; S, 10.98. In the FT-IR spectra below, the peak around 2052  $\text{cm}^{-1}$  is attributed to  $\gamma_{\text{CN}}$  vibration of  $\text{SCN}^-$  (Figure 3.1).

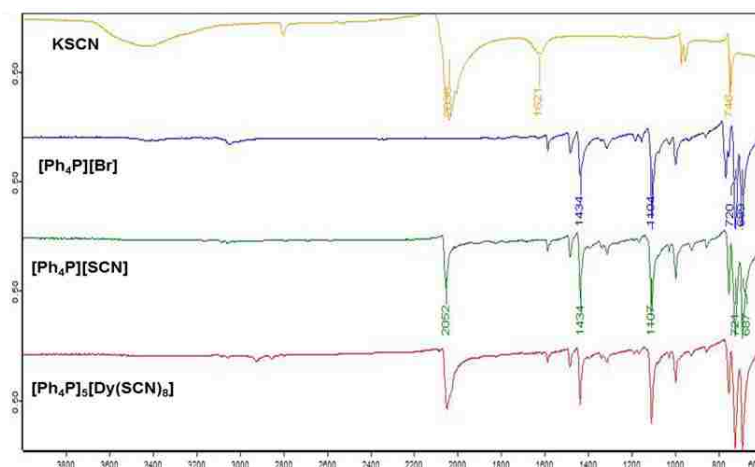


Figure 3.1. FT-IR spectra of KSCN,  $[\text{Ph}_4\text{P}][\text{Br}]$ ,  $[\text{Ph}_4\text{P}][\text{SCN}]$ ,  $[\text{Ph}_4\text{P}]_5[\text{Dy}(\text{SCN})_8]$ .

$[\text{Ph}_3\text{PBn}]_5[\text{Dy}(\text{SCN})_8]$ , pale yellow solid. Yield, 81%. Mp: 50-52  $^\circ\text{C}$ .  $^1\text{H}$  NMR (400 MHz,  $\text{DMSO-d}_6$ ),  $\delta$  (ppm): 7.89 (t, 3H,  $J=8\text{Hz}$ ), 7.56 (m, 6H), 7.45 (m, 6H), 7.33 (m, 2H), 7.23 (m, 2H), 7.13 (d, 1H), 5.23 (s, 1H), 5.21 (s, 1H).  $^{13}\text{C}$  NMR (100 MHz,  $\text{DMSO-d}_6$ ),  $\delta$  (ppm): 135.6, 135.5, 134.3, 131.3, 131.2, 130.6, 130.5, 129.3, 129.0, 128.4, 128.3, 118.7, 117.8, 80.0,

28.8, 28.4.  $^{31}\text{P}$  NMR (101 MHz, DMSO- $d_6$ ),  $\delta$  (ppm): 24.0. IR (neat),  $\nu$  ( $\text{cm}^{-1}$ ): 2912, 2852, 2035, 1436, 1112, 724, 687. Anal. Calcd for  $\text{C}_{133}\text{H}_{110}\text{DyN}_8\text{P}_5\text{S}_8$ : C, 66.72; H, 4.63; N, 4.68; S, 10.71. Found: C, 66.01; H, 4.83; N, 4.21; S, 10.62.

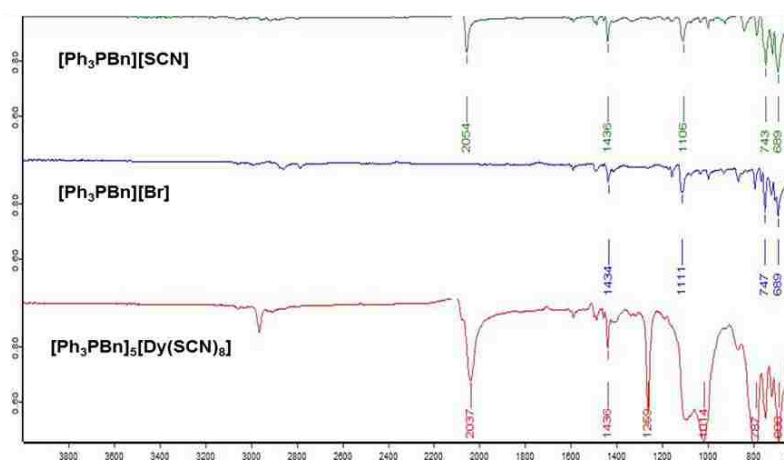


Figure 3.2. FT-IR spectra of  $[\text{Ph}_3\text{PBn}][\text{Br}]$ ,  $[\text{Ph}_3\text{PBn}][\text{SCN}]$ ,  $[\text{Ph}_3\text{PBn}]_5[\text{Dy}(\text{SCN})_8]$ .

$[\text{Ph}_3\text{PBnNO}_2]_5[\text{Dy}(\text{SCN})_8]$ , pale brown solid. Yield, 79%. Mp: 64-67  $^\circ\text{C}$ .  $^1\text{H}$  NMR (400 MHz, DMSO- $d_6$ ),  $\delta$  (ppm): 8.08 (d, 2H,  $J=8\text{Hz}$ ), 7.91 (m, 2H), 7.75 (m, 13H), 7.26 (dd, 2H), 5.53 (s, 1H), 5.48 (s, 1H).  $^{13}\text{C}$  NMR (100 MHz, DMSO- $d_6$ ),  $\delta$  (ppm): 147.8, 136.6, 136.5, 135.8, 134.6, 134.5, 132.6, 132.5, 130.8, 130.7, 130.0, 124.3, 118.1, 117.3, 28.7, 28.2.  $^{31}\text{P}$  NMR (101 MHz, DMSO- $d_6$ ),  $\delta$  (ppm): 24.5. IR (neat),  $\nu$  ( $\text{cm}^{-1}$ ): 2921, 2846, 2042, 1439, 720, 689. Anal. Calcd for  $\text{C}_{138}\text{H}_{105}\text{DyN}_{13}\text{P}_5\text{S}_8$ : C, 60.99; H, 4.04; N, 6.95; S, 9.79. Found: C, 60.46; H, 3.95; N, 6.79; S, 9.73.

$[\text{Ph}_3\text{PBnOEt}]_5[\text{Dy}(\text{SCN})_8]$ , pale yellow solid. Yield, 72%. Mp: 45-48  $^\circ\text{C}$ .  $^1\text{H}$  NMR (400 MHz, DMSO- $d_6$ ),  $\delta$  (ppm): 7.89 (t, 3H,  $J=8\text{Hz}$ ), 7.72 (m, 6H), 7.63 (m, 6H), 6.86 (dd, 2H), 6.73 (dd, 2H), 5.13 (s, 1H), 5.10 (s, 1H), 3.93 (q, 2H,  $J=8\text{Hz}$ ), 1.26 (t, 3H,  $J=8\text{Hz}$ ).  $^{13}\text{C}$  NMR (100 MHz, DMSO- $d_6$ ),  $\delta$  (ppm): 158.9, 135.5, 134.6, 134.5, 132.5, 132.4, 130.6, 130.5, 129.9, 119.5, 119.4, 118.9, 118.0, 115.1, 28.2, 27.7, 15.0.  $^{31}\text{P}$  NMR (101 MHz, DMSO- $d_6$ ),  $\delta$  (ppm): 23.0. IR

(neat),  $\nu$  ( $\text{cm}^{-1}$ ): 2923, 2859, 2038, 1435, 1106, 722, 691. Anal. Calcd for  $\text{C}_{143}\text{H}_{130}\text{DyN}_8\text{O}_5\text{P}_5\text{S}_8$ : C, 65.69; H, 5.01; 4.29; S, 9.81. Found: C, 66.58; H, 5.13; N, 4.20, S, 9.56.

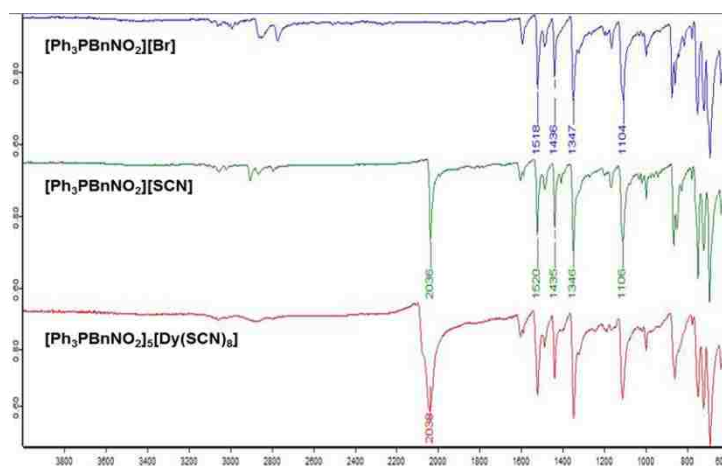


Figure 3.3. FT-IR spectra of  $[\text{Ph}_3\text{PBnNO}_2][\text{Br}]$ ,  $[\text{Ph}_3\text{PBnNO}_2][\text{SCN}]$ ,  $[\text{Ph}_3\text{PBnNO}_2]_5[\text{Dy}(\text{SCN})_8]$ .

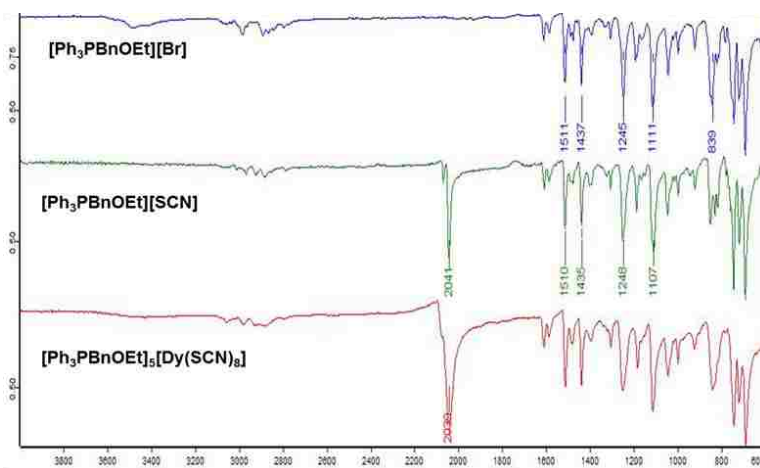


Figure 3.4. FT-IR spectra of  $[\text{Ph}_3\text{PBnOEt}][\text{Br}]$ ,  $[\text{Ph}_3\text{PBnOEt}][\text{SCN}]$ ,  $[\text{Ph}_3\text{PBnOEt}]_5[\text{Dy}(\text{SCN})_8]$ .

The hydrophobic triphenylarylphosphonium cations confer poor water solubility to the resulting phosphonium-dysprosium compounds, a feature useful in the synthesis of nanoparticles by reprecipitation method. In contrast,  $\text{K}_5\text{Dy}(\text{SCN})_8$ , a control compound containing a different cation is much more water soluble, clearly demonstrating the role played by the cation in dictating the solubilities of these compounds (Table 3.1). Resistivity of the saturated aqueous solution of  $[\text{Ph}_4\text{P}]_5[\text{Dy}(\text{SCN})_8]$  was  $14.58 \Omega$  compared to  $8.38 \Omega$  for the control compound



$K_5[Dy(SCN)_8]$ . The high resistivity displayed by the phosphonium-dysprosium compounds implies that they are stable and principally exist in a non-dissociated form in water.

Table 3.1. Solubility of phosphonium-dysprosium compounds in water\*

Compound	Solubility (g/L)	Solubility (mol/L)	Dissociation constant $K_s$ (mol <sup>6</sup> /L <sup>6</sup> )
$[Ph_3PBnNO_2]_5[Dy(SCN)_8]$	0.11	$4.73e^{-5}$	$3.50e^{-23}$
$[Ph_4P]_5[Dy(SCN)_8]$	0.16	$6.35e^{-5}$	$2.05e^{-22}$
$[Ph_3PBn]_5[Dy(SCN)_8]$	0.20	$7.65 e^{-5}$	$6.26e^{-22}$
$[Ph_3PBnOEt]_5[Dy(SCN)_8]$	0.12	$5.01 e^{-5}$	$4.94e^{-23}$
$K_5Dy(SCN)_8]$	> 17	-	>> 1

\* Reproduced from reference 19 with permission from Elsevier.

### 3.3.2. Physical and Morphological Properties of the Nanoparticles

The four compounds formed fairly spherical to slightly ovate nanoparticles of varying sizes ranging from 21 nm to 92 nm (Figure 3.5) as determined by TEM.

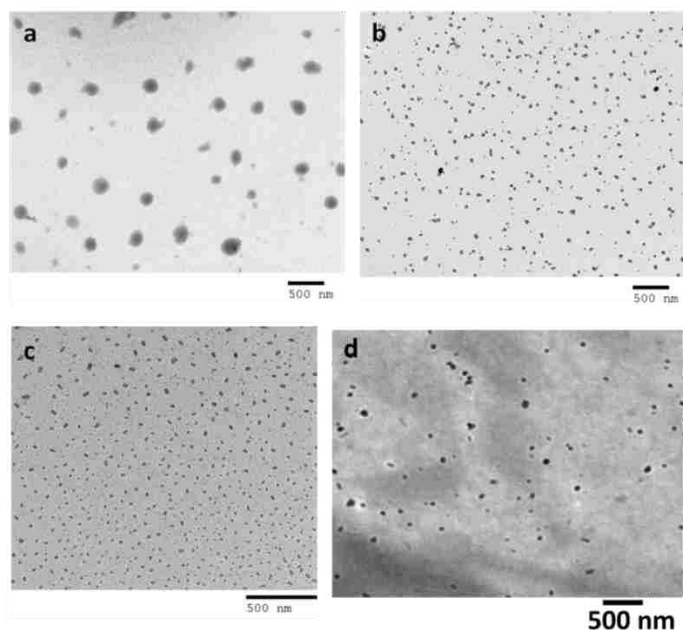


Figure 3.5. Transmission electron micrographs of a)  $[Ph_4P]_5[Dy(SCN)_8]$  nanoparticles, size:  $54 \pm 8$  nm b)  $[Ph_3PBnOEt]_5[Dy(SCN)_8]$  nanoparticles, size:  $65 \pm 13$  nm. c)  $[Ph_3PBnNO_2]_5[Dy(SCN)_8]$  nanoparticles, size:  $21 \pm 3$  nm and d)  $[Ph_3PBn]_5[Dy(SCN)_8]$  nanoparticles, size:  $92.3 \pm 15.2$  nm. Bars represent 500 nm.

The zeta potentials were determined to be -10 mV, -2 mV, -12 mV, and -6 mV for  $[\text{Ph}_4\text{P}]_5[\text{Dy}(\text{SCN})_8]$ ,  $[\text{Ph}_3\text{PBnOEt}]_5[\text{Dy}(\text{SCN})_8]$ ,  $[\text{Ph}_3\text{PBnNO}_2]_5[\text{Dy}(\text{SCN})_8]$ , and  $[\text{Ph}_3\text{PBn}]_5[\text{Dy}(\text{SCN})_8]$ , respectively. The differences in the nanoparticles sizes and corresponding zeta potentials clearly indicate the role played by the variations of the functional groups on the phosphonium moiety of these ionic compounds. It is worth noting that the concept in which the counterions influence the various properties of ionic compounds is in agreement with previous studies.<sup>18</sup>

### 3.3.3. Magnetic Properties

The phosphonium-dysprosium compounds have a magnetically active ion  $\text{Dy}^{3+}$  with a  $4f^9$  electron configuration and display paramagnetism at room temperature. Their magnetic susceptibilities were determined by use of a superconducting quantum interference device (SQUID) magnetometer. Magnetization at 300 K was measured in the magnetic field range of -70,000 to 70,000 Oe. Molar magnetic susceptibilities of the nanoparticles at 300 K were determined as 0.0301, 0.029, 0.0333, and 0.0298  $\text{cm}^3 \text{mol}^{-1}$  for  $[\text{Ph}_4\text{P}]_5[\text{Dy}(\text{SCN})_8]$ ,  $[\text{Ph}_3\text{PBnOEt}]_5[\text{Dy}(\text{SCN})_8]$ ,  $[\text{Ph}_3\text{PBnNO}_2]_5[\text{Dy}(\text{SCN})_8]$  and  $[\text{Ph}_3\text{PBn}]_5[\text{Dy}(\text{SCN})_8]$  respectively, which are similar to values obtained previously for  $\text{Dy}^{3+}$ .<sup>19,30</sup> The effective magnetic moment ( $\mu_{\text{eff}}$ ) for  $\text{Dy}^{3+}$  is reported as  $10.48 \mu_{\text{B}}$ .<sup>30</sup> The  $\mu_{\text{eff}}$  values were calculated from the slopes of the fitted lines (Table 3.2). Phosphonium-dysprosium compounds exhibited weak anti-ferromagnetic interactions as seen from their Curie-Weiss temperature (Table 3.2), confirming a lack of cluster formation within solution.

In this study, both field scans at a given temperature and temperature scans at a given field were performed. Figure 3.6, A, represents a plot of the field dependence of magnetization (M) at 300 K for  $[\text{Ph}_3\text{PBnNO}_2]_5[\text{Dy}(\text{SCN})_8]$  nanoparticles. Similar results were obtained for all

the other nanomaterials and bulk phosphonium-dysprosium compounds. This shows a linear field dependence of magnetization between -7 and +7 Tesla. Such behavior suggests paramagnetic interactions for these materials at 300 K.

Table 3.2. Summary of magnetic properties of phosphonium-dysprosium compounds\*

Compounds	$\chi_{\text{mol}}^{\text{a}}$ ( $\text{cm}^3 \text{mol}^{-1}$ )	$\mu_{\text{eff}}^{\text{b}}$ ( $\mu_{\text{B}}$ )	$\Theta^{\text{c}}$ (K)
$[\text{Ph}_3\text{PBnNO}_2]_5[\text{Dy}(\text{SCN})_8]$	0.0453	10.4	-4.3
$[\text{Ph}_3\text{PBnOEt}]_5[\text{Dy}(\text{SCN})_8]$	0.0400	10.2	-4.4
$[\text{Ph}_3\text{PBn}]_5[\text{Dy}(\text{SCN})_8]$	0.0385	9.9	-3.7
$[\text{Ph}_4\text{P}]_5[\text{Dy}(\text{SCN})_8]$	0.0353	9.6	-3.1

<sup>a</sup>Molar magnetic susceptibility. <sup>b</sup>Effective magnetic moment. <sup>c</sup>Curie-Weiss temperature.  
\*Reproduced from reference 19 with permission from Elsevier

Interestingly, the magnetic susceptibility  $\chi$  measured at 0.2 T shows little temperature dependence above  $\sim 80$  K, as plotted in Figure 3.6, B. While constant susceptibility usually suggests a small spin contribution, the nonlinear M vs. H curve obtained at 200 K (Figure 3.6, C) indicated superparamagnetic (S-shaped) behavior of  $[\text{Ph}_3\text{PBnNO}_2]_5[\text{Dy}(\text{SCN})_8]$ . Similar results were obtained with the other nanoparticles.

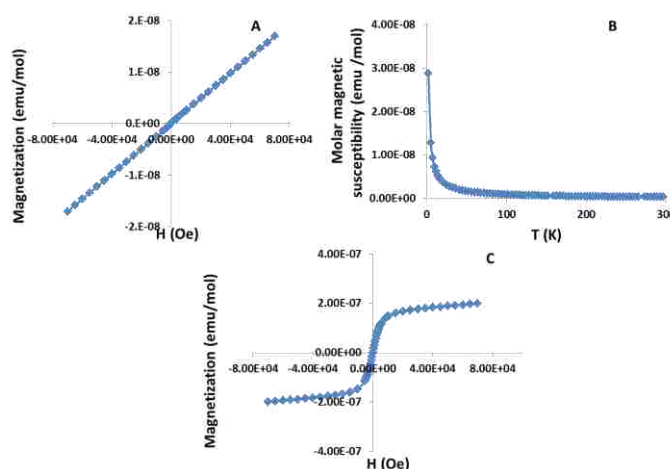


Figure 3.6. Magnetic property of  $[\text{Ph}_3\text{PBnNO}_2]_5[\text{Dy}(\text{SCN})_8]$ . a) Field dependence of molar magnetization at 300 K. b) Temperature dependence of static molar magnetic susceptibility  $\chi_{\text{mol}}$  at a field of 1,000 Oe and c) field dependence of molar magnetization at 200 K.

The bulk materials did not display this trend which may be attributed to the enhanced phase coherence of the magnetic dipoles within the nanomaterials as compared to the bulk material.<sup>31</sup> Therefore, the magnetic properties of the bulk material<sup>19</sup> were retained and enhanced in the nanoparticle formulations. The improved magnetism may prove useful as an external magnetic field may be used to direct the nanoparticles to tumors or diseased sites.<sup>17</sup>

### 3.3.4. UV-Vis Absorption and Fluorescence Spectroscopy

Luminescence properties of the nanoparticles were studied to ascertain that the dysprosium lanthanide moiety observed in the bulk material was retained in the nanoscale. All four compounds and the corresponding nanoparticles displayed two characteristic luminescence peaks (Figure 3.7) consistent with Dy<sup>3+</sup> containing compounds.<sup>32</sup>

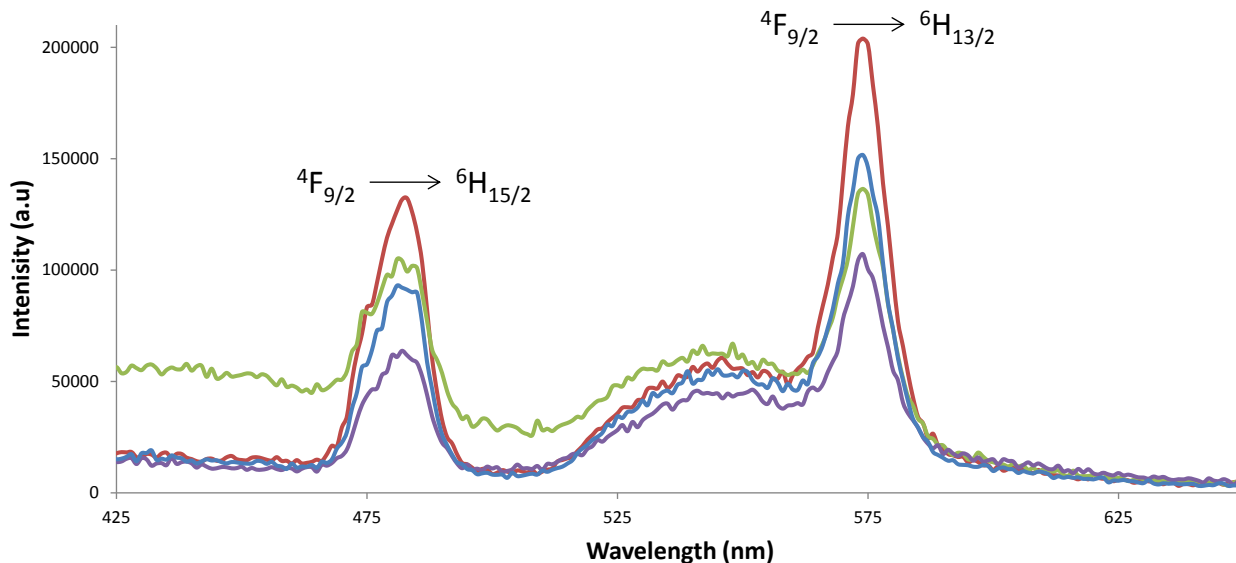


Figure 3.7. Fluorescence emission spectra of the phosphonium based nanoparticles with transition assignments for [Ph<sub>4</sub>P]<sub>5</sub>[Dy(SCN)<sub>8</sub>] (red), Ph<sub>3</sub>PBnOEt]<sub>5</sub>[Dy(SCN)<sub>8</sub>] (green), [Ph<sub>3</sub>PBnNO<sub>2</sub>]<sub>5</sub>[Dy(SCN)<sub>8</sub>] (purple), and [Ph<sub>3</sub>PBn]<sub>5</sub>[Dy(SCN)<sub>8</sub>] (blue) in acetonitrile (1 mM), λ<sub>ex</sub> = 365 nm.

The fluorescence peak around 483 nm (blue region) arises from 4f<sup>9</sup> electron configuration due to a transition from <sup>4</sup>F<sub>9/2</sub> to <sup>6</sup>H<sub>15/2</sub> while the peak around 573 nm (yellowish-green region) is a result of <sup>4</sup>F<sub>9/2</sub> to <sup>6</sup>H<sub>13/2</sub> transition. The latter peak is the most intense, consistent with their yellowish-green luminescence. Lanthanide ions are known to have very low absorption

coefficients because transitions within their 4f subshells are partially forbidden.<sup>33</sup> However, it is possible for a lanthanide to be excited outside its region of absorption if there is an organic antenna chromophore that can transfer energy to it. In addition, lanthanide ions are known to be quenchers of triplet states which mitigates against photobleaching.<sup>34</sup> The aryltriphenylphosphonium cations in the phosphonium–dysprosium compounds may have functioned as sensitizers (antenna) and therefore activated Dy<sup>3+</sup> through energy transfer. Fluorescence emanating from Dy<sup>3+</sup> may be useful for potential application as an imaging agent in cancer cells.

### 3.3.5. Cell Studies

An MTS assay method was used to evaluate the effectiveness of the nanoparticles *in vitro*. To compare the effect of nanoparticles towards normal and cancer cells, human breast carcinoma cells (Hs578T), and normal human breast fibroblast cells (Hs578Bst) were utilized. These cell lines are an interesting pair to study as they were both derived from the same patient. Hs578T is epithelial in origin and was derived from a carcinosarcoma while Hs578Bst was developed from a normal tissue bordering the tumor.<sup>35</sup> Other cancer cell lines investigated include hormone-independent human breast carcinoma cells (MDA-MB-231), human pancreatic carcinoma cells (PANC-1), and human colorectal adenocarcinoma cells (HT-29). The nanoparticle formulations of the phosphonium-dysprosium compounds were found to be fairly non-toxic to the normal breast cell line in comparison with the breast cancer cell line (Figure 3.8).

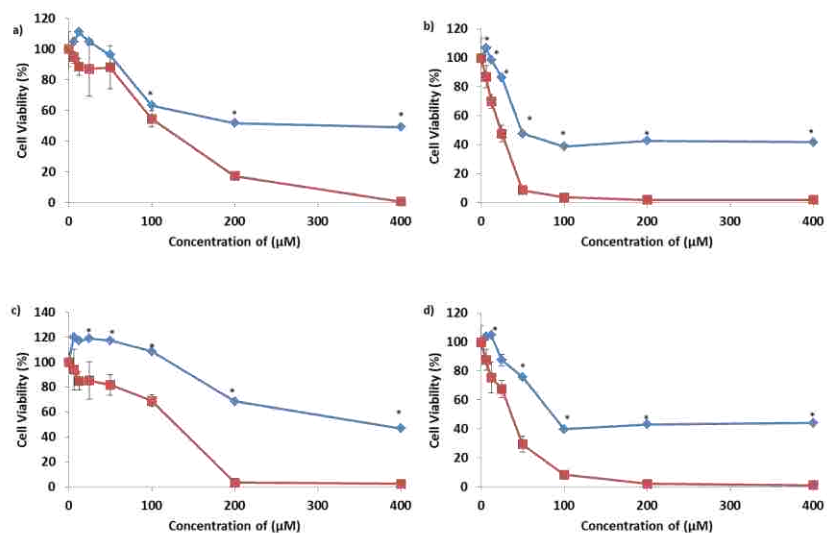


Figure 3.8. Cytotoxicity of a) [Ph<sub>4</sub>P]<sub>5</sub>[Dy(SCN)<sub>8</sub>], b) [Ph<sub>3</sub>PBnOEt]<sub>5</sub>[Dy(SCN)<sub>8</sub>], c) [Ph<sub>3</sub>PBnNO<sub>2</sub>]<sub>5</sub>[Dy(SCN)<sub>8</sub>], and d) [Ph<sub>3</sub>PBn]<sub>5</sub>[Dy(SCN)<sub>8</sub>] nanoparticles against breast cancer (Hs578T, red) and normal breast (Hs578Bst, blue) cell lines, 48 h incubation. All points are mean ± s.d of triplicate wells of three independent experiments. \*Statistically different from the corresponding concentration for the same compound in Hs578T (P < 0.05).

In addition, the IC<sub>50</sub> values revealed that the nanoparticle formulations were significantly more effective towards cancer cell lines in comparison to the native compounds<sup>19</sup>, while maintaining comparable non-toxicity towards the normal cell line (Table 3.3). Although this was true for almost all the cell lines investigated, the greatest difference was observed for PANC-1 cell line where the IC<sub>50</sub> was lower by an order of magnitude, except for [Ph<sub>3</sub>PBnNO<sub>2</sub>]<sub>5</sub>[Dy(SCN)<sub>8</sub>].<sup>19</sup> Consequently, the developed nanoparticles are more selective towards the cancer cell lines, consistent with previous literature.<sup>18,28</sup> The effectiveness of the nanoparticle formulations could be a result of increased surface area for interaction between the cells and the nanomaterials, allowing an increase in the amount of interaction occurring. Nanoparticle formulations have also been described to decrease non-specific targeting, alter drugs pharmacokinetic profiles, and increase drugs therapeutic indices.<sup>11</sup> Furthermore, nanoparticles are reported to achieve improved intracellular concentration with minimal toxicity to normal cells.<sup>36</sup>

Table 3.3. Summary of IC<sub>50</sub> values for phosphonium-dysprosium nanoparticles and the bulk materials.

Cell lines	IC <sub>50</sub> (μM)							
	[Ph <sub>4</sub> P] <sub>5</sub> [Dy(SCN) <sub>8</sub> ]		[Ph <sub>3</sub> PBnOEt] <sub>5</sub> [Dy(SCN) <sub>8</sub> ]		[Ph <sub>3</sub> PBnNO <sub>2</sub> ] <sub>5</sub> [Dy(SCN) <sub>8</sub> ]		[Ph <sub>3</sub> PBn] <sub>5</sub> [Dy(SCN) <sub>8</sub> ]	
	nps	Bulk*	nps	Bulk*	nps	Bulk*	Nps	Bulk*
Hs578Bst	164	>200	48	74	370	147	86	85
Hs578T	112	83	23	19	140	91	36	22
MDA-MB-231	5	121	8	28	152	141	11	194
HT29	5	251	58	86	169	303	74	85
PANC-1	68	>400	20	>450	208	>400	28	>400

\* Adapted from reference 19 with permission from Elsevier

Clonogenic assay revealed that nanoparticles from the four compounds prevented colony formation of MDA-MB-231 cancer cell lines when surviving cells were cultured with a low dosage of the nanoparticles after treatment (Figure 3.9). Accordingly, phosphonium-dysprosium derived nanoparticles may be good candidates for further investigations as possible chemotherapeutic agents.

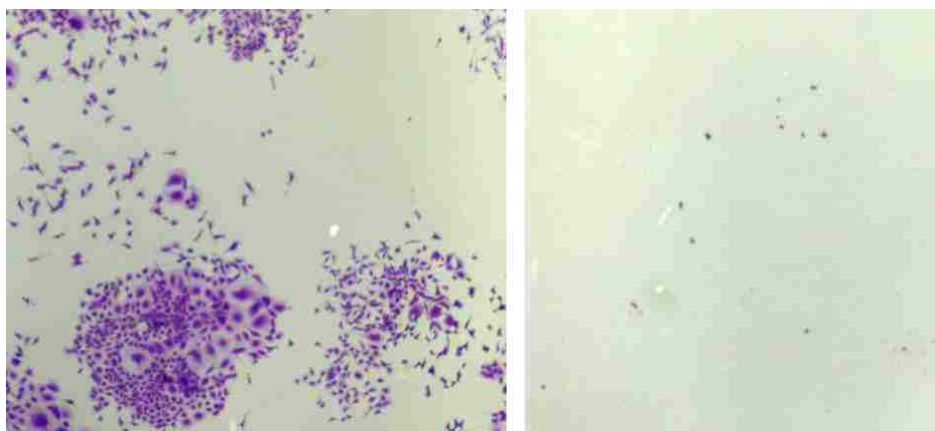


Figure 3.9. Clonogenic assay images of MDA-MB-231 breast cancer cells showing a) Colonies formed from control wells and b) zero colonies formed in wells treated with 5 μM [Ph<sub>3</sub>PBnNO<sub>2</sub>]<sub>5</sub>[Dy(SCN)<sub>8</sub>]. Similar results were obtained for all the other phosphonium-dysprosium nanoparticles.

### 3.4. Conclusion

In summary, multifunctional nanoparticles derived from phosphonium dysprosium salts were synthesized and evaluated for anticancer properties *in vitro*. The nanoparticles were designed to possess luminescence and paramagnetic properties from dysprosium containing anions, and cancer targeting properties from aryltriphenylphosphonium cations. The multifunctional properties have been evaluated in this study, and the nanoparticles developed are promising chemotherapeutic agents. This study has demonstrated that nanoparticle formulations derived from phosphonium dysprosium salts through a simple, additive free reprecipitation method are more selective towards cancer cell lines in comparison to normal cell lines. This finding provides an alternative avenue to drug design and development that is simple and time efficient.

### 3.5. References

1. Chatterjee, J.; Haik, Y.; Chen, C. J., Polyethylene magnetic nanoparticle: A new magnetic material for biomedical applications. *Journal of Magnetism and Magnetic Materials* **2002**, *246*, 382-391.
2. Holm, B. A.; Bergey, E. J.; De, T.; Rodman, D. J.; Kapoor, R.; Levy, L.; Friend, C. S.; Prasad, P. N., Nanotechnology in biomedical applications. *Molecular Crystals and Liquid Crystals* **2002**, *374*, 589-598.
3. Otsuka, H.; Nagasaki, Y.; Kataoka, K., Pegylated nanoparticles for biological and pharmaceutical applications. *Advanced Drug Delivery Reviews* **2003**, *55*, 403-419.
4. De, M.; Ghosh, P. S.; Rotello, V. M., Applications of nanoparticles in biology. *Advanced Materials* **2008**, *20*, 4225-4241.
5. Jordan, A. N.; Das, S.; Siraj, N.; de Rooy, S. L.; Li, M.; El-Zahab, B.; Chandler, L.; Baker, G. A.; Warner, I. M., Anion-controlled morphologies and spectral features of cyanine-based nanoGUMBOS - an improved photosensitizer. *Nanoscale* **2012**, *4*, 5031-5038.
6. Torchilin, V. P., Multifunctional nanocarriers. *Advanced Drug Delivery Reviews* **2006**, *58*, 1532-1555.
7. Alonso, M. J., Nanomedicines for overcoming biological barriers. *Biomedicine & Pharmacotherapy* **2004**, *58*, 168-172.
8. Cho, K.; Wang, X.; Nie, S.; Chen, Z.; Shin, D. M., Therapeutic nanoparticles for drug delivery in cancer. *Clinical Cancer Research* **2008**, *14*, 1310-1316.



9. Cheng, Z.; Al Zaki, A.; Hui, J. Z.; Muzykantov, V. R.; Tsourkas, A., Multifunctional nanoparticles: Cost versus benefit of adding targeting and imaging capabilities. *Science* **2012**, *338*, 903-910.
10. Nogueira, D. R.; Tavano, L.; Mitjans, M.; Perez, L.; Infante, M. R.; Vinardell, M. P., In vitro antitumor activity of methotrexate via pH-sensitive chitosan nanoparticles. *Biomaterials* **2013**, *34*, 2758-2772.
11. Sultana, S.; Khan, M. R.; Kumar, M.; Kumar, S.; Ali, M., Nanoparticles-mediated drug delivery approaches for cancer targeting: A review. *Journal of Drug Targeting* **2013**, *21*, 107-125.
12. Wasserscheid, P.; Keim, W., Ionic liquids - new "solutions" for transition metal catalysis. *Angewandte Chemie-International Edition* **2000**, *39*, 3772-3789.
13. Armand, M.; Endres, F.; MacFarlane, D. R.; Ohno, H.; Scrosati, B., Ionic-liquid materials for the electrochemical challenges of the future. *Nature Materials* **2009**, *8*, 621-629.
14. Gratzel, M., Dye-sensitized solar cells. *Journal of Photochemistry and Photobiology C-Photochemistry Reviews* **2003**, *4*, 145-153.
15. Seddon, K. R., Ionic liquids for clean technology. *Journal of Chemical Technology and Biotechnology* **1997**, *68*, 351-356.
16. Kaushik, N. K.; Attri, P.; Kaushik, N.; Choi, E. H., Synthesis and antiproliferative activity of ammonium and imidazolium ionic liquids against T98G brain cancer cells. *Molecules* **2012**, *17*, 13727-13739.
17. Egorova, K. S.; Ananikov, V. P., Toxicity of ionic liquids: Eco(cyto)activity as complicated, but unavoidable parameter for task-specific optimization. *ChemSusChem* **2014**, *7*, 336-360.
18. Magut, P. K. S.; Das, S.; Fernand, V. E.; Losso, J.; McDonough, K.; Naylor, B. M.; Aggarwal, S.; Warner, I. M., Tunable cytotoxicity of rhodamine 6g via anion variations. *Journal of the American Chemical Society* **2013**, *135*, 15873-15879.
19. Li, M.; Ganea, G. M.; Lu, C.; De Rooy, S. L.; El-Zahab, B.; Fernand, V. E.; Jin, R.; Aggarwal, S.; Warner, I. M., Lipophilic phosphonium-lanthanide compounds with magnetic, luminescent, and tumor targeting properties. *Journal of Inorganic Biochemistry* **2012**, *107*, 40-46.
20. Calabrese, G.; Gomes, A. C. N. M.; Barbu, E.; Nevell, T. G.; Tsibouklis, J., Carborane-based derivatives of delocalised lipophilic cations for boron neutron capture therapy: Synthesis and preliminary in vitro evaluation. *Journal of Materials Chemistry* **2008**, *18*, 4864-4871.
21. Morrison, D. E.; Issa, F.; Bhadbhade, M.; Groebler, L.; Witting, P. K.; Kassiou, M.; Rutledge, P. J.; Rendina, L. M., Boronated phosphonium salts containing arylboronic acid, closo-carborane, or nido-carborane: Synthesis, x-ray diffraction, in vitro cytotoxicity, and cellular uptake. *Journal of Biological Inorganic Chemistry* **2010**, *15*, 1305-1318.
22. Manetta, A.; Gamboa, G.; Nasserri, A.; Podnos, Y. D.; Emma, D.; Dorion, G.; Rawlings, L.; Carpenter, P. M.; Bustamante, A.; Patel, J.; Rideout, D., Novel phosphonium salts

- display in vitro and in vivo cytotoxic activity against human ovarian cancer cell lines. *Gynecologic Oncology* **1996**, *60*, 203-212.
23. Muratovska, A.; Lightowers, R. N.; Taylor, R. W.; Turnbull, D. M.; Smith, R. A. J.; Wilce, J. A.; Martin, S. W.; Murphy, M. P., Targeting peptide nucleic acid (PNA) oligomers to mitochondria within cells by conjugation to lipophilic cations: Implications for mitochondrial DNA replication, expression and disease. *Nucleic Acids Research* **2001**, *29*, 1852-1863.
  24. Roman Luque-Ortega, J.; Reuther, P.; Rivas, L.; Dardonville, C., New benzophenone-derived bisphosphonium salts as leishmanicidal leads targeting mitochondria through inhibition of respiratory complex ii. *Journal of Medicinal Chemistry* **2010**, *53*, 1788-1798.
  25. Plechkova, N. V.; Seddon, K. R., Applications of ionic liquids in the chemical industry. *Chemical Society Reviews* **2008**, *37*, 123-150.
  26. van Rantwijk, F.; Sheldon, R. A., Biocatalysis in ionic liquids. *Chemical Reviews* **2007**, *107*, 2757-2785.
  27. Bwambok, D. K.; El-Zahab, B.; Challa, S. K.; Li, M.; Chandler, L.; Baker, G. A.; Warner, I. M., Near-infrared fluorescent nanoGUMBOS for biomedical imaging. *ACS Nano* **2009**, *3*, 3854-3860.
  28. Kasai, H.; Murakami, T.; Ikuta, Y.; Koseki, Y.; Baba, K.; Oikawa, H.; Nakanishi, H.; Okada, M.; Shoji, M.; Ueda, M.; Imahori, H.; Hashida, M., Creation of pure nanodrugs and their anticancer properties. *Angewandte Chemie International Edition* **2012**, *51*, 10315-10318.
  29. Franken, N. A. P.; Rodermond, H. M.; Stap, J.; Haveman, J.; van Bree, C., Clonogenic assay of cells in vitro. *Nature Protocols* **2006**, *1*, 2315-2319.
  30. Mallick, B.; Balke, B.; Felser, C.; Mudring, A. V., Dysprosium room-temperature ionic liquids with strong luminescence and response to magnetic fields. *Angewandte Chemie-International Edition* **2008**, *47*, 7635-7638.
  31. Santra, S.; Kaittanis, C.; Grimm, J.; Perez, J. M., Drug/dye-loaded, multifunctional iron oxide nanoparticles for combined targeted cancer therapy and dual optical/magnetic resonance imaging. *Small* **2009**, *5*, 1862-1868.
  32. Getsis, A.; Balke, B.; Felser, C.; Mudring, A.-V., Dysprosium-based ionic liquid crystals: Thermal, structural, photo- and magnetophysical properties. *Crystal Growth & Design* **2009**, *9*, 4429-4437.
  33. Li, Z. F.; Zhou, L.; Yu, J. B.; Zhang, H. J.; Deng, R. P.; Peng, Z. P.; Guo, Z. Y., Synthesis, structure, photoluminescence, and electroluminescence properties of a new dysprosium complex. *Journal of Physical Chemistry C* **2007**, *111*, 2295-2300.
  34. Bunzli, J. C. G., Lanthanide luminescence for biomedical analyses and imaging. *Chemical Reviews* **2010**, *110*, 2729-2755.
  35. Hackett, A. J.; Smith, H. S.; Springer, E. L.; Owens, R. B.; Nelsonreese, W. A.; Riggs, J. L.; Gardner, M. B., 2 syngeneic cell lines from human breast-tissue - aneuploid

- mammary epithelial (hs578t) and diploid myoepithelial (hs578bst) cell lines. *Journal of the National Cancer Institute* **1977**, 58, 1795-1806.
36. Haley, B.; Frenkel, E., Nanoparticles for drug delivery in cancer treatment. *Urologic Oncology: Seminars and Original Investigations* **2008**, 26, 57-64.

## CHAPTER 4. MULTIMODAL STIMULI RESPONSIVE THERANOSTIC NANOMATERIALS DERIVED FROM IRON (III) PHTHALOCYANINE DEOXYCHOLATE SALT

### 4.1. Introduction

Design of nanometer sized vehicles for stimuli responsive delivery of therapeutic agents is extremely promising with respect to modern, evolving techniques developed for non-invasive treatment of diseases. In recent years, substantial efforts have been made towards development of engineered theranostic nanomaterials with multifunctional and multimodal characteristics that are capable of simultaneous therapy and diagnosis.<sup>1-3</sup> Nanotheranostics interact more effectively with biological systems which permits early detection of diseases. High surface area-to-volume ratio is a characteristic of nanoparticles that enable enhanced drug loading.<sup>1-3</sup> Drug encapsulated nanometric sized materials exhibit prolonged half-life due to improved circulation times within the body as compared to early excretion of free drug molecules before achieving their desired result.<sup>4</sup> Additionally, incorporation of target specificity to nanoscale delivery vehicles through response to external or internal stimuli enables administration of lower doses, thus reducing associated side-effects.<sup>5</sup>

Superparamagnetic iron oxide nanoparticles, magnetite ( $\text{Fe}_3\text{O}_4$ ) and maghemite ( $\gamma\text{-Fe}_2\text{O}_3$ ), are typically used magnetic nanoparticles which have found wide applications in biomedicine due to their inherent biocompatibility.<sup>6</sup> Iron oxide nanoparticles of dual functionality such as magnetic and target specific,<sup>7</sup> magnetic-fluorescent,<sup>8,9</sup> magnetic-pH sensitive<sup>10</sup> as well as magnetic-temperature sensitive<sup>11</sup> have also been reported. In most cases, surface modification with site specific ligands via covalent attachments is needed for incorporation of other desired functionalities into magnetic nanoparticles. For instance, conjugation of a protein or antibody adds target specificity to magnetic nanoparticles which improves contrast in MRI. This allows improved distinction between the site of interest and the

surrounding region.<sup>12,13</sup> Target specificity can also be incorporated by attaching a stimuli responsive element such as pH<sup>8,9</sup> or temperature sensitive polymers<sup>11</sup> to magnetic nanoparticles. Incorporation or conjugation of a fluorescent dye imparts fluorescent properties in combination with magnetism.<sup>14</sup> Magnetic-fluorescent nanoparticles have been designed in the form of core-shell nanostructures such as CdSe@Fe<sub>3</sub>O<sub>4</sub> nanoparticles.<sup>15</sup> Moreover, use of quantum dots also overcomes challenges associated with photostability. Presence of manifold functionalities within the same particle permits the performance of multiple therapies such as magnetic hyperthermia, photoinduced hyperthermia, chemotherapy as well as imaging. This improves the effectiveness of a treatment.<sup>5</sup>

Despite several advances, nearly all variations of multifunctional nanomaterials reported so far involve multistep, sophisticated and elongated synthetic approaches for incorporation of desired functionalities which inevitably result in low-yields and more expensive products. In this study, we demonstrate a facile approach to synthesis of a new class of multifunctional nanoparticles with magnetic, pH sensitive, and fluorescence properties based on the use of iron phthalocyanine. Iron (III) phthalocyanine has been previously used to coat the surface of Fe<sub>2</sub>O<sub>3</sub> nanoparticles in order to obtain better dispersion in organic solvents as well as increase their antioxidative properties.<sup>16</sup> Its derivatives have been used to design multilayered electrodes for use as resistive switching memory.<sup>17</sup> Phthalocyanines and phthalocyanine conjugated nanoparticles have been widely investigated for application in photodynamic therapy,<sup>18</sup> although iron phthalocyanines are not known to be used for such purposes. In all of the above mentioned studies, metal phthalocyanines have been used in combination with other materials in order to improve their redox properties.<sup>17,18</sup> However, to the best of our knowledge nanomaterials derived directly from Iron (III) phthalocyanine or its derivatives and its influence on the magnetic

properties attributed to its metallic core has not been explored. Moreover, the use of Iron (III) phthalocyanine or its nanomaterials for therapeutic or diagnostic purposes has not been reported.

This study was designed to develop multimodal nanoparticles directly from organic salts based on Iron (III) phthalocyanine and to determine their utility in theranostic applications. Multidimensional nanomaterials allow combined pH responsive drug delivery to cancer cells, as well as provide simultaneous imaging. Our studies reveal significantly high biocompatibility of this new class of nanomaterials. Hence, herein we have tailored an existing molecule using an extremely facile approach that demonstrated improved functionality upon nanoformulation for combined stimuli responsive therapeutic and diagnostic uses.

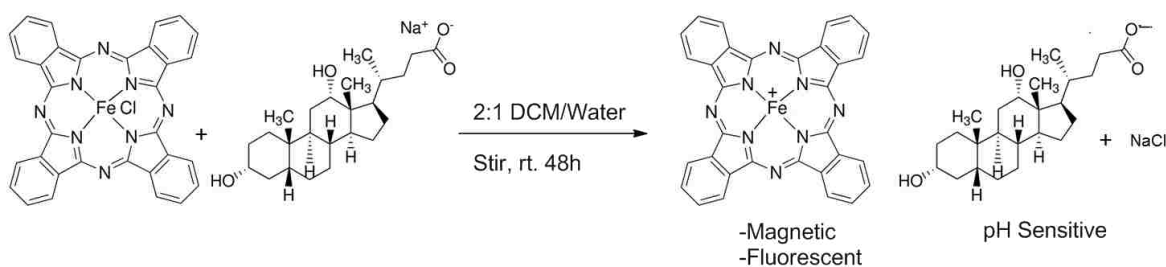
## **4.2. Materials and Methods**

### **4.2.1. Materials**

Sodium deoxycholate (97%), Doxorubicin hydrochloride, methylene chloride, Iron (III) phthalocyanine chloride, phosphate buffered saline, anhydrous tetrahydrofuran (THF), and ethanol (spectroscopic grade) were purchased from Sigma Aldrich (Milwaukee, WI). Cell viability MTT (3-[4, 5-Dimethylthiazol-2-yl]-2, 5-diphenyltetrazolium bromide) assay kit was purchased from Promega Corporation (Madison, WI). Triply deionized water (18.2 M $\Omega$ ·cm) from an Elga model PURELAB ultra water filtration system (Lowell, MA) was used for all experiments. A Branson 3510RDTH model bath ultrasonicator (335 W, 40 kHz frequency) (Branson Ultrasonics Corporation, Danbury, CT) was used at room temperature for preparation of nanomaterials. Normal human breast fibroblast cells (Hs578Bct, ATCC no. HTB-125) and hormone-independent human breast carcinoma cells (MDA-MB-231) were obtained from the American Tissue Culture Collection (ATCC, Manassas, VA) and grown to 90% confluence prior to any experiments according to ATCC protocol.

#### 4.2.2. Synthesis of [Ptc][DC]

A biphasic ion-metathesis reaction was performed. Dark green Iron (III) phthalocyanine chloride (PtcCl) dissolved in dichloromethane (DCM) was mixed with sodium deoxycholate (NaDC) dissolved in water and stirred for 48 hours (Scheme 4.1). The ([Ptc][DC]) which is soluble in DCM, was then washed repeatedly with water to remove NaCl byproduct. Presence of both ions in the final product was determined by use of  $^1\text{H}$  NMR and electrospray ionization (ESI) performed in positive and negative ion modes.



Scheme 4.1. Synthesis of Iron (III) phthalocyanine based pH sensitive organic salt [Ptc][Dc].

#### 4.2.3. Synthesis and Characterization of the Nanomaterials

The [Ptc][DC] derived nanoparticles were synthesized using a reprecipitation approach. In this method, 100  $\mu\text{L}$  of 1 mM stock of the compound in THF was injected in 5 ml of phosphate buffer at pH 7.4 under sonication. Nanoparticles were then allowed to age for half an hour before further experimentation. TEM micrographs were obtained using an LVEM5 transmission electron microscope (Delong America, Montreal, Canada). The nanoparticles dispersion (3  $\mu\text{L}$ ) were drop casted onto a carbon coated copper grid and allowed to air dry at room temperature before TEM imaging.

#### 4.2.4. UV-Vis Absorption and Fluorescence Spectroscopy

Absorbance measurements were performed using a Shimadzu UV- 3101PC, a UV-Vis-near-IR scanning spectrophotometer (Shimadzu, Columbia, MD). Fluorescence studies were performed using a Spex Fluorolog-3 spectrofluorimeter (model FL3-22TAU3); Jobin Yvon,

Edison, NJ). A 0.4 cm path length quartz cuvette (Starna Cells) was used for acquiring the fluorescence and absorbance against an identical cell filled with water as the blank. Fluorescence studies were performed with right angle geometry.

#### **4.2.5. Magnetic Property Measurement**

Magnetic properties of the bulk material and the lyophilized nanoparticles were investigated using Magnetic Property Measurement System (*Quantum Design*). Field scans (-7 T to +7 T) at a given temperature and temperature scans (0 to 300 K) at a given field were both performed.

#### **4.2.6. Drug Encapsulation in Nanoparticles**

Two hundred microliters of 1 mM [Ptc][DC] prepared in THF was rapidly injected to 10 mL water solution containing 0.4 mg/mL doxorubicin under sonication. The nanoparticles with the drug were sonicated for 30 min and then allowed to stand for 24 h for drug diffusion into the nanoparticles to reach equilibrium. Drug loaded nanoparticles were then centrifuged at 2000 rpm for 20 min and the supernatant separated and kept. The drug loaded nanoparticles were then lyophilized and drug delivery was studied under varying pH environments. Doxorubicin stock solution without nanoparticles was prepared at the same time as the ones with nanoparticles, sonicated and left for 24 h after which the absorbance was measured and compared to the absorbance of doxorubicin in the supernatant to determine the amount of drug encapsulated.

#### **4.2.7. Cell Studies**

Cytotoxicities of the synthesized drug free and drug loaded nanomaterials were determined against breast cancer (MDA-MB-23) and normal breast (Hs578Bst) cell lines by use of MTT assay kit, according to the manufacturer's instructions. Briefly, in a 96-well plate, 5000 cells in 0.1 mL culture medium were seeded to each well and incubated at 37 °C, in 5% CO<sub>2</sub>



humidified atmosphere for adherence. After 24 h, the old culture medium was aspirated and replaced with 0.1 mL of fresh culture medium containing 0-50  $\mu\text{M}$  of the salt dissolved in 1% DMSO. The cells were then incubated for 48 h at 37  $^{\circ}\text{C}$ , in a 5%  $\text{CO}_2$  humidified atmosphere. At the end of the incubation period, the cells were treated with 15  $\mu\text{L}$  MTT dye solution and incubated for 2 h. Subsequently, 100  $\mu\text{L}$  of stop solution was added per well and incubated overnight at room temperature. The plate was then shaken for 20 s and absorbance read at 570 nm with a reference wavelength of 650 nm using a micro plate spectrophotometer (Benchmark Plus, Bio-Rad Laboratories, Hercules, CA, USA). Cell viability as a percentage was determined by taking the ratio between absorbance of the treated and untreated (control) cells. For confocal microscopy, cells were incubated with the test compound at a final concentration of 20  $\mu\text{M}$  for 45 min. Cell images were acquired under an objective (x40) with a confocal laser microscope (Zeiss 510 confocal microscope) equipped with an argon laser excited at 488 nm.

### **4.3. Results and Discussions**

Ionic liquid chemistry was exploited in this work to incorporate various functionalities into a given material using a simple materials design. The organic salt [Ptc][DC] was synthesized from iron (III) phthalocyanine chloride ([Ptc][Cl]) and sodium deoxycholate (NaDC) using an ion metathesis reaction (Scheme 4.1). This molecular design was implemented with the idea that the iron (III) core of phthalocyanine would contribute the magnetic properties and deoxycholate counteranion would impart pH sensitive properties. In addition, the strong absorption of phthalocyanine in the near infrared (NIR) and visible regions would also contribute to the absorption and fluorescence properties of these materials.

### 4.3.1. Synthesis and Characterization of [Ptc][DC]

Successful incorporation of phthalocyanine cation and deoxycholate anion was ascertained by electrospray ionization mass spectrometry,  $^1\text{H}$  NMR, and FT-IR, and gave results consistent with expectations as follows:

Iron (III) phthalocyanine cation (MS, ESI $^+$ )  $m/z$  568 ( $\text{C}_{32}\text{H}_{16}\text{FeN}_8^+$ ), deoxycholate anion (MS, ESI)  $m/z$  392 ( $\text{C}_{24}\text{H}_{39}\text{O}_4^-$ ).

Iron (III) phthalocyanine cation.  $^1\text{H}$  NMR (400 MHz, DMSO- $d_6$ ),  $\delta$  (ppm): 7.81 (m, 8H), 7.16 (m, 8H). Deoxycholate anion.  $^1\text{H}$  NMR (400 MHz, DMSO- $d_6$ ),  $\delta$  (ppm): 4.45 (m, 1H), 4.20 (m, 1H), 3.76 (m, 2H), 2.19 (s, 1H), 2.50 (s, 1H) 1.63-1.14 (m, 24H), 0.90 (s, 3H), 0.88 (s, 3H), 0.57 (s, 3H).

The FT-IR spectra are displayed in Figure 4.1. Compared to the spectrum of the starting material (Figure 4.1, A), Figure 4.1, B, has new peaks near  $3000\text{ cm}^{-1}$  attributed to the deoxycholate anion.

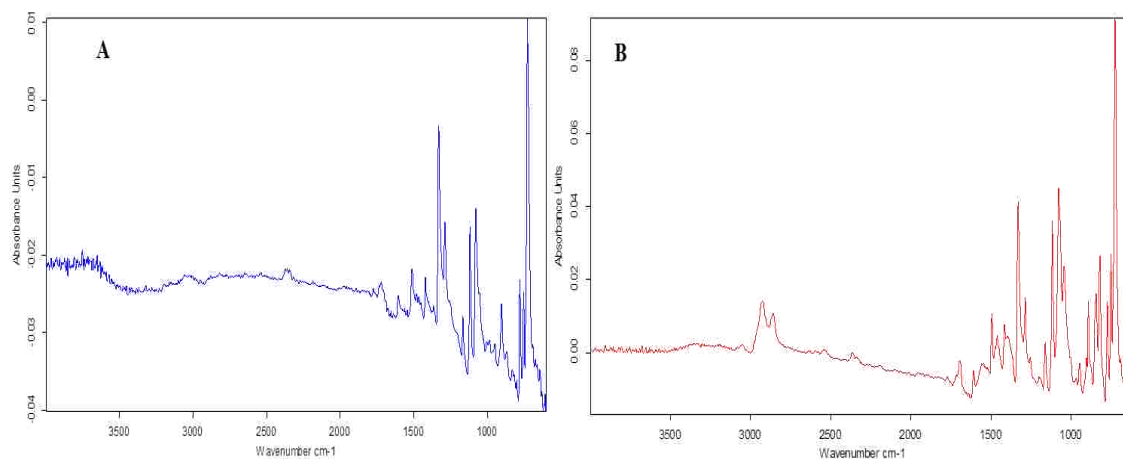


Figure 4.1. FT-IR spectrum of A) [Ptc][Cl] and B) [Ptc][DC].

### 4.3.2. Spectral Characterization of [Ptc][DC] Nanoparticles

Spectral properties of [Ptc][DC] nanoparticles in an aqueous medium (buffer pH 7.4) reveals the presence of two characteristic bands of phthalocyanines (Figure 4.2). These are the

intense and broad B-band lying in the UV region and a relatively less intense Q-band lying in the near infrared region (NIR) peaking at  $\sim 718$  nm. A broad fluorescence emission with a peak at  $\sim 500$  nm was observed when excited at a wavelength of 400 nm. However, no fluorescence emission was observed in the NIR region corresponding to absorption at 718 nm. This observation is in agreement with the previous literature which suggest that Iron(III) phthalocyanines are non-fluorescent in the NIR.<sup>19</sup> Spectral properties of both phthalocyanine based nanoparticles were slightly affected by variations in pH.

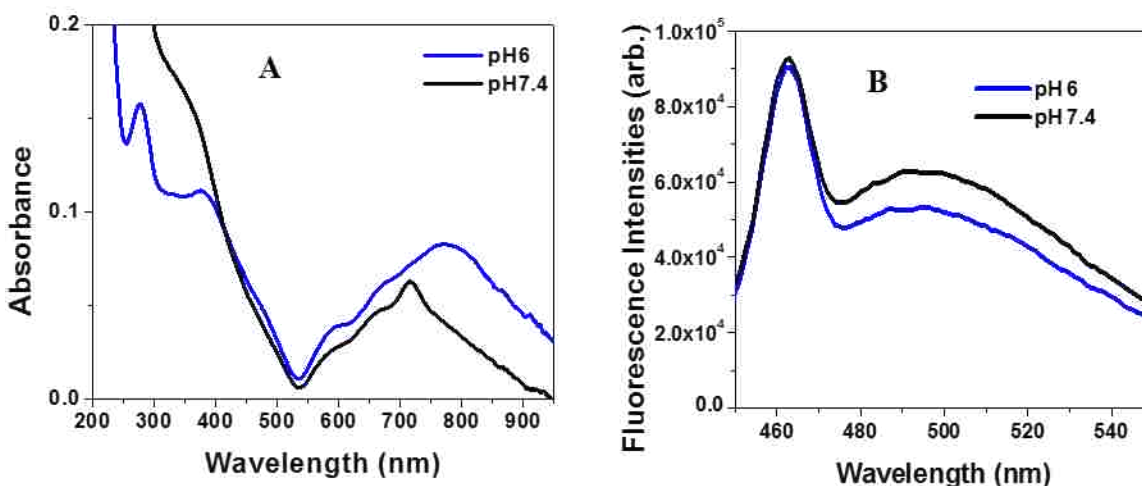


Figure 4.2. (A) Absorption spectra and (B) fluorescence emission spectra ( $\lambda_{\text{ex}}=400$  nm) of [Ptc][DC] nanoparticles with varying pH.

#### 4.3.3. TEM Studies of [Ptc][DC] Nanoparticles

Transmission electron micrographs (TEM) revealed formation of distinct spherical nanoparticles of average size 15-20 nm for [Ptc][DC] at pH 7.4 (Figure 4.3). The distinctly separated [Ptc][DC] nanoparticles, as observed under TEM, as well as their stability in the colloidal state, was further supported by their fairly high zeta potential value (+21.6 mV). The zeta potential remained constant with time pointing towards appreciable stability of this nano-dispersion. Moreover, the high positive zeta potential of these nanoparticles may facilitate adsorption on or penetration through the negatively charged cell membranes.<sup>20</sup>

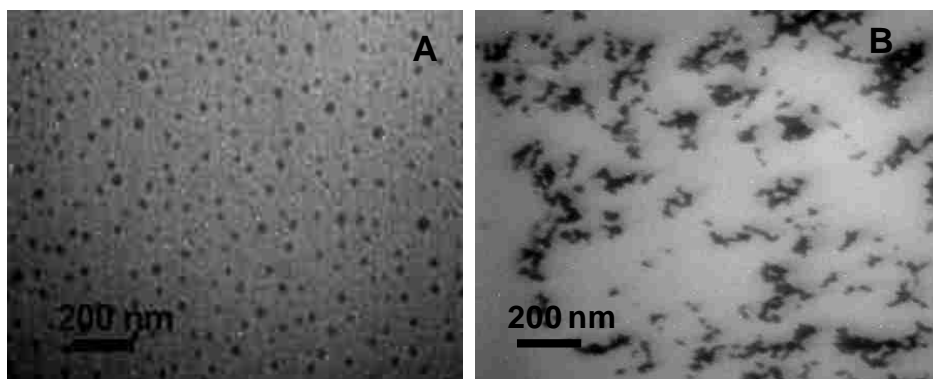


Figure 4.3. TEM micrographs of [Ptc][DC] nanoparticles respectively at A) pH 7.4 and B) pH 6.

Magnetic nanoparticles possess an inherent tendency to agglomerate and are rapidly cleared by macrophages of the mononuclear phagocyte system upon intravascular administration.<sup>11</sup> Therefore, several efforts have been made in order to prevent the nanoparticle agglomeration at physiological pH through surface modification keeping into account their non-toxicity as well as other factors.<sup>21,22</sup> Accordingly, the highly stable nanoparticle dispersion obtained in our case is considered an important improvement in this direction achieved through inherent characteristics of [Ptc][DC] nanoparticles, excluding the requirement for stabilization through surface modification. At pH 6, nanoparticles were observed to coalesce and lose their distinct shapes. Such pH sensitive behavior was ascribed to the presence of the deoxycholate counteranion. The counteranion has a pKa value near pH 6.8<sup>23</sup> suggesting protonation of the counteranion below this pH. Thus, at pH 6 the [Ptc][DC] salt is expected to decompose, leading to destabilization of the nanoparticles.

#### 4.3.4. Magnetic Properties of [Ptc][DC] Nanoparticles

Magnetic properties of the bulk material and the lyophilized [Ptc][DC] nanoparticles were investigated. In this study, both field scans at a given temperature and temperature scans at a given field were performed. Figure 4.4, A, represents a plot of the field dependence of magnetization ( $M$ ) at 300 K for bulk [Ptc][DC].

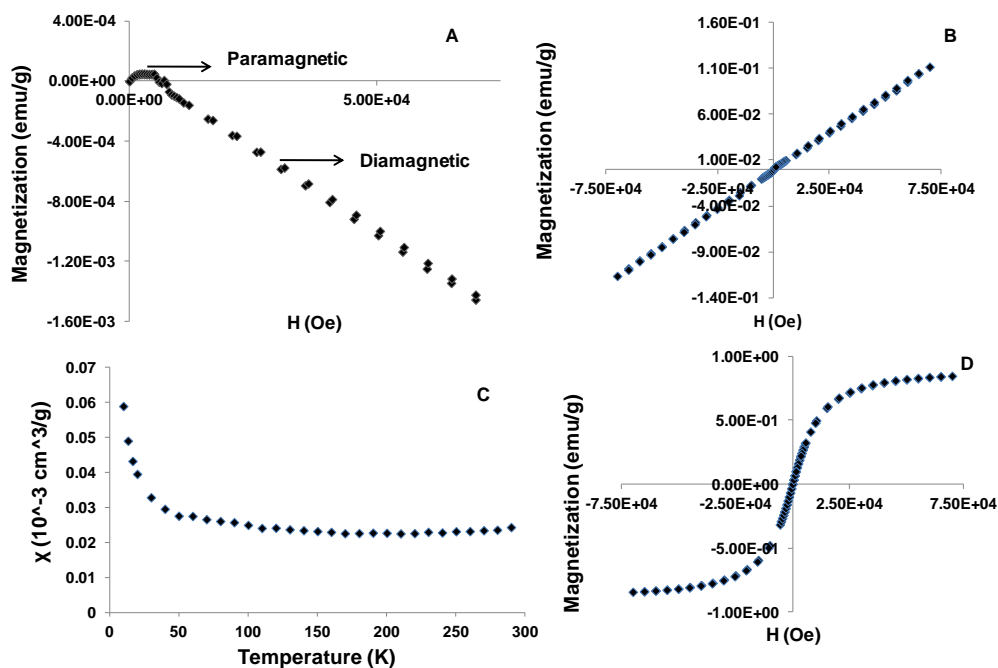


Figure 4.4. Magnetic properties of [Ptc][DC] (A) bulk M vs H at 300 K, (B) nanoparticles M vs H at 300 K, (C) nanoparticles  $\chi$  vs T at 0.2 Tesla and (D) nanoparticles M vs H at 200 K.

Note that M initially increases with increasing field, then decreases after reaching a maximum near  $xy$  Oe, and changes sign from positive at  $H < yz$  Oe to negative at  $H > yz$  Oe, suggesting mostly diamagnetic behavior of [Ptc][DC] bulk. This behavior also indicates that magnetic interactions in bulk [Ptc][DC] are highly field dependent. In contrast, the nanoparticle form of [Ptc][DC] exhibits linear field dependence of magnetization between -7 and +7 Tesla as shown in Figure 4.4, B. Such behavior suggests paramagnetic interactions at 300 K. Magnetic susceptibility ( $\chi$ ) measured at 0.2 T shows little temperature dependence above  $\sim 60$  K, as plotted in Figure 4.4, C. While constant susceptibility usually suggests a small spin contribution, the nonlinear M vs. H curve obtained at 200 K (Figure 4.4, D) indicated superparamagnetic (S-shaped) behavior of [Ptc][DC] nanoparticles.<sup>14</sup>

Thus, our studies reveal an interesting transition in magnetic behavior from [Ptc][DC] bulk to [Ptc][DC] nanoparticles which might be attributed to the enhanced phase coherence of

the magnetic dipoles within the nanomaterials as compared to the bulk material.<sup>14</sup> This indicates the potential utility of these nanoparticles for the desired applications as discussed earlier.

#### **4.3.5. pH Responsive Properties of [Ptc][DC] Nanoparticles**

The pH sensitive response of these nanoparticles was further investigated in order to examine its potential utility for pH responsive drug release. Doxorubicin was encapsulated into [Ptc][DC] nanoparticles and lyophilized. The lyophilized drug encapsulated nanoparticles were then exposed to buffers at physiological (pH 7.4) and pH 5.5 (Figure 4.5, C). Release of doxorubicin was monitored through changes in absorbance values of the drug in the supernatant buffer system. It was observed that only 17% of doxorubicin was released in the first three hours at the physiological pH 7.4. A 100% doxorubicin was released within the same time period at pH 5.5. Therefore [Ptc][DC] nanomaterials may be useful as stimuli responsive drug delivery vehicles under slightly acidic environments such as are found in tumors and bacterial infections.

#### **4.3.6. Cell Studies**

Cytotoxicity of doxorubicin loaded nanoparticles towards a normal breast (Figure 4.5, A), and breast cancer cell lines (Figures 4.5, B) was performed. Both cell lines were incubated with drug free and doxorubicin loaded [Ptc][DC] nanoparticles for 48 hours and cell viabilities were determined. It was observed that normal breast cells remained essentially unaffected by both drug free and doxorubicin loaded nanoparticles with increasing concentrations of the nanoparticles. However, with breast cancer cell lines a concentration dependent cell death ensued with doxorubicin loaded nanoparticles, demonstrating 37% cell viability at the highest concentration studied (48  $\mu$ M). In contrast, drug free [Ptc][DC] nanoparticles did not significantly inhibit cell proliferation even at the highest concentrations, indicating they are non-toxic.

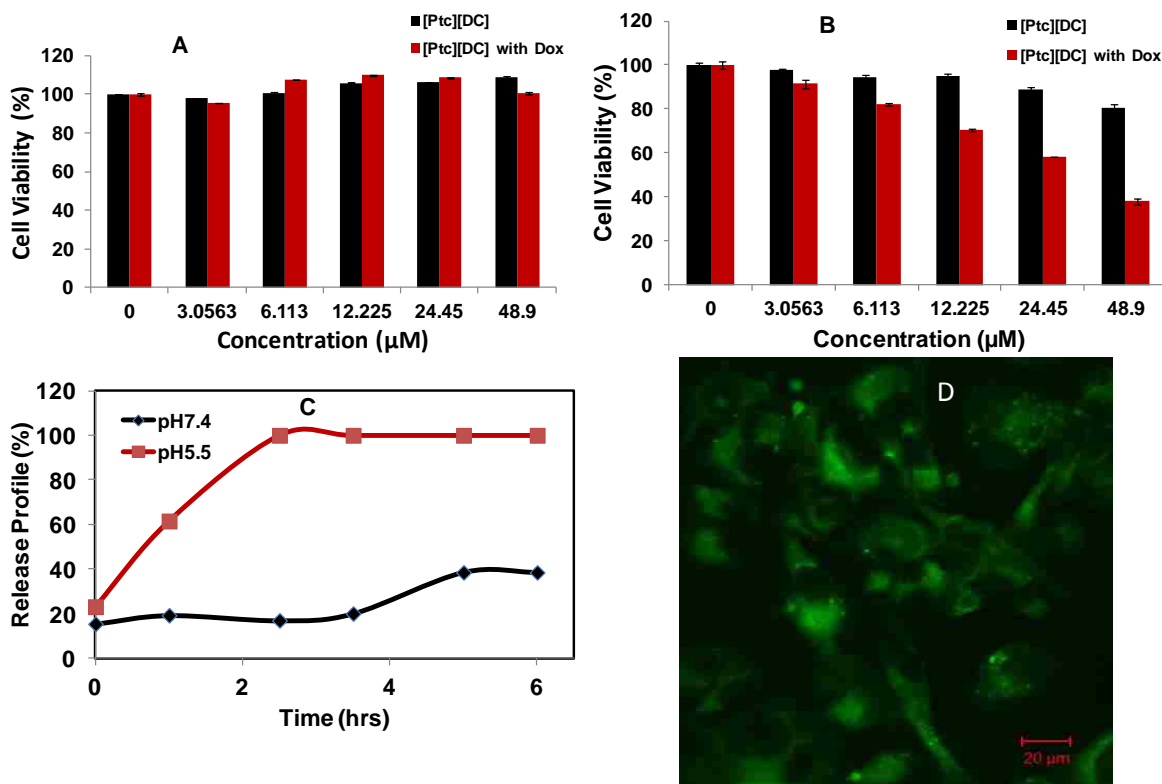


Figure 4.5. Cell viability studies of free [Ptc][DC] and doxorubicin loaded [Ptc][DC] nanoparticles in (A) Hs578Bst (normal breast) and (B) MDA-MB-231 (breast cancer) cell lines. (C) Release profile of doxorubicin from [Ptc][DC] nanoparticles with varying pH. (D) Confocal microscopic image of MDA-MB 231 cells after 2 h incubation with Dox free [Ptc][DC] nanoparticles.

These studies indicate that this novel, yet simple, approach to developing multifunctional pH sensitive nanoparticles may be used to provide stimuli responsive drug delivery to acidic environments such as cancer cells and infected tissues. The inherent biocompatibility excludes the need to induce biocompatibility through conjugation with more compatible polymers or proteins.

A confocal microscopy image (Figure 4.5, D) was obtained for MDA-MB-231 cell line after 2 h incubation with drug free [Ptc][DC] nanoparticles. This suggests the potential utility of these nanoparticles for simultaneous imaging and therapy. Since the deoxycholate is a non-fluorescent moiety, the observed fluorescence was attributed to the phthalocyanine counterpart,

thus exhibiting actual capability of these materials for theranostic applications. Most of the existing multimodal theranostics involve conjugation of separate moieties attributing each functionality, thereby leading to highly elongated synthetic procedures.<sup>1</sup> Therefore, the one-pot synthesis of the multifunctional theranostic nanomaterials as reported in this study is advancement in design of theranostics.

#### **4.4. Conclusions**

In summary, this study reports a facile one-pot approach for synthesizing pH responsive-magnetic-fluorescent nanoparticles by use of ionic liquid chemistry. These materials demonstrate nearly 100% cell viability at all concentrations in both normal and cancer cells studied, suggesting their fairly non-toxic characteristics. The pH responsive drug release property of these nanomaterials in actual cellular environment could be efficiently used for target specific delivery of therapeutic agents to tumors and other acidic environments. Besides, the interesting transition in magnetic properties switching from diamagnetic bulk material to paramagnetic nanoparticles indicate their potential to be exploited for applications in targeted drug delivery using an external magnetic field, magnetic hyperthermia as well as their possible utility as MRI contrast agents. Confocal fluorescence microscopic images obtained with MDA-MB-231 cells upon a short incubation period with [Ptc][DC] nanoparticles emphasize their application for simultaneous fluorescence imaging along with therapy. Thus, when one considers the simple synthetic approach to development of this new class of multimodal, multifunctional as well as highly biocompatible theranostic nanoparticles, these materials should be extremely promising candidates for use as stimuli responsive drug delivery systems.

#### **4.5. References**

1. Kelkar, S. S.; Reineke, T. M., Theranostics: Combining imaging and therapy. *Bioconjugate Chemistry* **2011**, 22, 1879-1903.



2. Ferrari, M., Cancer nanotechnology: Opportunities and challenges. *Nature Reviews Cancer* **2005**, *5*, 161-171.
3. Caldorera-Moore, M. E.; Liechty, W. B.; Peppas, N. A., Responsive theranostic systems: Integration of diagnostic imaging agents and responsive controlled release drug delivery carriers. *Accounts of Chemical Research* **2011**, *44*, 1061-1070.
4. Alexis, F.; Pridgen, E.; Molnar, L. K.; Farokhzad, O. C., Factors affecting the clearance and biodistribution of polymeric nanoparticles. *Molecular Pharmaceutics* **2008**, *5*, 505-515.
5. Cheng, Z.; Al Zaki, A.; Hui, J. Z.; Muzykantov, V. R.; Tsourkas, A., Multifunctional nanoparticles: Cost versus benefit of adding targeting and imaging capabilities. *Science* **2012**, *338*, 903-910.
6. Reddy, L. H.; Arias, J. L.; Nicolas, J.; Couvreur, P., Magnetic nanoparticles: Design and characterization, toxicity and biocompatibility, pharmaceutical and biomedical applications. *Chemical Reviews* **2012**, *112*, 5818-5878.
7. Nasongkla, N.; Bey, E.; Ren, J. M.; Ai, H.; Khemtong, C.; Guthi, J. S.; Chin, S. F.; Sherry, A. D.; Boothman, D. A.; Gao, J. M., Multifunctional polymeric micelles as cancer-targeted, mri-ultrasensitive drug delivery systems. *Nano Letters* **2006**, *6*, 2427-2430.
8. Choi, J. H.; Nguyen, F. T.; Barone, P. W.; Heller, D. A.; Moll, A. E.; Patel, D.; Boppart, S. A.; Strano, M. S., Multimodal biomedical imaging with asymmetric single-walled carbon nanotube/iron oxide nanoparticle complexes. *Nano Letters* **2007**, *7*, 861-867.
9. Mulder, W. J. M.; Koole, R.; Brandwijk, R. J.; Storm, G.; Chin, P. T. K.; Strijkers, G. J.; Donega, C. D.; Nicolay, K.; Griffioen, A. W., Quantum dots with a paramagnetic coating as a bimodal molecular imaging probe. *Nano Letters* **2006**, *6*, 1-6.
10. Gao, G. H.; Im, G. H.; Kim, M. S.; Lee, J. W.; Yang, J.; Jeon, H.; Lee, J. H.; Lee, D. S., Magnetite-nanoparticle-encapsulated ph-responsive polymeric micelle as an mri probe for detecting acidic pathologic areas. *Small* **2010**, *6*, 1201-1204.
11. Das, M.; Mishra, D.; Dhak, P.; Gupta, S.; Maiti, T. K.; Basak, A.; Pramanik, P., Biofunctionalized, phosphonate-grafted, ultrasmall iron oxide nanoparticles for combined targeted cancer therapy and multimodal imaging. *Small* **2009**, *5*, 2883-2893.
12. Mazzucchelli, S.; Colombo, M.; De Palma, C.; Salvade, A.; Verderio, P.; Coghi, M. D.; Clementi, E.; Tortora, P.; Corsi, F.; Prospero, D., Single-domain protein a-engineered magnetic nanoparticles: Toward a universal strategy to site-specific labeling of antibodies for targeted detection of tumor cells. *ACS Nano* **2010**, *4*, 5693-5702.
13. Smith, J. E.; Sapsford, K. E.; Tan, W. H.; Ligler, F. S., Optimization of antibody-conjugated magnetic nanoparticles for target preconcentration and immunoassays. *Analytical Biochemistry* **2011**, *410*, 124-132.
14. Santra, S.; Kaittanis, C.; Grimm, J.; Perez, J. M., Drug/dye-loaded, multifunctional iron oxide nanoparticles for combined targeted cancer therapy and dual optical/magnetic resonance imaging. *Small* **2009**, *5*, 1862-1868.

15. Wang, D.; Qian, F.; Yang, C.; Zhong, Z. H.; Lieber, C. M., Rational growth of branched and hyperbranched nanowire structures. *Nano Letters* **2004**, *4*, 871-874.
16. Liu, S. Y.; Jiang, X. Z.; Zhuo, G. L., In situ chemical formation of iron phthalocyanine (FePc) monolayer on the surface of magnetite nanoparticles. *New Journal of Chemistry* **2007**, *31*, 916-920.
17. Koo, B.; Baek, H.; Cho, J., Control over memory performance of layer-by-layer assembled metal phthalocyanine multilayers via molecular-level manipulation. *Chemistry of Materials* **2012**, *24*, 1091-1099.
18. Nyokong, T.; Antunes, E., Influence of nanoparticle materials on the photophysical behavior of phthalocyanines. *Coordination Chemistry Reviews* **2013**, *257*, 2401-2418.
19. Balraj, C.; Elango, K. P., Spectroscopic studies on the intermolecular charge transfer interaction of Fe (II)- and Fe (III)-phthalocyanines with 2,3,5,6-tetrachloro-1,4-benzoquinone and its application in colorimetric sensing of amino acids and amines. *Spectrochimica Acta Part a-Molecular and Biomolecular Spectroscopy* **2012**, *86*, 44-50.
20. Kandela, I. K.; Lee, W.; Indig, G. L., Effect of the lipophilic/hydrophilic character of cationic triarylmethane dyes on their selective phototoxicity toward tumor cells. *Biotechnic and Histochemistry* **2003**, *78*, 157-169.
21. Sonvico, F.; Mornet, S.; Vasseur, S.; Dubernet, C.; Jaillard, D.; Degrouard, J.; Hoebeke, J.; Duguet, E.; Colombo, P.; Couvreur, P., Folate-conjugated iron oxide nanoparticles for solid tumor targeting as potential specific magnetic hyperthermia mediators: Synthesis, physicochemical characterization, and in vitro experiments. *Bioconjugate Chemistry* **2005**, *16*, 1181-1188.
22. Mutin, P. H.; Guerrero, G.; Vioux, A., Hybrid materials from organophosphorus coupling molecules. *Journal of Materials Chemistry* **2005**, *15*, 3761-3768.
23. Rich, A.; Blow, D. M., Formation of a helical steroid complex. *Nature* **1958**, *182*, 423-426.

## CHAPTER 5. IONIC LIQUID-BASED NANOMATERIALS FOR PH SENSING AND CHEMOTHERAPY\*

### 5.1. Introduction

Smart materials capable of applications as inexpensive sensing tools using a simple colorimetric approach are highly desirable for analysis and diagnosis. One of the most important rationale for this observation is that colorimetric detection techniques minimize the need for more sophisticated instrumentation. Numerous nanoparticles have been developed for colorimetric biosensing, including gold, silver, graphene oxide, and carbon nanotubes.<sup>1</sup> Color changes observed due to aggregation and disaggregation of these nanoparticles have also been used as methods for detection of several biomaterials.<sup>1</sup> For example, magnetic nanoparticles such as Fe<sub>3</sub>O<sub>4</sub> undergo color change due to the catalysis of peroxidase substrates.<sup>2,3</sup> Aptamer-based colorimetric sensors are also reported, where aptamer binding events are transformed into a colorimetric response.<sup>4</sup> Colorimetric detection of adenosine and cocaine has also been performed using such sensors.<sup>4</sup>

The pH balance in mammalian tissues can be altered under several health conditions such as cancer, chronic pulmonary diseases, and renal failure.<sup>5</sup> The extracellular pH value usually lies in the range of 5 - 7 under various pathological conditions. Certain bacterial infections also produce an acidic environment where the pH may vary between 4.5 - 7.0.<sup>6</sup> On the basis of this observation, pH sensitive polymeric nanoparticles as well as nanoparticles embedded in pH sensitive gel matrices have been designed for local delivery of antibiotics.<sup>6</sup>

\*Part of this work was published by Das, S.; Magut, P. K. S.; de Rooy, S. L.; Hasan, F.; Warner, I. M., Ionic liquid-based fluorescein colorimetric pH nanosensors. *RSC Advances* **2013**, *3*, 21054-21061 and is Reproduced by permission of The Royal Society of Chemistry [DOI:10.1039/C3RA42394H](https://doi.org/10.1039/C3RA42394H)

Tumors and cancerous tissues have been found to exhibit acidic pH values as compared to normal tissues due to the production of lactic acid as well as hydrolysis of ATP in the hypoxic regions of tumors.<sup>5</sup> Thus, several pH responsive nanoparticles have been applied to stimuli responsive drug delivery for tumors and cancerous sites<sup>7</sup> through exploitation of their acidic environment.

As pH is an important indicator for advancement of numerous diseases and biological processes, development of smart nanomaterials for simple detection of pH using a colorimetric approach, in combination with additional measurable pH dependent parameters, is highly desirable. In this regard, various metal nanoparticles based colorimetric pH sensors have been reported, including modification of gold or silver nanoparticles with DNA,<sup>8</sup> protein antigens,<sup>9</sup> and polymers.<sup>10</sup> Although several nanomaterials have been designed toward this end, most of these materials involve multistep and very sophisticated synthetic procedures. Thus, a facile, cost efficient design in this direction would be extremely advantageous.

Room temperature ionic liquids (RTILs) have been applied to multiple analytical techniques such as separation science, MALDI-MS, quartz crystal microbalance sensors, as well as synthetic chemistry, as catalysts and solvents in electroanalysis.<sup>11</sup> Due to their versatility, several ionic liquids have been prepared using various combinations of ions in order to obtain desired properties. For example, a recent communication reports an RTIL-based colorimetric amine sensing on films.<sup>12</sup> In another study, ILs have been synthesized using indicator dyes and their pH sensitive properties have been investigated.<sup>13</sup> A recent report describes the design of an ionic liquid polymer gel-based barcode system derived from indicator dyes for determining the pH of sweat generated during an exercise period.<sup>14</sup> However, to the best of our knowledge, nanosensors based on RTILs with pH dependent colorimetric and morphological response have

not yet been reported. Optical nanosensors for a variety of sensing applications including pH, which involve encapsulation of dyes in polymeric nanoparticles, have been developed by Kopelman and co-workers.<sup>15</sup> However, pH dependent colorimetric and size changes have not been observed in such studies. Moreover, problems such as leaching and alteration of photophysical properties are often encountered upon encapsulation of fluorophores.<sup>15</sup> In recent years, our group has introduced nanoparticles derived from a Group of Uniform Materials Based on Organic Salts (GUMBOS), which are higher melting (solid phase) counterparts of ionic liquids with much wider scopes of variations. We have reported functional, as well as multifunctional nanoGUMBOS with various morphologies and spectral features.<sup>16-18</sup>

Herein, we report the synthesis, characterization, and pH dependent properties of two novel nanomaterials based on RTILs derived from fluorescein (FL) and trihexyltetradecylphosphonium (TTP) ions of two different stoichiometries. The present study involves development of nanosensors directly from a fluorophore in contrast to studies reported in the literature where the fluorophore is either encapsulated or covalently linked to polymeric nanoparticles.<sup>15,19</sup> The pH dependent optical and morphological properties of these nanosensors suggest their potential utility for applications in detection, *in vitro* pathological applications, as components for pH and size dependent chemical separation,<sup>20</sup> as well as pH sensitive drug delivery devices.<sup>21</sup>

## **5.2. Materials and Methods**

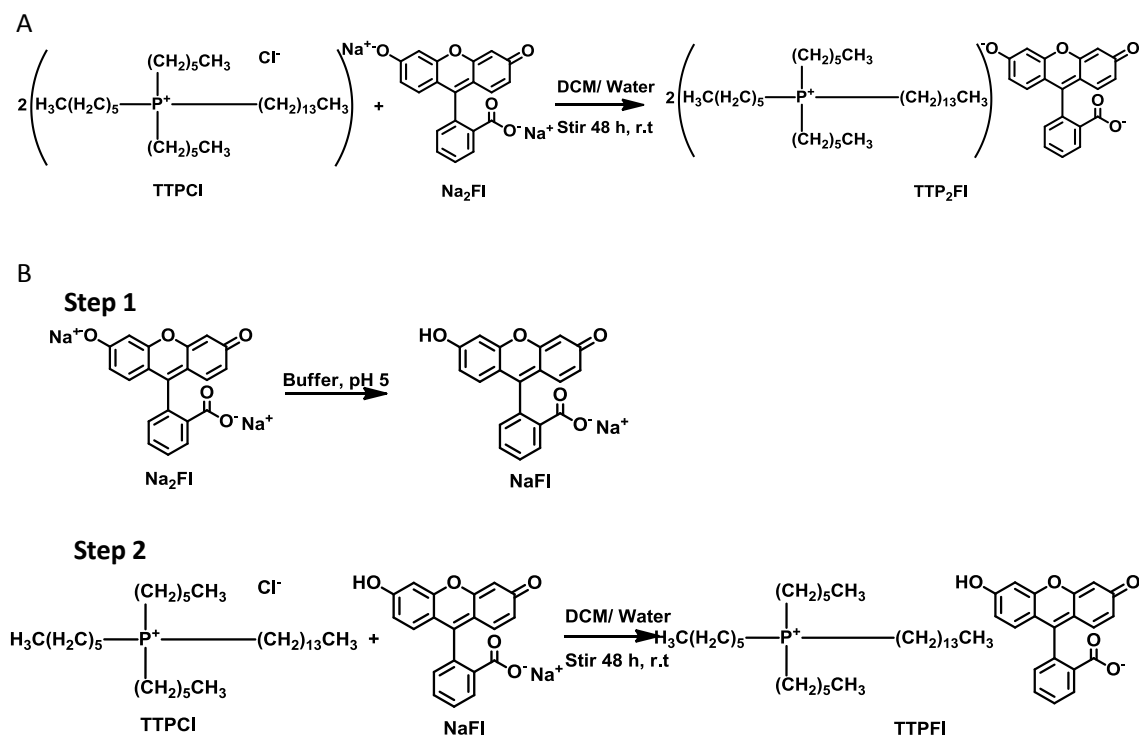
### **5.2.1. Materials**

Trihexyltetradecylphosphonium chloride, disodium fluorescein, tetrabutylphosphonium chloride, benzyltriphenylphosphonium chloride, 4-nitrobenzyltriphenylphosphonium chloride and tetraphenylphosphonium chloride were purchased from Sigma Aldrich and were used as

received. Citric acid (Sigma Aldrich), sodium phosphate dibasic heptahydrate (Fisher Scientific), and sodium phosphate monobasic monohydrate (Fisher Scientific) were used for the preparation of universal buffer (pH 2.2 - pH 5.5)<sup>22</sup> and phosphate buffer (pH 7.4). Triply deionized water (18.2 MΩ cm), obtained from an Elga model PURELAB ultra water-filtration system, was used for the preparation of all the solutions.

### 5.2.2. Synthesis and Characterization of Ionic Liquids

The [TTP]<sub>2</sub>[FL] IL was synthesized using an ion exchange reaction (Scheme 5.1, A) where TTPCl was dissolved in dichloromethane (DCM) and mixed with Na<sub>2</sub>Fl dissolved in water.



Scheme 5.1. Synthesis of (A) [TTP]<sub>2</sub>[FL] and (B) [TTP][FL] ionic liquids

Phosphonium chloride and disodium fluorescein were taken in a molar ratio of 2:1. The mixture was stirred for 48 h following which the two layers were separated. The DCM layers were washed several times with water to remove the water soluble impurities. The organic layer was dried over anhydrous sodium sulfate and the solvent was removed under reduced pressure. The

synthesis of [TTP][FL] was accomplished in two steps (Scheme 5.1, B). In the first step, monosodium fluorescein was synthesized by monoprotection of Na<sub>2</sub>FL by stirring it in a buffer of pH 5.<sup>23</sup> In the second step, the sodium ion was exchanged with the TTP cation in a 1:1 molar ratio using the same ion-exchange reaction described above. Both products were characterized by <sup>1</sup>H-NMR and electrospray ionization mass spectrometry. The formation of the 1:1 and 2:1 stoichiometries was confirmed by integrated <sup>1</sup>H NMR.

### **5.2.3. Synthesis and Characterization of Nanomaterials from Ionic Liquids**

Nanomaterials were synthesized from the ILs using a modified simple, additive-free reprecipitation method similar to that used for organic nanoparticles.<sup>24,25</sup> In a typical preparation, 250 µL of a 1 mM solution of GUMBOS precursor dissolved in ethanol was rapidly injected into 5 mL of triply-deionized water in an ultrasonic bath, followed by additional sonication for 2 min. All solvents used in this study were filtered prior to nanoparticle preparation using 0.2 µm nylon membrane filters. The particles were allowed a 15 min of equilibration time after preparation and then characterized using different techniques.

The average particle size and size distribution of the prepared nanomaterials were obtained by use of transmission electron microscopy (TEM). TEM micrographs were obtained using an LVEM5 transmission electron microscope (DeLong America, Montreal, Canada). The nanoGUMBOS dispersion (1 µL) were drop casted onto a carbon coated copper grid and allowed to dry in air at room temperature before TEM imaging. Dynamic light scattering (DLS) studies for size determination of nanomaterials were performed using a Malvern Zetasizer, UK. Zeta potentials of the nanomaterials were also determined using the same set up.

#### 5.2.4. Absorption and Fluorescence Studies

Absorbance measurements were performed using a Shimadzu UV- 3101PC, an UV-Vis-near-IR scanning spectrometer (Shimadzu, Columbia, MD). Fluorescence studies were performed using a Spex Fluorolog-3 spectrofluorimeter (model FL3-22TAU3); Jobin Yvon, Edison, NJ). A 0.4 cm path length quartz cuvette (Starna Cells) was used for acquiring the fluorescence and absorbance spectra against an identical cell filled with water as the blank. Fluorescence studies were performed adopting a synchronous scan protocol with right angle geometry. Fluorescence spectra were corrected for inner filter effects using a standard formula.<sup>26</sup>

Fluorescence anisotropy ( $r$ ) is a measure of the average angular displacement of the fluorophore between the absorption and subsequent emission of the photon and is given by the formula:

$$r = \frac{I_{VV} - GI_{VH}}{I_{VV} + 2GI_{VH}}$$

The parameters  $I_{VV}$  and  $I_{VH}$  are the fluorescence emission intensity measured parallel and perpendicular to the vertically polarized excitation, respectively.  $G$  is the grating factor included to correct for the wavelength response for polarization of the emission optics and the detector. Its given by the formula:

$$G = \frac{I_{HV}}{I_{HH}}$$

The parameters  $I_{HH}$  and  $I_{HV}$  are the fluorescence emission intensity measured parallel and perpendicular to the horizontally polarized excitation.<sup>26</sup> Fluorescence lifetime measurements were performed at Horiba Jobin Yvon, NJ using time domain mode. A picoseconds pulsed excitation source of 450 nm was used and emission was collected at 545 nm for [TTP]<sub>2</sub>[FL] and



515 nm for [TTP][FL] with a TBX detector. The time correlated single photon counting (TSCPC) mode was used for data acquisition with a resolution of 7 ps/channel.

### **5.2.5. Cytotoxicity Studies**

Cytotoxicities of [TTP]<sub>2</sub>[FL] and [TTP][FL] nanomaterials were determined against breast cancer (MCF-7, ATCC no. HTB-22, MDA-MB-231, ACC no. HTB-26) and normal breast (Hs578Bst, ATCC no. HTB-125) cell lines using an MTT Assay kit (Promega Corporation, Madison, WI, USA), according to the manufacturer's instructions. Briefly, in a 96-well plate, 5000 cells in 0.1 mL culture medium were seeded to each well. After 24 h, the old culture medium was removed and discarded and 0.1 mL of new culture medium containing 0-40 μM ILs dissolved in 1% DMSO was introduced to the cells. The cells were then incubated for 48 h at 37 °C, in 5% CO<sub>2</sub> atmosphere. At the end of the incubation period, the cells were treated with 15 μL 3-(4,5-dimethylthiazol-2-yl)-2,5-diphenyltetrazolium bromide (MTT) and incubated for 4 h. After 4 h, 100 μL of the stock solution was added per well and incubated overnight. The plate was shaken for 20 s and absorbance was then read at 570 nm with a reference wavelength of 650 nm using a micro plate spectrophotometer (Benchmark Plus, Bio-Rad Laboratories, Hercules, CA, USA). Cell viability as a percentage was determined by taking the ratio between absorbance of the treated cells and the absorbance of untreated (control) cells taken as 100%.

### **5.3. Results and Discussions**

Aqueous solutions of disodium fluorescein (Na<sub>2</sub>FL) has been known to exhibit pH sensitive spectral changes, which are attributable to the presence of different ionic forms of fluorescein.<sup>23</sup> However, to the best of our knowledge and as demonstrated in this study, Na<sub>2</sub>FL is not known to exhibit any significant pH dependent colorimetric response. Moreover, Na<sub>2</sub>FL is highly soluble in aqueous medium, and, thus, nanoformulation is not possible.

Herein, hydrophobic salts of fluorescein were synthesized in two different stoichiometries in combination with TTP counterions. The presence of both the ions was determined by electrospray ionization mass spectrometry performed in positive and negative ion modes. The  $^1\text{H}$  NMR results were as follows; [TTP][FL]: Dark orange sticky solid. Yield, 93%.  $^1\text{H}$ -NMR (DMSO, 400 MHz):  $\delta$  7.95 (d,  $J$ = 8.32, 1H), 7.55 (m, 2H), 7.13 (d,  $J$ = 7.44 Hz, 1H), 6.57 (d,  $J$ = 9 Hz, 2H), 6.34 (s, 1H), 6.30 (d,  $J$ = 8.88 Hz, 2H), 2.15 (m, 8H), 1.45-1.23 (m, 48H), 0.85 (m, 12H).

[TTP] $_2$ [FL]: Orange viscous liquid. Yield, 88%.  $^1\text{H}$ -NMR (DMSO, 400 MHz):  $\delta$  7.88 (d,  $J$ = 6.92 Hz, 1H), 7.40 (m, 2H), 7.00 (d,  $J$ = 7.04 Hz, 1H), 6.57 (d,  $J$ = 9.12 Hz, 2H), 6.08 (m, 3H), 2.15 (m, 16H), 1.46-1.23 (m, 96H), 0.87 (m, 24H).

The bulky TTP cation not only induces hydrophobicity in the resulting salt but also drops its melting point below or close to room temperature, resulting in the formation of fluorescein based ILs. Hydrophobic properties were introduced in order to obtain fluorescein nanoparticles with pH sensitive spectral properties. The initial idea was to achieve these properties when these nanoparticles were suspended in aqueous medium for expansion of their applications as stimuli responsive carriers for therapeutic agents; however, the synthesized nanodroplets unexpectedly exhibited numerous pH sensitive effects, as well as potential therapeutic characteristics, which may allow several applications of these new materials.

### **5.3.1. Physical Characterization of the ILs**

Two ILs were synthesized using ion metathesis reactions in two different stoichiometric ratios, yielding the salts [TTP] $_2$ [FL] and [TTP][FL]. [TTP] $_2$ [FL] was an orange viscous liquid at room temperature, while the latter, [TTP][FL], was a dark orange sticky solid (Figure 5.1).

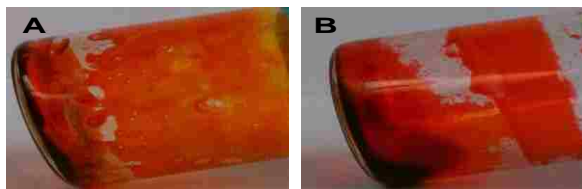


Figure 5.1. Pictures of the compounds (A) [TTP][FL] and (B) [TTP]<sub>2</sub>[FL].

A variation in their viscoelastic properties was expected, since the presence of two bulky cations leads to further frustrated packing,<sup>27</sup> resulting in a lower melting IL. Thermogravimetric analyses of these compounds suggested a fairly high decomposition temperature for both compounds. [TTP]<sub>2</sub>[FL] was stable up to 348.6 °C, while [TTP][FL] exhibited a decomposition temperature of 354.6 °C (Figure 5.2).

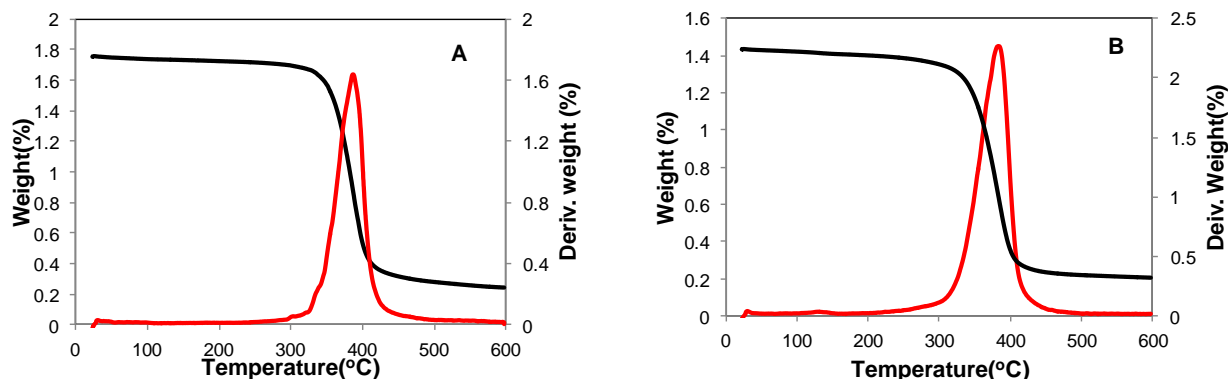


Figure 5.2. Thermogravimetric analysis of (A) [TTP][FL] and (B) [TTP]<sub>2</sub>[FL].

### 5.3.2. Optical Properties of pH Dependent TTP Nanomaterials

Nanomaterials derived from the two fluorescein-based ILs through a reprecipitation<sup>18</sup> technique produced contrasting pH dependent colorimetric responses. The [TTP]<sub>2</sub>[FL] nanodroplet suspension exhibited a red color in water whose inherent pH was 8.4 and in phosphate buffer of pH 7.4. These nanodroplets displayed distinct color changes with further variations of buffer pH (universal buffer)<sup>22</sup> in the acidic region. In a buffer of pH 5.5, the solution was orange, orange green at pH 4, and light green at pH 2.2 (Figure 5.3, a). However, [TTP][FL] nanoparticles did not exhibit a significant color change as a function of changes in pH value (Figure 5.3, b). A control experiment was also performed with the parent compound

( $\text{Na}_2\text{FL}$ ) at the same concentration, which displayed little or no pH dependent colorimetric response (Figure 5.3, c).

Absorption spectra of  $[\text{TTP}]_2[\text{FL}]$  nanodroplets revealed a 23 nm red-shift in unbuffered water and a 40 nm red-shift in buffer of pH 7.4, as compared to the same concentration of the parent compound ( $\text{Na}_2\text{FL}$ ) in the corresponding media. A red shift in the absorption spectrum of a dye is usually attributed to head to tail type of stacking, often referred to as J-type aggregation.<sup>18</sup>

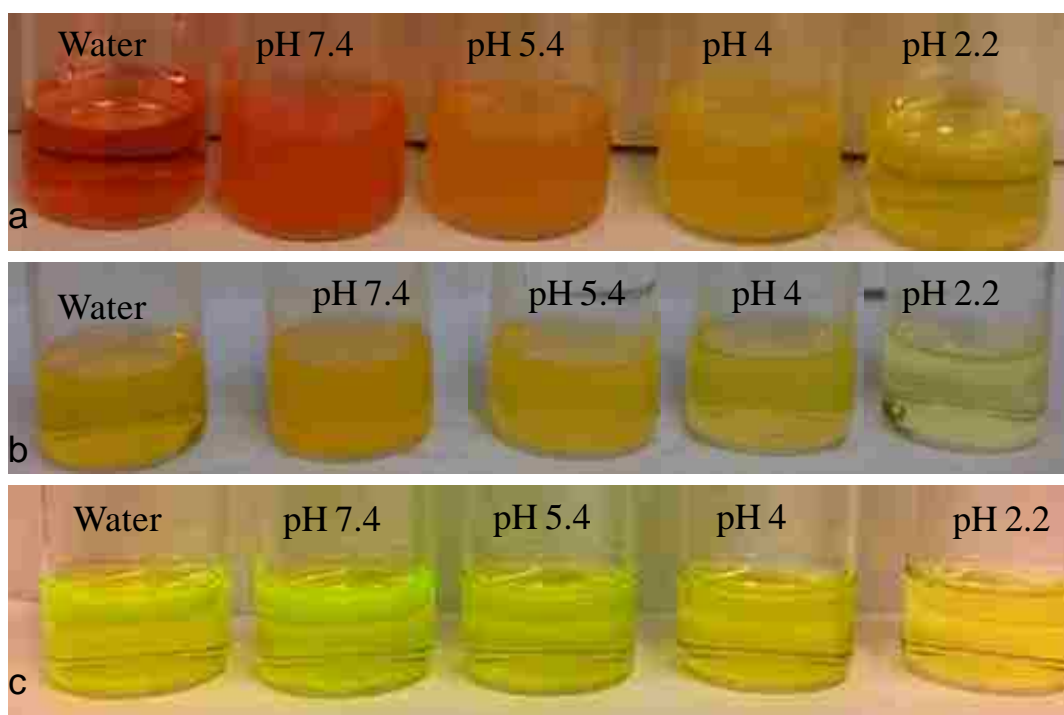


Figure 5.3. pH dependent color change of (a)  $[\text{TTP}]_2[\text{FL}]$  nanodroplets, (b)  $[\text{TTP}][\text{FL}]$  nanoparticles and (c)  $\text{Na}_2\text{FL}$  in water (inherent pH 8.4) and buffers of different pH.

A gradual blue shift in absorption maxima was observed with a lowering of the pH value below 7.4 (Figure 5.4, a). In spite of this blue shift in acidic buffers, the absorption maxima of the nanomaterials were red-shifted as compared to the parent compound. This observation suggests J-type aggregates of various stacking angles in different pH environments, which results in variable red-shifts.<sup>28</sup> In order to further confirm this as an aggregation effect and not just the

inherent characteristic of this IL, concentration dependent absorption spectra were collected. Examination of these spectra indicated that the absorption maxima were identical with those of the parent compound (490 nm) in the micromolar region. A concentration dependent change in shape and position of the absorption spectra and a complete red-shift in the absorption peak at higher concentrations further confirmed this as an aggregation effect, and, thus, the red shift is attributed to J-type of aggregation within these nanomaterials at higher concentrations.<sup>18</sup>

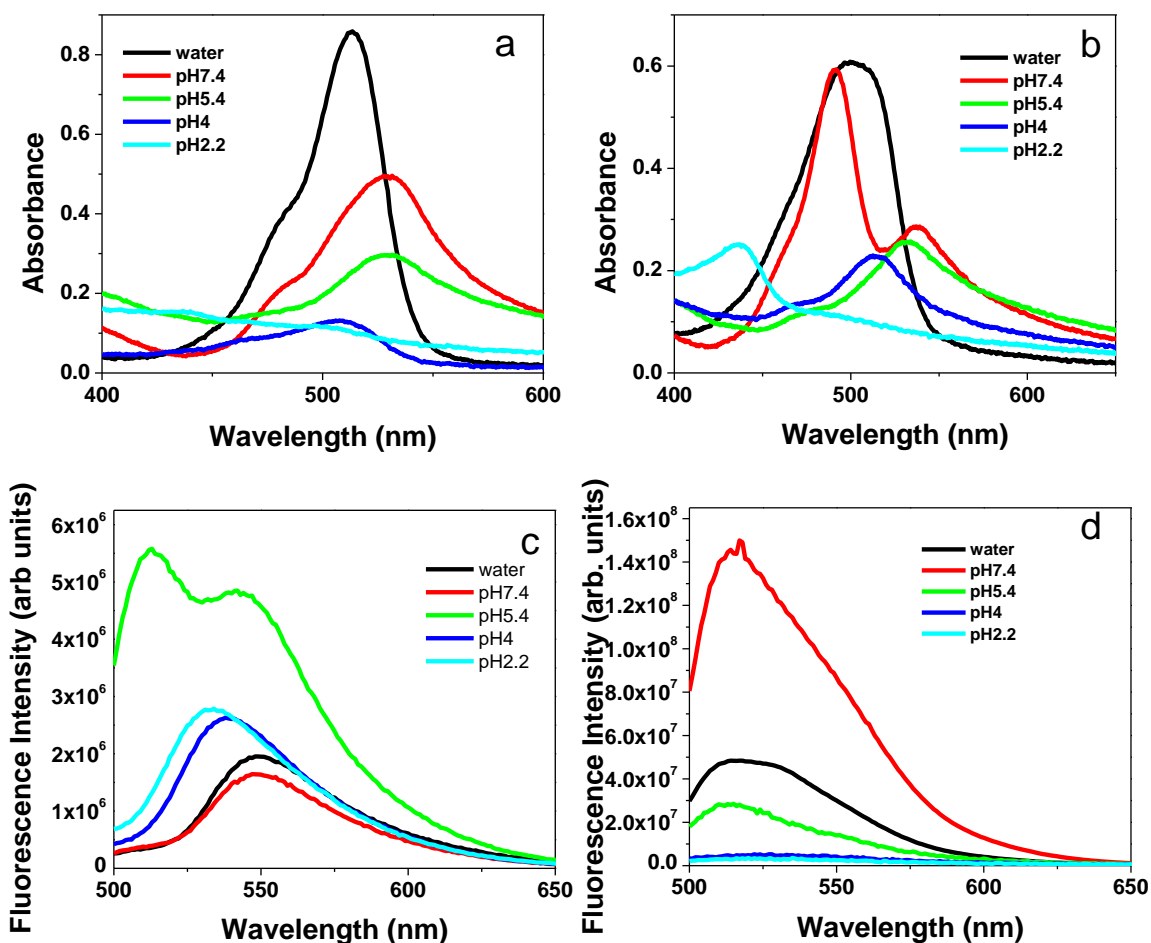


Figure 5.4. (a, c) absorption and fluorescence spectra of  $[TTP]_2[FL]$  and (b, d) of  $[TTP][FL]$ , respectively.

In addition to the observed colorimetric response,  $[TTP]_2[FL]$  nanodroplets were also observed to display a pH dependent fluorescence emission and excitation spectra. In water (pH 8.4) and pH 7.4 buffer, the fluorescence emission and excitation spectra of the  $[TTP]_2[FL]$

nanodroplets (50  $\mu\text{M}$ ) were red-shifted as compared to the parent compound ( $\text{Na}_2\text{FL}$ ) and to the same compound ( $[\text{TTP}]_2[\text{FL}]$ ) at lower concentrations. In an acidic environment, the fluorescence spectrum was gradually blue-shifted towards the monomeric region, also suggesting a change in molecular stacking with pH (Figure 5.4).<sup>18,28</sup> It is worth noting that the Stokes shift of these nanomaterials was extremely low and, in some cases (at pH 7.4 and 5.4), nearly resonance fluorescence was observed, which is a well-established signature of J-aggregation.<sup>18</sup> In addition to the red-shifted absorption spectra and the small Stokes shifts (Figure 5.4), J-aggregation was also confirmed by use of fluorescence lifetime measurements. Lifetime studies suggested that in water and at pH 7.4,  $[\text{TTP}]_2[\text{FL}]$  nanodroplets were found to be composed entirely of a shorter lifetime component (73 ps) which is characteristic of J-aggregates as compared to its lifetime of 4 ns in the monomeric state in water. The monomeric lifetime was found to be similar to that of the parent compound in an aqueous medium.<sup>29</sup> The relatively lower fluorescence intensity of  $[\text{TTP}]_2[\text{FL}]$  J-aggregates is attributed to the formation of higher order aggregates which leads to quenching.<sup>30</sup>

Although,  $[\text{TTP}][\text{FL}]$  nanodroplets did not demonstrate any significant pH dependent color change, shifts (Figure 5.4, d) and the appearance of distinct peaks/ shoulders in the absorption spectra (Figure 5.4, b) with varying pH suggest a similar change in molecular aggregation for various pH environments.<sup>18</sup> The fluorescence emission maxima in water was centered around the monomeric emission peak (513 nm), revealing that the predominant emitting species were likely monomers, which is also complemented by a two component fluorescence lifetime decay with 79% contribution from the monomer with a lifetime of 3.9 ns and 21% contribution from a 109 ps component attributed to J-aggregates. The fluorescence emission maxima of  $[\text{TTP}][\text{FL}]$  at all pH values being centered on 513 nm is consistent with the fact that

the primary fluorescence emission was contributed by the monomeric component. The decrease in fluorescence emission was however attributed to the formation of weakly fluorescent or non-fluorescent aggregates in various pH environments.

Thus, it can be summarized from the optical properties thus far that the presence of two TTP cations favors J-aggregation to a greater extent compared to one TTP cation. The two bulky TTP cations might force the two adjacent  $FL^{2-}$  anions to stack in a head-to-tail fashion (Figure 5.5) in order to have minimum steric hindrance from each other. However, only one TTP cation in  $[TTP][FL]$  allows the two  $FL^-$  anions to mostly stack in a random fashion, therefore resembling the monomeric species in their spectral behaviour, and partly stacking into head-to-tail manner (J-type of aggregates) (Figure 5.5, B).

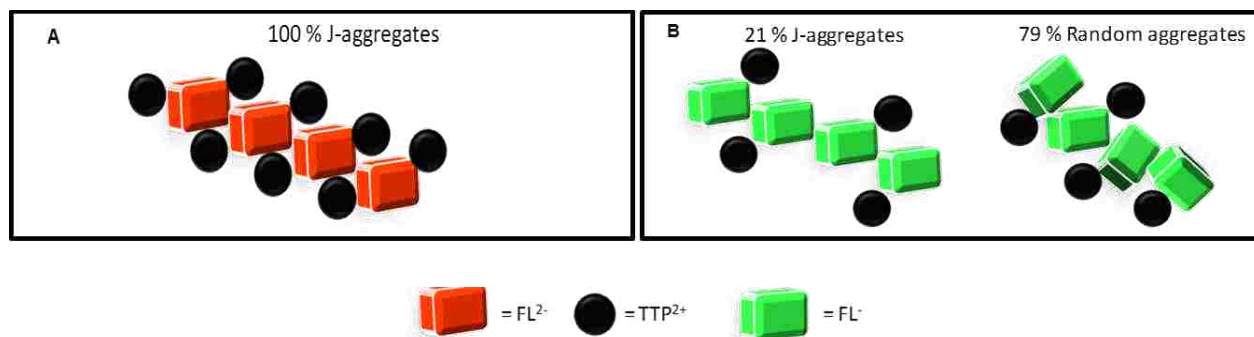


Figure 5.5. Schematic representation of the type of aggregation in (A)  $[TTP]_2[FL]$  and (B)  $[TTP][FL]$ .

Examination of data from photostability studies of  $[TTP]_2[FL]$  nanoparticles indicated extremely high photostability upon prolonged (2500 s) irradiation under maximum exposure (Figure 5.6, a). The photostability of  $[TTP]_2[FL]$  in ethanolic solution were found to increase under similar conditions. Such an effect was also observed in previous studies and was attributed to irradiation induced J-aggregation.<sup>31</sup> We note that photostability of fluorescent nanomaterials is an extremely important factor for determining sensor applicability in adverse conditions. Thus, the observed enhanced photostability in solutions and extremely high (100 %) photostability of the nanodroplets of these materials are considered an additional advantage of the materials.

Fluorescence anisotropy (FA) studies of the  $[TTP]_2[FL]$  nanodroplets (Figure 5.6, b) also suggest a change in molecular aggregation with variation of pH, exhibiting negative and lower FA values in water and at pH 7.4 where J-aggregation is maximum. FA was found to increase with increasing acidity of the buffer, suggesting alteration in molecular stacking and formation of different types of aggregates. J-aggregates have often been reported to demonstrate lower as well as negative FA upon excitation at a wavelength blue to J-band, and are attributed to faster exciton relaxation and energy migration compared to randomly oriented or H-type of aggregates.<sup>18,32</sup>

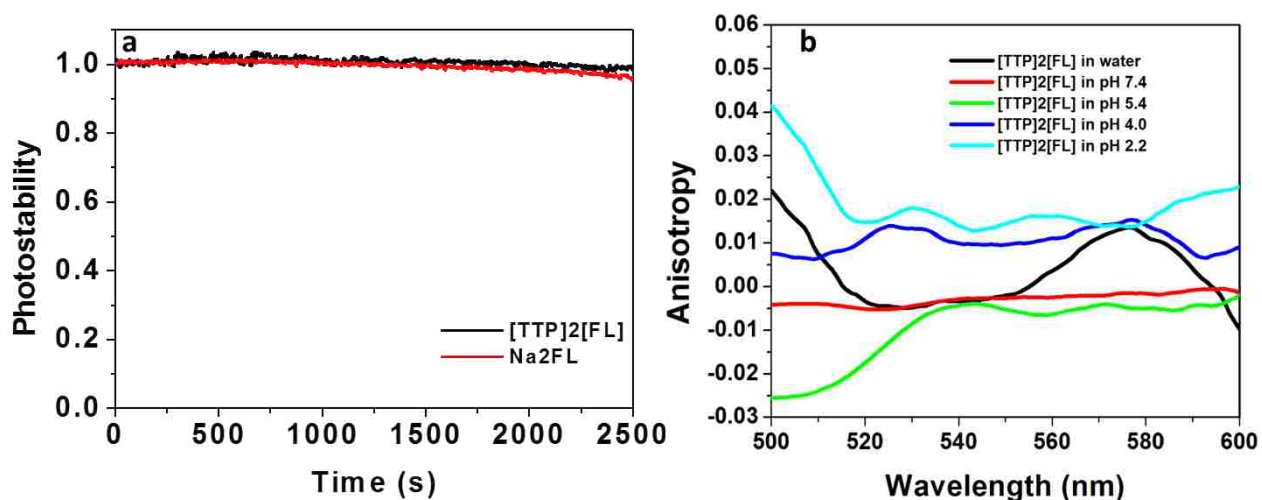


Figure 5.6. a) Photostabilities of  $[TTP]_2[FL]$  nanoparticles compared to  $Na_2FL$  solution in water and b) fluorescence emission anisotropy of  $[TTP]_2[FL]$  nanodroplets in buffer of varying pHs.

Fluorescence anisotropy studies provide a molecular level picture of the nanodroplets, and a better understanding of the intermolecular aggregation behavior under various pH conditions.

### 5.3.3. Morphological Changes in TTP Nanomaterials with Changes in pH

The pH dependent colorimetric response was also accompanied by a change in particle size, as illustrated in the transmission electron microscopic images (Figure 5.7) of the  $[TTP]_2[FL]$  nanodroplets. These nanodroplets demonstrated a size of  $28 \pm 8$  nm at pH 7.4,



gradually increasing in size with lowering of pH, attaining a size of  $1.6 \pm 0.2 \mu\text{m}$  at pH 4, followed by the appearance of two distinctly different sizes at pH 2.2 viz.  $797 \pm 171 \text{ nm}$ ,  $167 \pm 46 \text{ nm}$  (Figure 5.7). This observation was also complemented by data obtained from DLS (Table 5.1). Examination of data from DLS studies indicated similar expansion of the nanodroplets with decreasing pH up to pH 4, followed by a sudden drop in size at pH 2.2 accompanied with some micron sized particles. It was noted during these studies that the nanodroplet dispersions were extremely stable for hours with insignificant particle growth or change in surface charge over time.

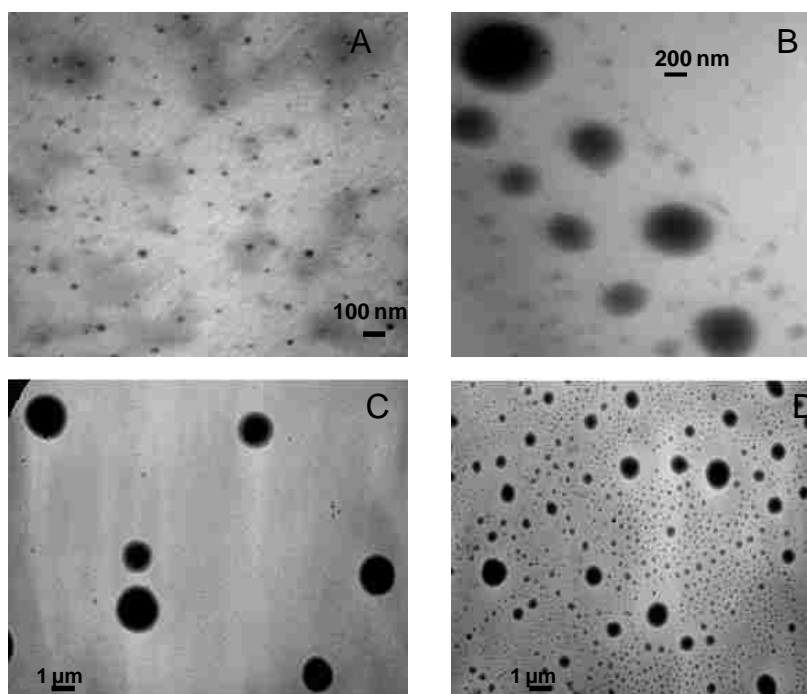


Figure 5.7. TEM micrographs of [TTP]<sub>2</sub>[FL] nanoparticles in (A) water (pH 8.4) ( $28 \pm 8 \text{ nm}$ ) and buffers of (B) pH 5.4 ( $453 \pm 197 \text{ nm}$ ), (C) pH 4.0 ( $1.6 \pm 0.2 \mu\text{m}$ ), (D) pH 2.2 ( $797 \pm 171 \text{ nm}$ ,  $167 \pm 46 \text{ nm}$ ).

Examination of TEM micrographs indicates relatively less dense mesodroplets in the acidic environments which is recognized as an effect of expansion in these media. One possible explanation for the observed nanoparticle swelling is attributed to an alteration in molecular stacking within the nanodroplets under various pH conditions due to the formation of various

protolytic states of FL. It has been reported in the literature that both covalent and non-covalent interactions, such as  $\pi$ - $\pi$  interaction, play a significant role in molecular organization at the nanoscale level.<sup>33</sup> Fluorescein is known to exist in four protolytic forms with dissociation constants (pKa) of 2.08, 4.31 and 6.43 corresponding to respective transitions from cationic to neutral, neutral to monoanionic, and monoanionic to dianionic.<sup>23</sup>

Table 5.1. Size of [TTP]<sub>2</sub>[FL] and [TTP][FL] nanodroplets at various pH values obtained from dynamic light scattering.

System	Peak 1 (nm)	Peak1 ar. Int. (%)	Peak 2 (nm)	Peak2 ar. Int. (%)	Z-average (nm)	PDI
[TTP] <sub>2</sub> [FL] in water	85.8	100	-	-	77.1	0.144
[TTP] <sub>2</sub> [FL] in pH 7.4	173.9	100	-	-	188.3	0.18
[TTP] <sub>2</sub> [FL] in pH 5.4	763	100	-	-	874	1
[TTP] <sub>2</sub> [FL] in pH 4.0	1592	100	-	-	1592	1
[TTP] <sub>2</sub> [FL] in pH2.2	124.5	98.8	2490	1.2	114.7	0.141
[TTP][FL] in water	100.7	100	-	-	96.62	0.088
[TTP][FL] in pH 7.4	534.7	100	-	-	538.1	0.039
[TTP][FL] in pH 5.4	402.4	100	-	-	521.1	0.057
[TTP][FL] in pH 4.0	795.9	100	-	-	717.4	0.17
[TTP][FL] in pH2.2	124.1	100	-	-	115.1	0.108

The neutral to monoanionic and monoanionic to dianionic protolytic constants were determined for [TTP]<sub>2</sub>[FL] using UV-visible spectrophotometry, and were found to be 4.52 and 6.37, respectively. These values are very close to the reported values for disodium fluorescein. Thus, the smallest particle size was obtained when fluorescein was in its dianionic form (water and pH 7.4) within the [TTP]<sub>2</sub>[FL] nanodroplets, which corresponds to an ordered head-to-tail type of stacking, as suggested by the examination of the absorption and fluorescence steady state

spectra, as well as time domain measurements. Monoprotonation of fluorescein at pH 5.4, leading to its monoanionic form, disturbs this ordered arrangement, as suggested by shifts in the absorption and fluorescence properties resulting in swelling. A further disordered arrangement ensues when the neutral form of fluorescein is formed at pH 4, which in combination with the hydrophobic phosphonium cations, results in an additional increase in particle size. However, the formation of cationic fluorescein at pH 2.2 should lead to repulsion with the phosphonium cations, possibly causing complete deformation of the pre-existing particles and formation of smaller particles of a different size distribution. Both fluorescein and phosphonium cations under such conditions are obviously considered to be associated with other counterions present in the buffer. The changes in ionic states of fluorescein with variation of pH values, affect the number of TTP ions associated with each FL, as well as the ionic and other non-covalent interactions within the particles. This change in interactions leads to different molecular orientations and stacking within the nanomaterial which contributes to the color changes of the dispersion.

Examination of zeta potential measurements indicates a systematic change in surface charge with varying pH. The variation in molecular orientation at various pH values possibly contributes to the variable surface charge. In water and at pH 7.4, the surface charge was highly positive ( $\sim +40\text{mV}$ ) (Table 5.2), which is also consistent with the observed high stability of these particles. The surface charge becomes less positive with lower pH values and then becomes negative. The surface charge is nearly zero at pH 4 and attains a high positive value at pH 2. The change in zeta potential (Table 5.2) of the particles at different pH values may also indicate altered orientations and the presence of variable numbers of TTP ions associated with different ionic forms of FL. A highly positive zeta potential at pH 2.2 is attributed to the presence of both fluorescein and phosphonium cations under such conditions. Similarly, a very small value of zeta

potential at pH 4 can be attributed to the presence of neutral fluorescein at this pH. In addition, the presence of monoanionic FL at pH 5.5, where one TTP cation is associated with one FL, yields a net negative surface charge. However, two TTP cations associated with the dianionic FL present at a physiological pH results in a net positive surface charge. Thus it is the molecular orientation and the presence of various ionic forms of FL under various pH conditions which determine the net charge on the nanoparticles.

Table 5.2. Zeta potential of [TTP][FL] and [TTP]<sub>2</sub>[FL] nanodroplets at various pH values.

Ionic liquid	pH	Zeta potential (mV)
[TTP] <sub>2</sub> [FL] in water	8.4	+45.50
[TTP] <sub>2</sub> [FL]	7.4	+36.45
[TTP] <sub>2</sub> [FL]	5.4	-9.89
[TTP] <sub>2</sub> [FL]	4.0	+1.45
[TTP] <sub>2</sub> [FL]	2.2	+55.9
[TTP][FL] in water	8.4	+25.1
[TTP][FL]	7.4	-12.35
[TTP][FL]	5.4	-12.00
[TTP][FL]	4.0	+0.09
[TTP][FL]	2.2	+60.15

In addition to these two ILs, four other phosphonium based disubstituted and monosubstituted ILs were synthesized through ion-exchange with the tetrabutylphosphonium, benzyltriphenylphosphonium, 4-nitrobenzyltriphenylphosphonium, and tetraphenylphosphonium counterions and their pH dependent characteristics were studied. A pH dependent color change was not observed for any of these ILs, including the parent sodium salt. Thus, the observed pH

dependent properties appear to be a unique characteristic of the nanoparticles based on  $[TTP]_2[FL]$ .

### 5.3.4. Anticancer Activity of TTP-based ILs

The extracellular pH of tumors is acidic (pH 4-6) as compared to normal cells. This is typically attributed to the lower buffering capacity of interstitial fluids and increased production of lactic acid within cancer cells.<sup>5</sup> Several pH sensing techniques including  $^{13}P$  NMR spectroscopy (using inorganic phosphates), pH sensitive  $^{19}F$  resonance, pH sensitive  $^1H$  NMR using appropriate probes, and pH sensitive Gadolinium relaxation using Gd based contrast agent, have been reported for probing such environments.<sup>5</sup> Incubation of  $[TTP]_2[FL]$  nanoparticles in acidified aqueous medium (with HCl) to pH 4 for an hour followed by removal of the solvent, indicated carboxylic acid protons (via NMR) in deuterated DMSO (Figure 5.8). Acidified aqueous medium was selected for these studies instead of buffer in order to avoid interferences from carboxylic acid protons present in the salts constituting the buffer. This study indicates the possible application of these particles in detecting acidic environments such as tumors by use of  $^1H$  NMR as well.

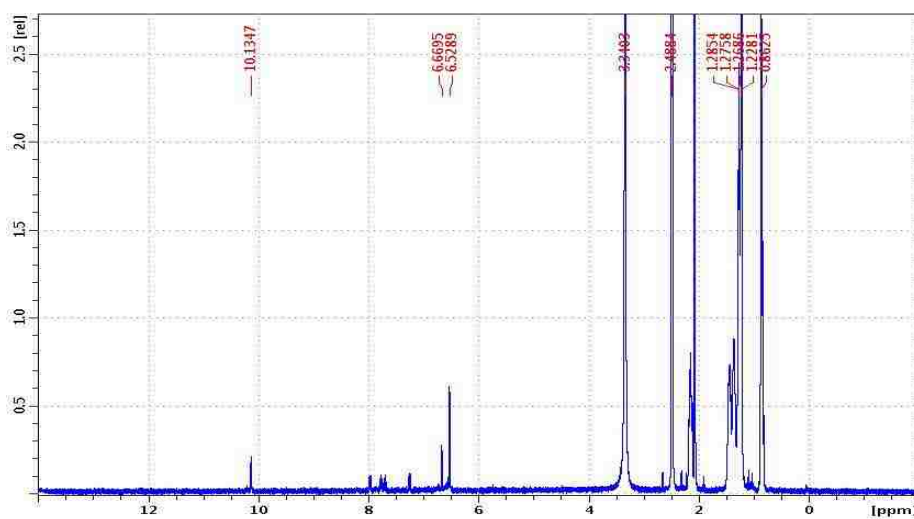


Figure 5.8. NMR of  $[TTP]_2[FL]$  nanodroplets synthesized and incubated at pH 4.

As discussed earlier, the reported anticancer activity of some phosphonium based ionic liquids<sup>34,35</sup> suggested exploration of the same for these new phosphonium salts. Tetraphenylphosphonium salts have been found to selectively accumulate in the mitochondrial membrane of cancer cells which is considered the possible pathway for their anticancer activities.<sup>35</sup> Anticancer activity of these salts were also found to correlate with the chain length of alkyl substitution on the phosphonium cation.<sup>34</sup> Cytotoxicity of the [TTP][FL] and [TTP]<sub>2</sub>[FL] nanoparticles towards a normal breast cell line (Hs578Bst) and two breast cancer cell line (MCF7 and MDA-MB-231) were studied. Examination of data from these studies showed that [TTP]<sub>2</sub>[FL] were more cytotoxic toward cancer cell lines as compared to [TTP][FL] (Figure 5.9). Since [TTP]<sub>2</sub>[FL] leads to greater cell death in the studied cancer cells, this possibly signifies that the phosphonium cation is primarily responsible for cytotoxic effects against cancer cells. In addition, the IC<sub>50</sub> values of the two compounds reveal that they are fairly non-toxic to normal cells and highly toxic towards cancer cell lines (Table 5.3).

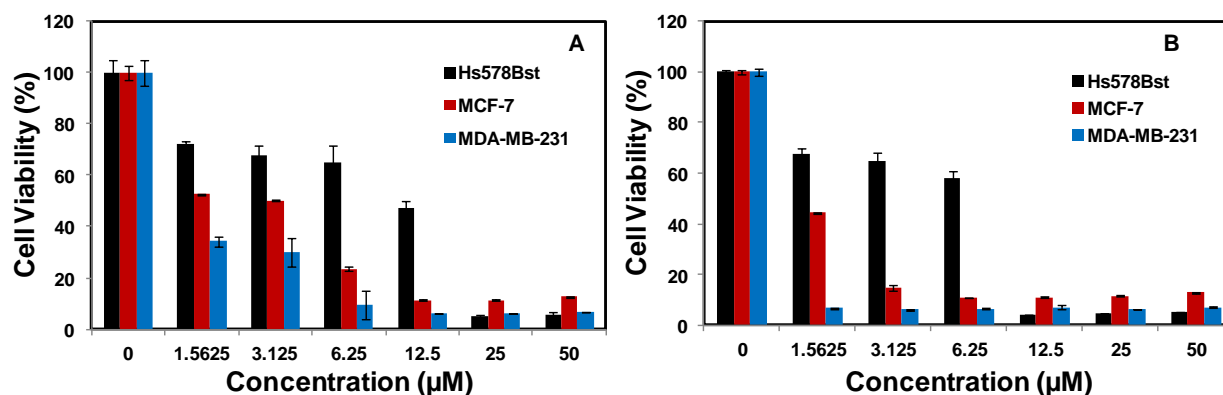


Figure 5.9. Cytotoxicity studies of (A) [TTP][FL] and (B) [TTP]<sub>2</sub>[FL] in normal breast (Hs578Bst) and breast cancer (MDA-MB-231, MCF-7) cell lines.

In order to confirm this finding, control studies were also performed with both starting materials and it was observed that Na<sub>2</sub>FL did not display any concentration dependent cell death in the investigated concentration range. In contrast, TTPCl did exhibit a concentration dependent cell death although their IC<sub>50</sub> were much higher than those of the ILs reported in this study

(Table 5.3). Thus, it is reasonable to infer that the cation and anion combination play a cooperative effect in the observed selectivity towards cancer cell lines.

Table 5.3. IC<sub>50</sub> values of [TTP][FL], [TTP]<sub>2</sub>[FL] and the starting materials [TTP][Cl] and Na<sub>2</sub>FL ILs in breast normal and cancer cell lines.

Cell line	IC <sub>50</sub> [TTP][FL]	IC <sub>50</sub> [TTP] <sub>2</sub> [FL]	IC <sub>50</sub> [TTP][Cl]	IC <sub>50</sub> Na <sub>2</sub> FL
Hs578Bst	10.17	7.17	5.0	>50
MCF-7	0.84	0.8	12.82	>50
MDA-MB-231	1.19	0.84	17.06	>50

Examination of the results outlined above suggest potential applications of [TTP]<sub>2</sub>[FL] nanoparticles for use as a therapeutic agent against breast cancer cell lines since its toxicity toward these cell lines are quite high as compared to normal cells. Although anticancer activities of some phosphonium and ammonium based ILs have been reported in the literature against several categories of human tumors, most studies do not report their activity in normal cell lines.<sup>34</sup> Lower cytotoxicities of our reported nanomaterials in normal breast cell lines clearly suggest their potential applicability in simultaneous detection and treatment of cancer.

Recently, several studies have demonstrated the challenge of delivering a requisite amount of drug to tumor cells due to the extremely high porosity of such cells. Owing to their high porosity, the rate of drug diffusion out of the tumors may be appreciably high as compared to the rate of drug penetration into them.<sup>36</sup> In this regard, the expansive properties of [TTP]<sub>2</sub>[FL] nanomaterials under acidic environment may be considered an advantage for addressing this challenging problem, since the diffusion of the expanded nanoparticles out of the tumors will likely be relatively slower.

## 5.4. Conclusions

In summary, two novel fluorescent pH dependent IL based nanomaterials have been successfully synthesized and characterized. The pH dependent colorimetric response of [TTP]<sub>2</sub>[FL] nanodroplets suggests possible applications of these materials for determination of acidosis *in vitro* or *in vivo* as biosensor for cancer and bacterial infections. The change in size of the nanodroplets with decrease of pH as suggested from the TEM and DLS studies may also be exploited for pH dependent molecular recognition as well as pH dependent drug delivery vehicles.<sup>37</sup> Furthermore, appearance of the carboxylic acid proton in <sup>1</sup>H NMR in an acidic environment can also be used as an additional detection tool. The anticancer activity displayed by these nanomaterials adds to the utility of their pH dependent colorimetric and morphological changes and thus may be further used for treating certain specific types of cancers as suggested from the results demonstrated in this study. Considerably large zeta potential of these nanoparticles suggests that the nanoparticles are stable in solution. In addition, the alteration in fluorescence properties with pH may also be utilized in fluorescence imaging to detect various pathological conditions.

## 5.5. References

1. Song, Y. J.; Wei, W. L.; Qu, X. G., Colorimetric biosensing using smart materials. *Advanced Materials* **2011**, *23*, 4215-4236.
2. Gao, L. Z.; Zhuang, J.; Nie, L.; Zhang, J. B.; Zhang, Y.; Gu, N.; Wang, T. H.; Feng, J.; Yang, D. L.; Perrett, S.; Yan, X., Intrinsic peroxidase-like activity of ferromagnetic nanoparticles. *Nature Nanotechnology* **2007**, *2*, 577-583.
3. Asati, A.; Santra, S.; Kaittanis, C.; Nath, S.; Perez, J. M., Oxidase-like activity of polymer-coated cerium oxide nanoparticles. *Angewandte Chemie-International Edition* **2009**, *48*, 2308-2312.
4. Liu, J. W.; Lu, Y., Fast colorimetric sensing of adenosine and cocaine based on a general sensor design involving aptamers and nanoparticles. *Angewandte Chemie-International Edition* **2006**, *45*, 90-94.
5. Gillies, R. J.; Raghunand, N.; Garcia-Martin, M. L.; Gatenby, R. A., pH imaging. *IEEE Engineering in Medicine and Biology Magazine* **2004**, *23*, 57-64.



6. Pichavant, L.; Bourget, C.; Durrieu, M. C.; Heroguez, V., Synthesis of pH-sensitive particles for local delivery of an antibiotic via dispersion romp. *Macromolecules* **2011**, *44*, 7879-7887.
7. Soppimath, K. S.; Liu, L. H.; Seow, W. Y.; Liu, S. Q.; Powell, R.; Chan, P.; Yang, Y. Y., Multifunctional core/shell nanoparticles self-assembled from pH-induced thermosensitive polymers for targeted intracellular anticancer drug delivery. *Advanced Functional Materials* **2007**, *17*, 355-362.
8. Saha, S.; Chakraborty, K.; Krishnan, Y., Tunable, colorimetric DNA-based pH sensors mediated by a-motif formation. *Chemical Communications* **2012**, *48*, 2513-2515.
9. Thanh, N. T. K.; Rosenzweig, Z., Development of an aggregation-based immunoassay for anti-protein a using gold nanoparticles. *Analytical Chemistry* **2002**, *74*, 1624-1628.
10. Liu, L. X.; Li, W.; Liu, K.; Yan, J. T.; Hu, G. X.; Zhang, A. F., Comb like thermoresponsive polymers with sharp transitions: Synthesis, characterization, and their use as sensitive colorimetric sensors. *Macromolecules* **2011**, *44*, 8614-8621.
11. Baker, G. A.; Baker, S. N.; Pandey, S.; Bright, F. V., An analytical view of ionic liquids. *Analyst* **2005**, *130*, 800-808.
12. Yung, K. Y.; Schadock-Hewitt, A. J.; Hunter, N. P.; Bright, F. V.; Baker, G. A., 'Liquid litmus': Chemosensory ph-responsive photonic ionic liquids. *Chemical Communications* **2011**, *47*, 4775-4777.
13. Zhang, Q. H.; Zhang, S. G.; Liu, S. M.; Ma, X. Y.; Lu, L. J.; Deng, Y. Q., Ionic liquid-modified dyes and their sensing performance toward acids in aqueous and non-aqueous solutions. *Analyst* **2011**, *136*, 1302-1304.
14. Benito-Lopez, F.; Coyle, S.; Byrne, R.; O'Toole, C.; Barry, C.; Diamond, D. Simple barcode system based on inonogels for real time ph-sweat monitoring. In *Body Sensor Networks (BSN), 2010 International Conference on* 2010, p 291-296.
15. Lee, Y. E. K.; Smith, R.; Kopelman, R. Nanoparticle pebble sensors in live cells and in vivo. In *Annual review of analytical chemistry* 2009; Vol. 2, p 57-76.
16. Li, M.; De Rooy, S. L.; Bwambok, D. K.; El-Zahab, B.; DiTusa, J. F.; Warner, I. M., Magnetic chiral ionic liquids derived from amino acids. *Chemical Communications* **2009**, 6922-6924.
17. de Rooy, S. L.; El-Zahab, B.; Li, M.; Das, S.; Broering, E.; Chandler, L.; Warner, I. M., Fluorescent one-dimensional nanostructures from a group of uniform materials based on organic salts. *Chemical Communications* **2011**, *47*, 8916-8918.
18. Das, S.; Bwambok, D.; El-Zahab, B.; Monk, J.; de Rooy, S. L.; Challa, S.; Li, M.; Hung, F. R.; Baker, G. A.; Warner, I. M., Nontemplated approach to tuning the spectral properties of cyanine-based fluorescent nanoGUMBOS. *Langmuir* **2010**, *26*, 12867-12876.
19. Sun, H.; Scharff-Poulsen, A. M.; Gu, H.; Almdal, K., Synthesis and characterization of ratiometric, ph sensing nanoparticles with covalently attached fluorescent dyes. *Chemistry of Materials* **2006**, *18*, 3381-3384.

20. Ghaemy, M.; Naseri, M., Synthesis of chitosan networks: Swelling, drug release, and magnetically assisted bsa separation using Fe<sub>3</sub>O<sub>4</sub> nanoparticles. *Carbohydrate Polymers* **2012**, *90*, 1265-1272.
21. Griset, A. P.; Walpole, J.; Liu, R.; Gaffey, A.; Colson, Y. L.; Grinstaff, M. W., Expansile nanoparticles: Synthesis, characterization, and *in vivo* efficacy of an acid-responsive polymeric drug delivery system. *Journal of the American Chemical Society* **2009**, *131*, 2469-2471.
22. McIlvaine, T. C., A buffer solution for colorimetric comparison. *Journal of Biological Chemistry* **1921**, *49*, 183-186.
23. Sjoback, R.; Nygren, J.; Kubista, M., Absorption and fluorescence properties of fluorescein. *Spectrochimica Acta Part a-Molecular and Biomolecular Spectroscopy* **1995**, *51*, L7-L21.
24. Kasai, H.; Nalwa, H. S.; Oikawa, H.; Okada, S.; Matsuda, H.; Minami, N.; Kakuta, A.; Ono, K.; Mukoh, A.; Nakanishi, H., A novel preparation method of organic microcrystals. *Japanese Journal of Applied Physics Part 2* **1992**, *31*, L1132-L1134.
25. Kasai, H.; Kamatani, H.; Okada, S.; Oikawa, H.; Matsuda, H.; Nakanishi, H., Size-dependent colors and luminescences of organic microcrystals. *Japanese Journal of Applied Physics Part 2-Letters* **1996**, *35*, L221-L223.
26. Lakowicz, J. R. *Principles of fluorescence spectroscopy*; Springer, 2007.
27. Del Popolo, M. G.; Voth, G. A., On the structure and dynamics of ionic liquids. *Journal of Physical Chemistry B* **2004**, *108*, 1744-1752.
28. von Berlepsch, H.; Bottcher, C., Supramolecular structure of ttbc j-aggregates in solution and on surface. *Langmuir* **2013**, *29*, 4948-4958.
29. De, S.; Das, S.; Girigoswami, A., Environmental effects on the aggregation of some xanthene dyes used in lasers. *Spectrochimica Acta Part a-Molecular and Biomolecular Spectroscopy* **2005**, *61*, 1821-1833.
30. Lin, H. Z.; Camacho, R.; Tian, Y. X.; Kaiser, T. E.; Wurthner, F.; Scheblykin, I. G., Collective fluorescence blinking in linear j-aggregates assisted by long-distance exciton migration. *Nano Letters* **2010**, *10*, 620-626.
31. Lu, C. F.; Das, S.; Magut, P. K. S.; Li, M.; El-Zahab, B.; Warner, I. M., Irradiation induced fluorescence enhancement in pegylated cyanine-based NIR nano- and mesoscale GUMBOS. *Langmuir* **2012**, *28*, 14415-14423.
32. Scheblykin, I. G.; Drobizhev, M. A.; Varnavsky, O. P.; VanderAuweraer, M.; Vitukhnovsky, A. G., Reorientation of transition dipoles during exciton relaxation in j-aggregates probed by fluorescence anisotropy. *Chemical Physics Letters* **1996**, *261*, 181-190.
33. Jia, H.; Bai, X. T.; Shi, L. J.; Lu, F.; Zheng, L. Q., The effects of the pi-pi stacking interactions on the patterns of gold nanoparticles formed at the air-water interface. *Nanoscale* **2012**, *4*, 3162-3167.

34. Kumar, V.; Malhotra, S. V., Study on the potential anti-cancer activity of phosphonium and ammonium-based ionic liquids. *Bioorganic & Medicinal Chemistry Letters* **2009**, *19*, 4643-4646.
35. Li, M.; Ganea, G. M.; Lu, C.; De Rooy, S. L.; El-Zahab, B.; Fernand, V. E.; Jin, R.; Aggarwal, S.; Warner, I. M., Lipophilic phosphonium-lanthanide compounds with magnetic, luminescent, and tumor targeting properties. *Journal of Inorganic Biochemistry* **2012**, *107*, 40-46.
36. Minchinton, A. I.; Tannock, I. F., Drug penetration in solid tumours. *Nature Reviews Cancer* **2006**, *6*, 583-592.
37. Dalmau, M.; Lim, S. R.; Wang, S. W., Design of a pH-dependent molecular switch in a caged protein platform. *Nano Letters* **2009**, *9*, 160-166.

## CHAPTER 6. CONCLUSIONS AND FUTURE DIRECTIONS

The work presented and discussed in my dissertation covers two classes of materials that differ only in their melting points, namely ionic liquids and a Group of Uniform Materials Based on Organic Salts. While ILs melt below 100 °C, the GUMBOS counterparts widen this range to between 25 °C to 250 °C. By developing these solid phase materials, we have been able to expand applications of low melting salts without worrying about their state of matter. From ILs and GUMBOS, new nanomaterials were developed, and interesting biomedical applications have been elucidated and discussed in this dissertation. It is exciting to realize that these nanomaterials have such broad applications that this work only explores and expounds on a very small fraction of possible applications. Their tunability in properties such as photophysical properties, melting points, solubility, magnetism, toxicity, just to name a few opens a new frontier of research in the sciences. This work focusses mainly on biomedical applications of ILs and GUMBOS

The first chapter provides a brief overview of one application namely cancer, the ancient group of diseases that has evaded man's innovativeness in the quest for its cure. A brief discussion on the approaches being explored in its treatment is provided. Secondly, a synopsis of previous studies, and foundations on ionic liquids, GUMBOS, nanomaterials, absorbance, and fluorescence among others, is provided. The various major analytical techniques employed in this research are also discussed to help the reader get a grasp of the principles behind them.

The second chapter discusses the synthesis, characterization and application of rhodamine 6G-based GUMBOS in the biomedical field. In particular, application of these compounds in cancer research *in vitro* is widely explored. Rhodamines have been investigated previously for utility as chemotherapeutic agents with observed toxicity to both normal and cancer cells. However, this study demonstrates that apart from tuning physicochemical properties, cytotoxicity is also varied by changing the counter anion on a rhodamine 6G

compound. The nanomaterials developed from the hydrophobic ones of the synthesized rhodamine 6G-based GUMBOS turned out to be non-toxic to an investigated breast normal cell line and toxic to breast cancer cell lines. This study demonstrated that both the cation and anion in a drug play an active and cooperative role in anti-tumor cell proliferation potential.

The third chapter introduces a new frontier in development of multifunctional nanomaterials based on phosphonium containing cations and dysprosium containing anions. Emboldened by the selectivity observed in the rhodamine based nanomaterials, we sought to synthesize nanomaterials from our previously reported chemotherapeutic candidates. Phosphonium-dysprosium derived nanoparticles were more effective than the bulk materials in killing select cancer cell lines while maintaining non-toxicity to a normal cell line. In addition, the nanomaterials retained the properties inherent in the bulk compounds such as paramagnetism, fluorescence, and cancer targeting. Therefore, if the phosphonium-dysprosium compounds prove to be useful as chemotherapeutic agents, the nanoformulation would improve its efficacy without loss of multifunctional properties.

In the fourth chapter another class of multifunction nanomaterials synthesized from iron (III) phthalocyanine chloride and sodium deoxycholate is discussed. These nanomaterials were designed to exhibit magnetism and fluorescence from the iron (III) phthalocyanine moiety and pH sensitivity from the deoxycholate. The resulting GUMBOS were non-toxic to both normal and cancer cell lines. This chapter demonstrates that the synthesized nanomaterial decompose or break apart in acidic environments which would be useful in releasing drugs at the target site. Drug release data revealed that doxorubicin encapsulated nanoparticles led to cell death *in vitro* while free nanoparticles did not. The pH responsive drug release property in actual cellular environment points toward possible utility as drug delivery vehicles to diseased tissue known to

be acidic. Besides, the paramagnetism may be useful in targeted drug delivery of these nanomaterials using an external magnetic field.

The fifth chapter introduces the second application namely pH sensing using an ionic liquid based sensor. Ionic liquids and IL nanodroplets were synthesized from trihexyltetradecylphosphonium (TTP) cation and a fluorescein anion. The pH dependent colorimetric response of [TTP]<sub>2</sub>[FL] nanodroplets suggests possible application in determination of acidosis *in vitro* or *in vivo* as biosensor for cancer and bacterial infections. The nanodroplets were also shown to expand at acidic pHs which may be improve retention if applied in the leaky vasculature of cancer tissue. Overall, all the compounds and nanomaterials synthesized and reported in this dissertation were fluorescent. This may allow utility as cellular probes in cancer cells.

The works presented in my dissertation are in no way exhaustive but serve as a springboard for further research. The hydrophobic rhodamine based compounds as well as all the nanomaterials reported in subsequent chapters displayed selectivity toward investigated cancer cell lines. More work need to be done to elucidate the mechanisms behind observed selectivity. It is worth noting that various factors influence the effect of a drug towards a disease. In particular factors such as drug resistance, cellular uptake, chemical structure of the drug, and hydrophobicity greatly determine the final effect of the drug. These factors need to be investigated further to establish their role in the reported works. In the case of nanoparticles, the surface charge, size, and composition play a great role. This list is by no means exhaustive and therefore this field is rich in terms of the many factors that need to be investigated before a theory is formulated. Generally, nanoparticle cellular uptake is via different types of endocytosis. Although we demonstrated improved uptake of nanoGUMBOS by a breast cancer cell line, the

actual mode of uptake was not investigated. This should be performed in the future to establish if it is the main reason behind the selectivity. Another question that remains to be answered through future work is whether the observed selectivity is a general trend for nanoGUMBOS derived from cationic compounds. Hence, more nanoGUMBOS from different cationic compounds should be investigated. Besides, it would be interesting to perform *in vivo* studies with the reported nanoGUMBOS as theranostics as well as actual pharmacophores. Promising results *in vivo* would edge nanoGUMBOS closer to the market which is the main goal of drug discovery related work. A future direction for the pH responsive colorimetric nanosensors may be actual fabrication of a hand held device that can be used in detection of diseased or infected tissue.

## APPENDIX: LETTERS OF PERMISSION

3/17/2014

RightsLink by Copyright Clearance Center



# RightsLink<sup>®</sup>

Account info

Help



**Title:** Intraoperative tumor-specific fluorescence imaging in ovarian cancer by folate receptor- $\alpha$  targeting: first in-human results

**Author:** Gooitzen M van Dam, George Themelis, Luda M A Crane, Niels J Harlaar, Rick G Pleijhuis, Wendy Keider, Athanasios Sarantopoulos, Johannes S de Jong, Hennette J G Arts, Até G J van der Zee, Joost Bart, Philip S Low, Vasilis Ntzichristos

**Publication:** Nature Medicine

**Publisher:** Nature Publishing Group

**Date:** Sep 18, 2011

Copyright © 2011, Rights Managed by Nature Publishing Group

Logged in as:  
Paul Magut  
Account #: 1000746949

LOGOUT

### Order Completed

Thank you very much for your order.

This is a License Agreement between Paul K. S Magut ("You") and Nature Publishing Group ("Nature Publishing Group"). The license consists of your order details, the terms and conditions provided by Nature Publishing Group, and the [payment terms and conditions](#).

License number	Reference confirmation email for license number
License date	Mar 17, 2014
Licensed content publisher	Nature Publishing Group
Licensed content publication	Nature Medicine
Licensed content title	Intraoperative tumor-specific fluorescence imaging in ovarian cancer by folate receptor- $\alpha$ targeting: first in-human results
Licensed content author	Gooitzen M van Dam, George Themelis, Luda M A Crane, Niels J Harlaar, Rick G Pleijhuis, Wendy Keider, Athanasios Sarantopoulos, Johannes S de Jong, Hennette J G Arts, Até G J van der Zee, Joost Bart, Philip S Low, Vasilis Ntzichristos
Licensed content date	Sep 18, 2011
Type of use	I don't see my intended use
Volume number	17
Issue number	10
Requestor type	academic/university or research institute
Special requirements	I would like to use figure 3 in the introduction of my dissertation
Author of this NPG article	no
Your reference number	
Billing Type	Invoice
Billing address	222 Choppin Hall Baton Rouge, LA 70803 United States
Total	0.00 USD

<https://rightslink.com/App/DispatchServlet>

1/2





# RightsLink

[Home](#)
[Account Info](#)
[Help](#)

**Title:**

Tunable Cytotoxicity of Rhodamine 6G via Anion Variations

Logged in as:

Paul Magut

**Author:**

Paul K. S. Magut, Susmita Das, Vivian E. Femand, Jack Lasso, Karen McDonough, Brittini M. Naylor, Sita Aggarwal, and Isiah M. Warner

[LOGOUT](#)
**Publication:** Journal of the American Chemical Society

**Publisher:** American Chemical Society

**Date:** Oct 1, 2013

Copyright © 2013, American Chemical Society

### PERMISSION/LICENSE IS GRANTED FOR YOUR ORDER AT NO CHARGE

This type of permission/license, instead of the standard Terms & Conditions, is sent to you because no fee is being charged for your order. Please note the following:

- Permission is granted for your request in both print and electronic format, and translations.
- If figures and/or tables were requested, they may be adapted or used in part.
- Please print this page for your records and send a copy of it to your publisher/graduate school.
- Appropriate credit for the requested material should be given as follows: "Reprinted (adapted) with permission from (COMPLETE REFERENCE CITATION). Copyright (YEAR) American Chemical Society." Insert appropriate information in place of the capitalized words.
- One-time permission is granted only for the use specified in your request. No additional uses are granted (such as derivative works or other editions). For any other uses, please submit a new request.

[BACK](#)
[CLOSE WINDOW](#)

Copyright © 2014 Copyright Clearance Center, Inc. All Rights Reserved. [Privacy statement](#)  
 Comments? We would like to hear from you. E-mail us at [custhelp@copyright.com](mailto:custhelp@copyright.com).



# RightsLink®

[Home](#)
[Account Info](#)
[Help](#)


**Title:** Lipophilic phosphonium-lanthanide compounds with magnetic, luminescent, and tumor targeting properties

**Author:** Min Li, Gabriele M. Ganes, Chengfei Lu, Sergio L. De Rooy, Bilal El-Zahab, Vivian E. Fernandez, Rongying Ju, Sita Aggarwal, Isiah M. Warner

**Publication:** Journal of Inorganic Biochemistry

**Publisher:** Elsevier

**Date:** February 2012  
Copyright © 2012, Elsevier

Logged in as:  
Paul Magut  
Account #: 0000746948

[LOGOUT](#)

## Order Completed

Thank you very much for your order.

This is a License Agreement between Paul K. S Magut ("You") and Elsevier ("Elsevier"). The license consists of your order details, the terms and conditions provided by Elsevier, and the [payment terms and conditions](#).

### [Get the printable license](#)

License Number	3353050393084
License date	Mar 20, 2014
Licensed content publisher	Elsevier
Licensed content publication	Journal of Inorganic Biochemistry
Licensed content title	Lipophilic phosphonium-lanthanide compounds with magnetic, luminescent, and tumor targeting properties
Licensed content author	Min Li, Gabriele M. Ganes, Chengfei Lu, Sergio L. De Rooy, Bilal El-Zahab, Vivian E. Fernandez, Rongying Ju, Sita Aggarwal, Isiah M. Warner
Licensed content date	February 2012
Licensed content volume number	107
Licensed content issue number	1
Number of pages	7
Type of Use	reuse in a thesis/dissertation
Portion	figures/tables/illustrations
Number of figures/tables/illustrations	All
Actual number of figures/tables/illustrations	21
Format	both print and electronic
Are you the author of this Elsevier article?	No
Will you be translating?	No
Title of your thesis/dissertation	IONIC LIQUIDS AND GROUPS OF UNIFORM MATERIALS BASED ON ORGANIC SALTS FOR BIOMEDICAL AND SENSING APPLICATIONS
Expected completion date	Mar 2014
Estimated size (number of pages)	150
Elsevier VAT number	GB 494 6272 12



My Orders > Orders > All Orders

## License Details

Thank you very much for your order.

This is a License Agreement between Paul K. S Magui ("You") and Elsevier ("Elsevier"). The license consists of your order details, the terms and conditions provided by Elsevier, and the [general terms and conditions](#).

[Get the embargo license.](#)

License Number	3353051163533
License date	Mar 20, 2014
Licensed content publisher	Elsevier
Licensed content publication	Journal of Inorganic Biochemistry
Licensed content title	Lipophilic phosphonium–lanthanide compounds with magnetic, luminescent, and tumor targeting properties
Licensed content author	Min Li, Gabriela M. Ganea, Chengfei Lu, Sergio L. De Rooy, Bilal El-Zahab, Wylan E. Fernandez, Rongying Jin, Sita Aggarwal, Isiah M. Warner
Licensed content date	February 20 12
Licensed content volume number	107
Licensed content issue number	1
Number of pages	7
Type of Use	reuse in a thesis/dissertation
Portion	excerpt
Number of excerpts	5
Actual number of figures/tables/illustrations	21
Format	both print and electronic
Are you the author of this Elsevier article?	No
Will you be translating?	No
Title of your thesis/dissertation	IONIC LIQUIDS AND GROUPS OF UNIFORM MATERIALS BASED ON ORGANIC SALTS FOR BIOMEDICAL AND SENSING APPLICATIONS
Expected completion date	Mar 2014
Estimated size (number of pages)	150
Elsevier VAT number	GB 494 6272 12
Permissions price	0.00 USD
VAT/Local Sales Tax	0.00 USD / 0.00 GBP
Total	<b>0.00 USD</b>



Paul Magut <[pmagut1@tigers.lsu.edu](mailto:pmagut1@tigers.lsu.edu)>

## Permission

1 message

Paul Magut <[pmagut1@tigers.lsu.edu](mailto:pmagut1@tigers.lsu.edu)>  
To: [contracts-copyright@rsc.org](mailto:contracts-copyright@rsc.org)

Tue, Mar 18, 2014 at 7:55 PM

To Whom It May Concern:

I am the second author in: Das, S.; Magut, P. K. S.; de Rooy, S. L.; Hasan, F.; Warner, L. M., Ionic liquid-based fluorescein colorimetric pH nanosensors. *RSC Advances* 2013, 3, 21054-21061.

I would like to use this paper in my dissertation.

Please let me know what forms and information is necessary to make this possible.

Regards,

Paul Sang Magut  
Ph.D. Candidate  
Warner Research Group  
Louisiana State University  
432 Choppin Hall  
Baton Rouge, LA 70803  
Office: (225) 578 - 3919  
Fax: (225) 578-3071

### Websites:

[www.rsc.org/condpub/author/e-mail/16/100/000/](http://www.rsc.org/condpub/author/e-mail/16/100/000/)

<http://www.usstream.lync.com/Join/312842376/>

CONTRACTS-COPYRIGHT (shared) <[Contracts-Copyright@rsc.org](mailto:Contracts-Copyright@rsc.org)>  
To: Paul Magut <[pmagut1@tigers.lsu.edu](mailto:pmagut1@tigers.lsu.edu)>

Wed, Mar 26, 2014 at 9:30 AM

Dear Paul

The Royal Society of Chemistry (RSC) hereby grants permission for the use of your paper(s) specified below in the printed and microfilm version of your thesis. You may also make available the PDF version of your paper(s) that the RSC sent to the corresponding author(s) of your paper(s) upon publication of the paper(s) in the following ways: in your thesis via any website that your university may have for the deposition of theses, via your university's Intranet or via your own personal website. We are however unable to grant you permission to include the PDF version of the paper(s) on its own in your institutional repository. The Royal Society of Chemistry is a signatory to the STM Guidelines on Permissions (available on request).

Please note that if the material specified below or any part of it appears with credit or acknowledgement to a third party then you must also secure permission from that third party before reproducing that material.

3/26/2014

TigerMail Mail - Permission

Please ensure that the thesis states the following:

Reproduced by permission of The Royal Society of Chemistry

and include a link to the paper on the Royal Society of Chemistry's website.

Please ensure that your co-authors are aware that you are including the paper in your thesis.

Regards

Gill Cockhead  
Publishing Contracts & Copyright Executive

Gill Cockhead  
Publishing Contracts & Copyright Executive  
Royal Society of Chemistry,  
Thomas Graham House,  
Science Park, Milton Road,  
Cambridge, CB4 0WF, UK  
Tel +44 (0) 1223 432134

Follow the Royal Society of Chemistry:  
[www.rsc.org/follow](http://www.rsc.org/follow)

Winner of The Queen's Award for Enterprise, International Trade 2013

## VITA

Paul Kipkorir Sang Magut was born in Nakuru County, Kenya, to Mr. Joel Kimuigei Arap Magut and Mrs. Esther Chelagat Magut. He was raised in Sosirot village where he attended Kenana Primary School. He attended Kapsabet Boys High School in Nandi County. It was at Kapsabet Boys that Paul developed a passion of Chemistry intrigued by color changes that acids and bases displayed in presence of indicators during titrations. Mr. Willy Mutai, the Chemistry Teacher recognized Paul's talent and passion and started mentoring him more closely in the subject. They would prepare experiments and solutions together and at one point Paul was even allowed to supervise fellow students performing experiments! Thereafter, he received his Bachelor of Education (Science) in Chemistry and Mathematics (November 2001) from Egerton University, Kenya. After teaching high school for five years, Paul's unquenched desire for science saw him apply for study leave from the Kenyan government through the Teachers Service Commission to pursue a Master of Science Degree in Chemistry from Moi University, Kenya. It was while pursuing the Master of Science Degree under the guidance of Dr. Claire I. Muhanji that Paul received an assistantship to pursue a Doctoral of Philosophy Degree in Chemistry at Louisiana State University (Fall 2009).

In the spring of 2010, Paul joined the Warner Research group where he performed research under the diligent tutelage of Professor Isiah M. Warner. Paul has since been productive in research and teaching. His research has resulted in five publications in peer reviewed journals with 10 more under preparation or submission as well as 19 conference presentations and a provisional patent. His efforts have been recognized through several awards and honors. Most notably, he was selected as the Louisiana State university Department of Chemistry nominee for the American chemical Society's 2014 Dr. Irving Sigal Post-doctoral fellowship. He also

received the Charles E. Harrington outstanding graduate student award, the James W. Robison outstanding research in analytical sciences award and the teaching assistant scholar award in the course of his graduate career. He is a member of the American Chemical Society (ACS) and the National Organization for the Professional Advancement of Black Chemists and Chemical Engineers (NOBCChE). He served as the Vice President of the NOBCChE LSU chapter in 2012-2013. Paul anticipates graduating with a Doctor of Philosophy Degree in Chemistry in August 2014.